Isoporous double layer hollow fiber by co-extrusion for membrane and other applications

Dissertation submitted in partial fulfillment of the requirements for the

degree of Doctor of Science (Dr. rer. nat.)

to

The University of Hamburg,

Institute of Physical Chemistry, Department of Chemistry, MIN Faculty

Submitted by

Nazia Noor

Hamburg, 2018

Reviewer 1: Prof. Dr. Volker Abetz

Reviewer 2: Prof. Dr. Gerrit A. Luinstra

Date of Defense: 15.03.2019

Examiner 1: Prof. Dr. Volker Abetz

Examiner 2: Prof. Dr. Hans-Ulrich Moritz

Examiner 3: Priv. Doz. Dr. Christoph Wutz

The work presented in this dissertation was conducted from July, 2013 – June, 2017 at the Institute of Polymer Research, Helmholtz-Zentrum Geesthacht (HZG) under the supervision of Prof. Dr. Volker Abetz.

List of Publications

1. A Facile Method to Prepare Double-Layer Isoporous Hollow Fiber Membrane by *in-situ* Hydrogen-bond Formation in the Spinning Line. **Nazia Noor**, Joachim Koll, Maryam Radjabian, Clarissa Abetz, Volker Abetz; Macromolecular Rapid Communications **2016**, *37*, 414 (**Front Cover page: 5/2016**).

2. Continuous Production of Macroporous Films from Commercially Accessible Polymers: An Alternative to Breath Figure Assembly. **Nazia Noor**, Joachim Koll, Clarissa Abetz, Heiko Notzke, Volker Abetz; Scientific Reports **2017**, *7*: 8050.

3. Hollow Fiber Membranes of Blends of Polyethersulfone and Sulfonated Polymers. **Nazia Noor**, Joachim Koll, Nico Scharnagl, Clarissa Abetz, Volker Abetz. Membranes **2018**, *8* (3), 54.

Patent Application

Macroporous or Mesoporous Polymer Films in Hollow Fiber Geometry. **Nazia Noor**, Volker Abetz, Joachim Koll. (Submitted to European Patent Office (EPO) (RO/EP)).

Table of Content

List of Figures

List of Schemes

List of Tables

List of Symbols

A	effective area of the inner surface of the hollow fiber acting in transporting water
A-B	Diblock block copolymer with A and B blocks
b	Grafting distance
d_O	Outer diameter of hollow fiber
f	Fraction of the minor blocks in the block copolymer
I	Integral peak
L	Liter
L_{Air}	Air-gap distance
N	degree of polymerization
P	pressure normalized permeation flux
Δp	transmembrane pressure across the wall thickness of the hollow fiber
Q_B	Flow rate of bore fluid
Q_P	Flow rate of polymer solution
Q_I	Flow rate of inner layer dope
Q_O	Flow rate outer layer dope
Rc	Radius of the core of a micelle

Rg	Radius of gyration
Rh	Hydrodynamic radius
Rm	Overall radius of the micelle
t	Time
V	Volume of water
Z	the aggregation number
χ	Flory-Huggins interaction parameter

List of Abbreviations

C or C′	Cylinder
CA	Cellulose acetate
CaH_2	Calcium hydride
CMC	Critical micelle concentration
$CHCl_3$	Chloroform
$ClSO_3H$	Chlorosulfonic acid
CMT	Critical micelle temperature
DCM	Dichloromethane
DMAc	Dimethylacetamide
DMF	N-N-dimethylformamide
DS	Degree of sulfonation
DSC	Differential Scanning Calorimetry
EDS	Elemental Analysis by Energy Dispersive Microanalysis
EG	Ethylene glycol
G or G′	Gyroid
GBL	γ-butyrolactone
GH 62	Styroclear® (PS-b-PB-b-PS)
ISR	Intermediate segregation region
L	Lammelar
LASER	Light amplification by stimulated emission of radiation
$MgBu_2$	Dibutylmagnesium
NG	Nucleation and growth
NIPS	Non-solvent induced phase separation

NMP	1-methyl-2-pyrrolidone
NMR	Nuclear Magnetic Resonance Spectroscopy
ODT	Order to disorder transition
PEG	Poly(ethylene glycol)
PEI	Polyetherimide
PESU	Polyethersulfone
PPSU	Polyphenylenesulfone
PS	Polystyrene
PS-*b*-PB-b-PS	polystyrene-*block*-polybutadiene-block-polystyrene
PS-*b*-P4VP	polystyrene-*block*-poly(4-vinylpyridine)
PSSNa	poly(sodium 4-styrene sulfonate) (PSSNa)
PVDF	Polyvinyledenefluoride
RED	Relative energy difference
S or S′	Spherical
SANS	Small-angle neutron scattering
SAXS	Small-angle X-ray scattering (SAXS)
S_{cp} or S'_{cp}	Closed pack sphere
sec-BuLi	sec-butyllithium
SD	Spinodal decomposition
SDS	Sodium lauryl sulfate
SEM	Scanning Electron Microscopy
SNIPS	Self-assembly and non-solvent induced phase separation
sPESU	Sulfonated polyethersulfone
sPPSU	Sulfonated polyphenylenesulfone
SSL	Strong segregation limit
TEM	Transmission Electron Microscopy
TGA	Thermogravimetric Analysis
THF	Tetrahydrofuran
TIPS	Temperature induced phase separation
VIPS	Vapor induced phase separation
4VP	4-vinyl pyridine
WSL	Weak segregation limit
XPS	X-ray Photoelectron Spectroscopy

Zusammenfassung

Das Ziel dieser Arbeit war es, die Zweckmäßigkeit des Koextrusionsverfahrens für die Herstellung stabiler isoporöser Hohlfasermembranen zu untersuchen. Zur Erzeugung der isoporösen Struktur auf der selektiven, äußeren Oberfläche der Membran mittels des SNIPS-Verfahrens (Kombination aus der Selbstorganisation amphiphiler Blockcopolymere und der Nicht-Lösemittel induzierten Phasenseparation) wurde Polystyrol-*block*-poly(4-vinylpyridin) (PS-*b*-P4VP) als Material gewählt. Diese Ergebnisse dienten als Ausgangspunkt für die Koextrusionsoptimierung. Die wichtigste Herausforderung bei der Koextrusion bestand darin, die Delamination der Schichten zu verhindern und diese an den Grenzflächen zu verbinden. Mittels der Bildung von Grenzflächenbindungen zwischen den Schichten gelang es letztendlich, delaminationsfreie Doppelschichthohlfasern in einem einstufigen Koextrusionsprozess herzustellen. Hierfür wurde das kommerziell erhältliche Polymer Polyethersulfon (PESU) zu sulfoniertem PESU (sPESU) funktionalisiert. Ein Polymerblend aus PESU und sPESU wurde für die Bildung der Stützschicht verwendet.[1]

Um eine Stützschicht mit geringerem Fließwiderstand gegenüber Wasser zu erzeugen, wurden verschiedene Blends aus PESU und sulfonierten Polymeren untersucht und modifiziert. PESU/sPESU enthaltende Hohlfasern erwiesen sich weiterhin als wasserundurchlässig, obwohl eine höhere Menge an Sulfonsäuregruppen an deren Oberflächen durch Röntgenphotoelektronenspektroskopie (XPS) nachgewiesen wurde. Die Zugabe von Ethylenglykol und Poly(Natrium-4-Styrolsulfonat) zur Spinnlösung der PESU/sPESU-Blends führte zu einer permeablen Hohlfasermembran. Unter Verwendung dieses Additivsystems wurde ebenfalls eine Zunahme der Wasserpermeabilität bei Hohlfasern aus Blends von PESU und sulfoniertem Polyphenylensulfon (sPPSU) verzeichnet.[2]

Am Ende wird ein innovativer Ansatz für die makroporöse Filmbildung vorgestellt. Dies erlaubte das simultane Koextrudieren von bis zu vier verschiedenen Flüssigkeiten. Die Umsetzung des Konzepts des „Eindiffundierens, der Tröpfchenbildung und dann Auskondensierens" von Glyzerin in einem Koextrusionsverfahren des Hohlfaserspinnens ermöglichte eine kontinuierliche makroporöse Filmbildung, die die Verwendung der etablierten Breath-Figure-Methode umgeht. Darüber hinaus wurde die kontinuierliche Filmbildung durch den vorgeschlagenen Mechanismus auch in einer Flachmembrangeometrie realisiert, indem zwei Gießklingen in einer Gießmaschine verwendet wurden.[3]

Abstract

The aim of this work was to examine the feasibility of the co-extrusion method for the fabrication of sturdy isoporous hollow fiber membranes. To fabricate the isoporous structure on the selective surface of the membranes by the SNIPS method (combination of self-assembly and non-solvent induced phase separation), polystyrene-*block*-poly(4-vinylpyridine) (PS-*b*-P4VP) was selected as the outer layer forming material. The biggest challenge in co-extrusion was to prevent delamination between the layers and to integrate them at the interface. The challenge of fabricating a delamination free double layer hollow fiber by a one step co-extrusion was overcome by utilizing the concept of interfacial bond formation between the layers. For this purpose, a commercial polymer, polyethersulfone (PESU) was sulfonated (sPESU) and the blend of PESU and sPESU was engaged in forming the support layer.[1]

PESU/sulfonated polymer blend solutions were analyzed and modified with the aim to find the compositions that would render into a support layer with less resistance. Hollow fibers containing a PESU/sPESU blend were found to be impermeable to water, although the higher amount of sulfonic acid groups was detected on their surface by X-ray Photoelectron Spectroscopy (XPS). The addition of ethylene glycol and poly(sodium 4-styrene sulfonate) to the spinning dopes of PESU/sPESU blends resulted in permeable hollow fiber membranes. By using this additive system, an increase in the water permeation of PESU/sulfonated polyphenylenesulfone (sPPSU) blend hollow fibers was evident as well.[2]

In the end, an innovative approach for the macroporous film formation is introduced. The implementation of the concept of "diffuse-in, droplet formation, and then condense-out" behavior of glycerol in a co-extrusion method of hollow fiber spinning made macroporous film

formation possible in an interminable way sidestepping the use of the established breath figure assembly method. Moreover, the continuous film formation by the proposed mechanism was also authenticated in flat sheet geometry by employing two casting blades in a casting machine.[3]

0.5 μm
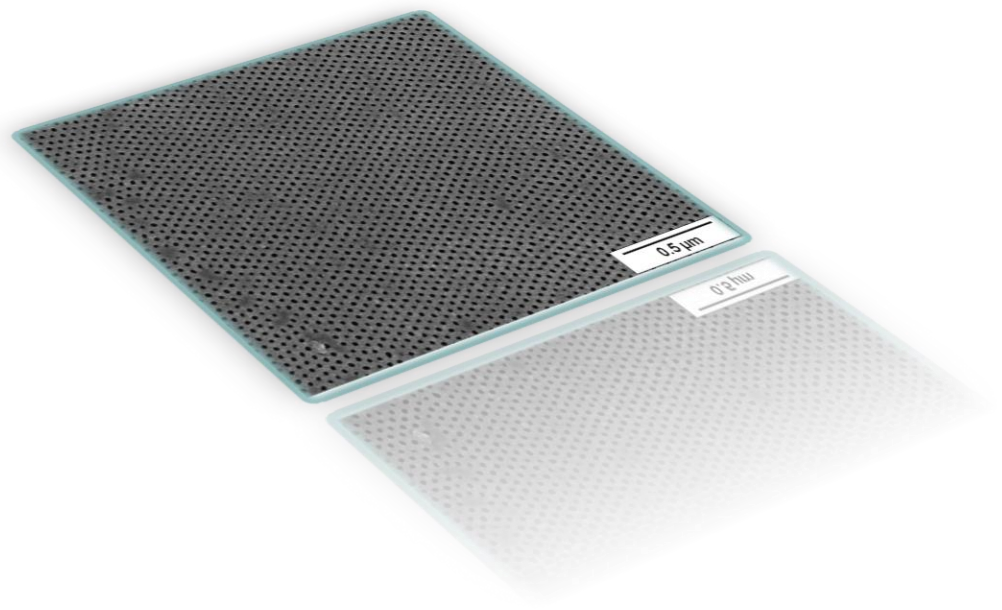
Chapter 1

Introduction

1.1 Objective

Synthetic membranes refer to an interface that can separate chemical entities from their mixture with other chemical entities as the biological cell membrane does to isolate the redundant components for the living beings. A membrane acts as a barrier between the feed molecules which are introduced on its surface and the permeate molecules which are permeated crossing this barrier when a driving force (e.g. pressure) is applied across it.[4] Pressure driven membrane separation techniques to separate solid and ionic entities from liquids are broadly categorized in different classes according to the size of the retentate entities (**Figure. 1.1**).
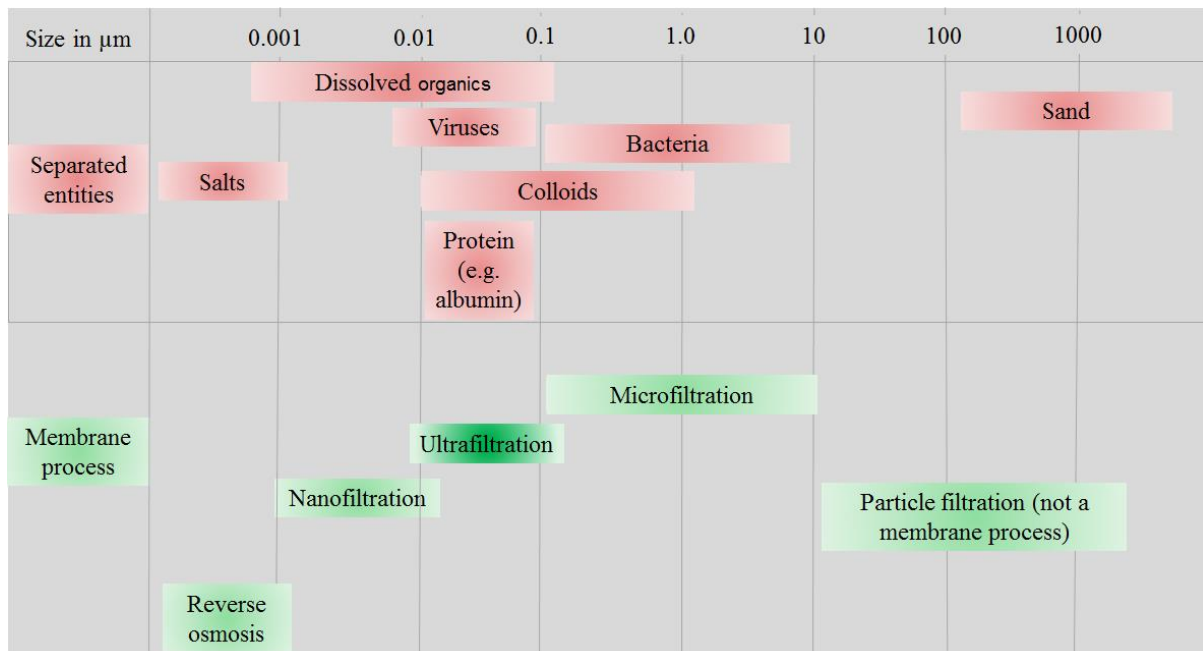
Figure 1.1. Pressure driven membrane processes.[5, 6]

Among the pressure driven separation processes ultrafiltration falls in the range by which bacteria, viruses, proteins or other macromolecules can be separated from feed solutions. Membranes with a pore size ranging from 2-100 nm are in use for pressure driven ultrafiltration (UF) processes. Ultrafiltration is widely used in several industries such as in food and beverage processing, water purification and treatment, biotechnological and pharmaceutical industries

etc.[5-7] A major application of this category of membranes is found in protein separation or purification. According to a study by MarketsandMarkets™ Research the global protein purification and isolation market was worth 3,970 million dollar in 2014 and is foreseen to be worth 6,370 million dollar by 2020.[8]

Protein study is necessary to understand the protein functions which may unveil many questions like biochemical mechanisms of disease and may lead to new drug development. To understand the protein function and regulation they need to get separated from other proteins or impurities, pyrogens and viruses.[7] In this regard, many techniques have been developed such as precipitation, packed bed chromatography, preparative chromatography, electrodialysis, electrophoresis, membrane chromatography, western blotting, dialysis, diafiltration, centrifugation, and ultrafiltration.[7, 9, 10] Among them the membrane based technology offers some advantages over others in terms of low energy consumption, low foot print, environmental friendliness, and high efficiency.[11] Though every method has its own pros and cons, the pressure driven ultrafiltration is a winsome choice regarding the scaling up of the process and functionality. However, earlier works showed that most ultrafiltration membranes made by the phase inversion method do not promise an acceptable separation performance unless the ratio of the molecular weight of the proteins is larger than seven. There still exists a question of how much the imperfect structure of the UF membranes contribute to the resolving power of UF membranes and to which extent it can be solved regarding the fundamental restriction of the method itself.[7, 12, 13] However, one of the possible routes to approach the answer may lie in the development and analysis of a membrane with a nearly perfect pore orientation on its selective surface. Separation of similar sized particles can be facilitated by using membranes with ordered pores of similar diameter (isoporous membranes) for reducing the energy consumption. Moreover, isoporous membranes with a sharp molecular weight cut-

off for high selectivity without interfering the transport properties are not only welcome for protein separation but also for other applications as well such as for water purification, biosensing, enzyme immobilization, selective separation of chemical and biological species, emulsification, molecular sieving, drug delivery, pathogen detection, tissue engineering, microfluidic, etc.[1, 14] The goal of this PhD work was to contribute in quest of a feasible method for isoporous membrane fabrication which would be potential to be integrated in the industrial scale.

1.2 Isoporous Double Layer Hollow Fiber Membrane

The key features of isoporous membranes i.e. pore size area and morphology can be tuned according to the intended applications. The available techniques for isoporous membrane formation include microfabrication techniques, LASER interference lithography, silicon micromachining technology, polymeric isoporous membrane fabrication by replication method using anodic porous alumina template, phase separation micromolding, excimer LASER, aperture array lithography, track-etched membranes, etc. High cost and sophistication of the processes do not promise mass production of isoporous membranes by these fabrication methods.[14-20]

In recent years, a considerable number of papers have been published that offer self-assembly of block copolymers as a key tool for fabricating membranes with high pore density and pore uniformity.[21-27] Research on architecture of highly selective membranes from block copolymer microdomain segregation got a propulsive force with the hope of large scale industrial production after the introduction of an intriguing method of membrane formation which combines block copolymer self-assembly and non-solvent induced phase separation (SNIPS).[28] Since then many studies have tended to focus on the tunability of pore size,

biocidal activity, and separation performances of isoporous block copolymer membranes.[27, 29-33] In order to meet the requirements by many membrane applications, the transformation of the geometry from flat to hollow fiber was necessary. However, winding up of self-ordered monodisperse pores of nanometer range scale on the top surface of a self-supporting hollow fiber requires optimization of several parameters of fiber processing and SNIPS mechanism such as block copolymer chemical composition, solution concentration, coagulant composition (both internal and external), air gap distance between spinneret and coagulation bath (adjusted with the required evaporation time of the structure formation), volumetric flow rates of bore fluid and dope solution, shear stress within spinneret etc. This impediment was successfully overcome in previous studies by developing a procedure of SNIPS based membrane in hollow fiber geometry using polystyrene-*block*-poly(4-vinylpyridine) (PS-*b*-P4VP) block copolymers.[34, 35] But the poor mechanical property of the continuous phase (PS) at room temperature detains the possibility of application of this innovative membrane. Functionalization of PS block[36, 37] or introduction of a third block[38] may offer improvement in properties of isoporous block copolymer membranes but these approaches neither suffice the requirement of lessening the usage of tailor-made expensive materials nor ensure the sturdiness of membrane for module fabrication. So in this study the work was continued with an engineering approach called co-extrusion[39] which is a well-studied method for improving mechanical stability of hollow fibers. This method is favorable among other processes of composite membrane fabrication because of its simplicity and feasibility of upscaling in expense of minimum amount of high performance material.[1]

By co-extrusion a support layer of commercially available materials was incorporated underneath the isoporous block copolymer layer by simultaneous extrusion of both layers. The solution characteristics and spinning parameters for single layer isoporous PS-*b*-P4VP hollow

fiber membrane fabrication were finely tuned and intricately discussed in the previous work.[35] However, double layer hollow fiber membrane fabrication by co-extrusion welds some other parameters to the loads of existing extrusion parameters of single layer hollow fiber like compatibility and different degree of shrinkage of polymer solutions used in both layers, ratio of extrusion rates of two layers, etc. The system of double layer hollow fiber where block copolymer is used as a selective layer on a support layer of different homopolymers always comes up with the problem of delamination of layers irrespective of processing methods.[1, 40, 41]

1.3 Strategy of the Work and Layout of the Thesis

The block copolymer chosen in this work for isoporous surface formation by a SNIPS process was PS-*b*-P4VP which is the most studied block copolymer so far to produce isoporous membranes by the SNIPS method.[28-30, 42] This tailor-made polymer was synthesized in house by living anionic polymerization. Initially, the hollow fiber formation method was studied by using commercially available polymers to optimize the parameters and to have an understanding of the process under the existing arrangement of the devices. The steps were then followed by the double layer hollow fiber formation by co-extrusion where the inner layer was formed by the solutions of commercial polymers and the outer layer was formed by the solutions of PS-*b*-P4VP.

The aim of this PhD work was to study the feasibility of the co-extrusion method for double layer isoporous hollow fiber membrane fabrication and to optimize the processing parameters towards this goal.

This thesis presents the analysis and discussion of the results obtained by the methodology followed in the aim of fabricating sturdy isoporous hollow fiber membranes by co-extrusion and is organized in the following way-

- In **Chapter 2**, theoretical background is presented in short on membrane types, non-solvent induced phase separation (NIPS), microphase separation of block copolymers, and the isoporous membrane formation by the SNIPS method.

- In **Chapter 3**, the materials used in this work are introduced and the experimental procedures are explained.

- **Chapter 4** shows the results of *in-situ* analysis of the hollow fiber formation method by using a LASER micrometer. Along with the diameter analysis this chapter highlights some other phenomena associated with the hollow fiber membrane formation method.

- Initially the hollow fiber formation method was studied by using commercially available polymers to optimize the parameters and to have an understanding of the process under the existing instrumental set-up. **Chapter 5** portrays the results obtained from a co-extrusion method where both layers were spun from commercially available polymers.

- Before applying PS-*b*-P4VP solution as the outer layer solution in the co-extrusion method the solutions of the block polymer were analyzed and optimized to bring in the isoporous structure on the membrane surface by the flat sheet casting method. Some representative results are discussed in **Chapter 6**.

- **Chapter 7** discusses the results of co-extrusion where the inner layer was formed by the solutions of commercially available polymers and the outer layer was formed by the solutions of PS-*b*-P4VP.

- Functionalization of the inner layer forming material was necessary for the adherence of the layers spun by co-extrusion. **Chapter 8** shows the results obtained for the double layer co-

extruded hollow fiber when using a functionalized polymer at the interface between inner and outer layer.

- **Chapter 9** explains the detailed characterization and modification of the functionalized polymer containing dope which potentially can be implemented as an inner or support layer forming material for composite isoporous membrane formation.

- The experimentation with isoporous double layer hollow fiber formation led to an idea of macroporous film formation in both flat sheet and hollow fiber geometry in a continuous process. **Chapter 10** sheds light on this newly reported work.

- **Chapter 11** depicts the summary of this work.

- **Chapter 12** and **13** are dedicated to references and appendix, respectively.

Chapter 2

Theoretical Background

2.1 Types of Membranes

A membrane, the barrier creating interface between the retentate and the permeate can be homogeneous with uniform composition and structure or can be chemically and/or physically heterogeneous.[4, 43, 44] According to their physical structures membranes can be categorized in different groups-

2.1.1 Symmetric Membrane

Isotropic microporous membrane

In an isotropic microporous membrane separation of the components is guided by the molecular size of the components and the pore size distribution of the membrane. These membranes serve the similar function as the filters do. However, the membranes have pore sizes much less in diameter compared to the filter (pore size of larger than 10 µm).[4, 43]

Dense membrane

In the nonporous or dense membranes, components are separated depending on their relative transport rate within the membrane. The transport rate is defined by the diffusivity and solubility of the component in the membrane forming material.[4, 43]

2.1.2 Anisotropic Membrane

Asymmetric membrane

In this type of membrane there is a gradient in pore sizes i.e. pore sizes get bigger from the surface to the bottom of the membranes. The separation behavior is determined mainly by the pore sizes of the upper layer whereas the substructure underneath functions as a mechanical support. Modern day's high flux membranes inspired by the method invented by Loeb and Sourirajan in 1960s are mostly fit into this category.[4, 43]

Composite membrane

Composite membrane constitutes of layers fabricated by different materials. The thin layer at the top controls the separation mechanism and the support layer (which can be asymmetric or symmetric) contributes as the support to the top layer or the selective layer.[4, 43]

2.2 Ultrafiltration Membrane

The membranes that are used for the separation that falls in the ultrafiltration category have smaller surface pores than the particles which need to be excluded. These membranes are usually anisotropic where a relatively fine micro/nanoporous structure on the surface is supported by the more open porous support. Particles in the permeating fluid are rejected on the surface of these membranes.[45]
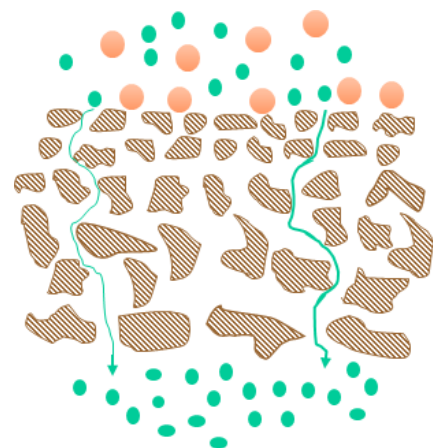
Anisotropic membranes can be named differently according to their fabrication methods such as- phase inversion membranes, interfacial polymerization membranes, solution-coated composite membranes, and other techniques with a variety of specialized processes e.g. plasma deposition.[46]

In this work, the phase inversion method was followed to fabricate the membranes and so this method is outlined in the following two sections.

2.2.1 Phase Inversion Membrane

The membrane fabrication technique what was introduced by Loeb and Sourirajan to produce reverse osmosis membrane is now recognized as a general category of membrane fabrication process called phase separation or phase inversion process, or the polymer precipitation process.[46]

The phase inversion process defines the process where a homogeneous polymer solution is brought into phase separation by any of the following means[46]-

i) Water precipitation (the Loeb-Sourirajan process): When the casted polymer solution is immersed into the non-solvent (mostly water) bath the exchange of non-solvent from the bath and the solvent from the polymer solution makes the asymmetric membrane formation possible. This process is known as non-solvent induced phase separation or NIPS.

 ii) Vapor absorption: In this process a casted polymer solution is brought into a non-solvent atmosphere or vapor to induce the phase separation in it. This is termed as vapor induced phase separation or VIPS.

iii) Thermal gelation: In this procedure the precipitation starts in the casted solution or film with a temperature change (usually cooling). This process is named as temperature induced phase separation or TIPS.

iv) Solvent evaporation: When a polymer solution is prepared with a mixture of solvents of different volatility the more volatile solvent induces the precipitation while evaporating.

Different combinations of these processes are also employed for fabrication of membranes with a desired morphology.[46]

In this study non-solvent induced phase separation or NIPS is used and therefore this process is introduced in more detail.

2.2.2 Theory of Membrane Formation by Non-solvent Induced Phase Separation (NIPS)

In this process, a homogeneous polymer solution is cast (for flat sheet geometry) or spun (for hollow fiber geometry) and then immersed in the coagulation bath. The coagulation bath consists of non-solvent for the polymer solution which is usually water or a water-based mixture. As the cast film or spun fiber is immersed into the precipitation bath phase separation is induced by the diffusion of the non-solvent into the polymer solution and the outflow of the solvent/s from the polymer solution. After plunging the homogeneous (in other words, thermodynamically stable) solution into the non-solvent bath the system becomes unstable by the exchange of solvent and non-solvent. Moreover, this is followed by the phase separation into a polymer-rich phase (higher polymer concentration) and polymer-lean phase (lower polymer concentration) which transform into the matrix and pores of the membranes, respectively. At this stage the minimum Gibb's free energy is favored by the co-existence of the two separated phases. By this method, membranes of asymmetric structure are formed with a selective surface sitting on top of a more open porous substructure.[43, 46, 47]

In the NIPS process the change of the composition of the membrane forming solution from its initial state to the final membrane formation state can be explained by polymer-solvent-precipitation medium phase diagrams. A typical three-component phase diagram showing the

trajectory for a NIPS membrane is presented in **Figure 2.1**. The three corners of the triangle represent polymer, solvent, and non-solvent (or water). The membrane formation path starts at a point having the initial composition of the original membrane forming solution followed by the points in the triangle which represent the mixture of the three components with different compositions. The path ends in a point which represents the final membrane composition. The diagram consists of two main regions- one phase region and two phase region. All three components are miscible in the one phase region whereas the system separates into a solid phase (or polymer rich phase) and a liquid phase (polymer poor phase) in the two phase region. As the membrane forming solution precipitates the composition of the solution moves from the one phase region to the two phase region by losing solvent and gaining non-solvent.
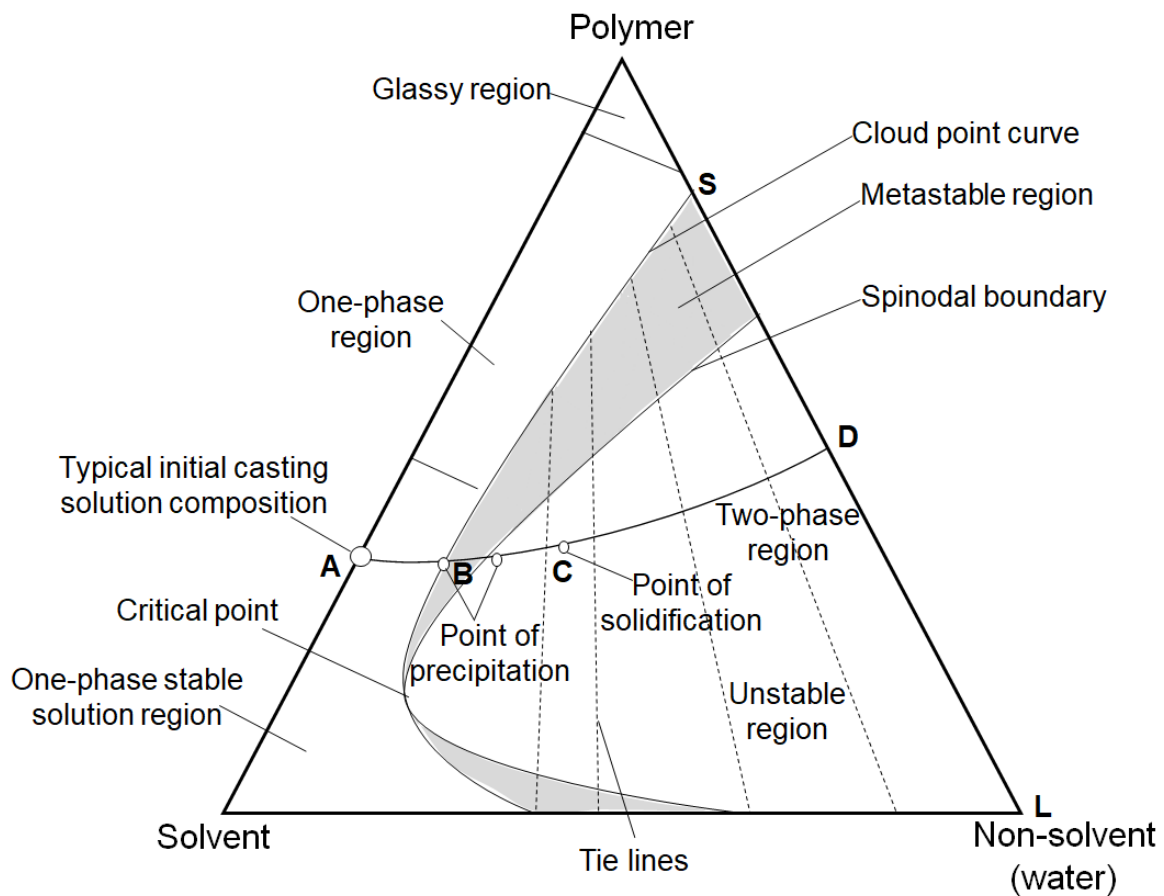
Figure 2.1 Membrane formation by phase inversion method (water precipitation) is explained by a three-component phase diagram where membrane formation is dipicted through a path

from the initial polymer casting solution (A) to the final membrane (D). This figure is adapted from reference [46].

The thermodynamically stable one-phase region can be subdivided into a liquid polymer solution region, a polymer gel region, and a glassy polymer region depending on polymer concentration. The solution composition behaves as a viscous liquid when the polymer concentration is low, whereas high enough concentration of the polymer behaves as a solid gel. When the casting solution crosses the cloud point it reaches into a metastable two phase region. As the solution composition approaches to the polymer-non-solvent axis, depletion of more solvent from the solution and increase in the non-solvent concentration in the solution lead the composition of the system to a thermodynamically unstable state by crossing the spinodal boundary. The point at which the cloud point curve and spinodal lines meet is called the critical point. The whole membrane formation process by NIPS is followed by a line in the phase diagram which was shown by Strathmann, Smolders and their co-workers.[46, 48, 49] As shown in **Figure 2.1** the initial composition A advances to the final membrane composition D. Two phases are in equilibrium at composition D- one is the polymer rich phase or solid phase which forms the matrix (S) and the other one is the polymer lean or liquid phase which forms the pores in the membrane (L). The tie lines link the compositions of these two phases. The overall porosity of the membrane is guided by the composition of D on the S-L line. Throughout the entire precipitation process along the path A-D, the solvent is replaced by the precipitant. B represents the composition at the initial precipitation and as more solvent is lost the solution composition at C gets viscous enough to solidify the polymer. The line A-D represents the average composition of the membrane.[46]

As the membrane formation goes on, different layers of the membrane forming solution follow different routes through the phase diagram. In the cast film, the top surface starts to precipitate

first and this precipitated layer acts as a barrier for the further exchange of the solvent and the non-solvent in the cast film. The precipitation rate slows down from top to bottom of the film, as the change of concentration of the non-solvent increases slower in deeper parts of the polymer solution, leading to a weaker thermodynamic driving force for phase separation which leads to larger concentration fluctuation wavelengths. And that is how the pore size increases from top to bottom since increased time duration is provided for phase separation from top to bottom. This phenomenon renders into an asymmetric structure along the thickness of the finally formed membrane.[46] The precipitation rates and path at different layers of a cast film immersed in the precipitation bath is illustrated in **Figure 2.2**.
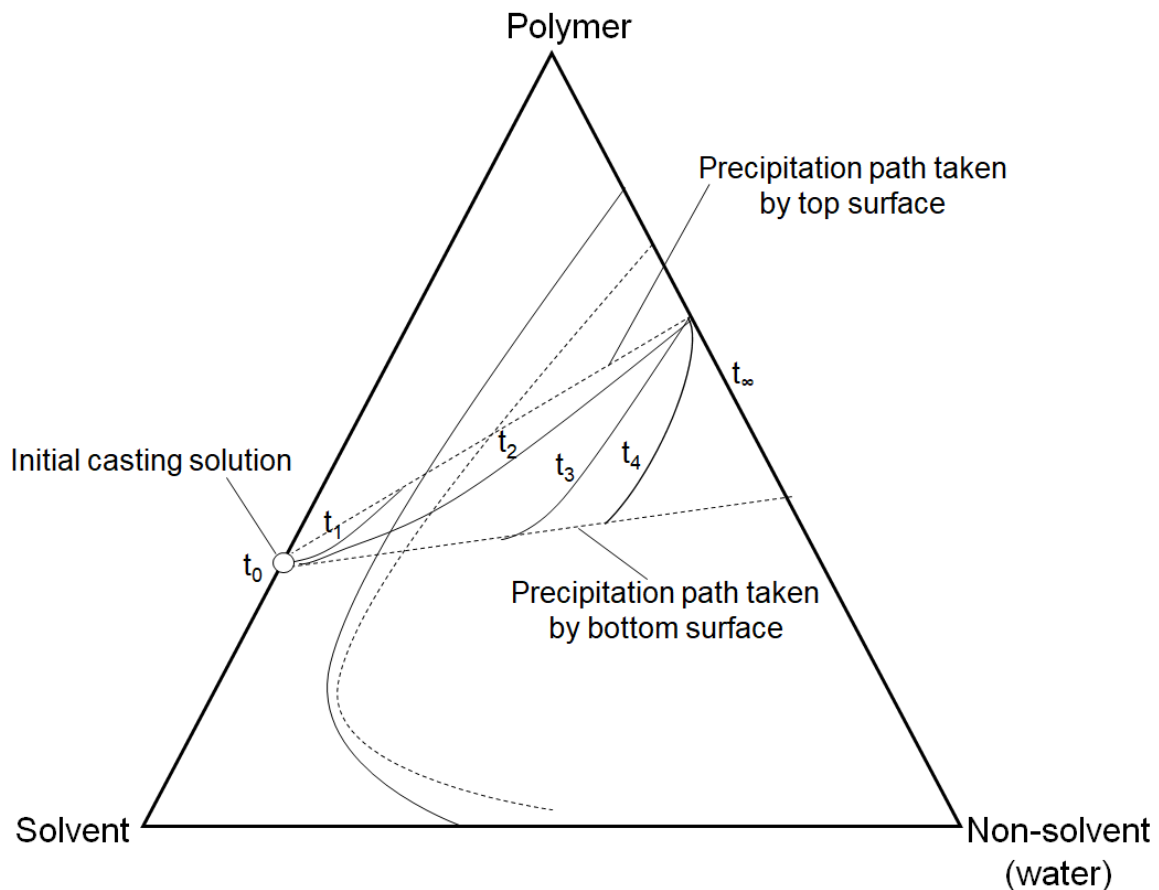
Figure 2.2 Different layers of a phase inversion membrane follow different routes with different time intervals. This figure is adapted from reference [46].

At a definite time interval the solution shows different compositions at different points. As the time proceeds they follow different routes to their final membrane composition. For example, at time t_2 the top surface composition may precipitate completely and reach to the final membrane composition whereas the bottom layer composition may start from the initial membrane forming solution composition and reach at the final membrane composition following a different path after a longer time period. The precipitation path enters from the one phase region to the two-phase region across a point above or below the critical point would define the structure of the membrane as well such as closed cell, open cell, or nodular structure.[46, 50]

The structure of NIPS membranes is governed by the interplay between thermodynamics and kinetics. Thermodynamics regulates the tendency to phase separate and kinetics plays a role determining the diffusion of non-solvent and solvent.[51, 52]

The pores in this type of membranes can be formed by two mechanisms- **i**) nucleation and growth (NG) and **ii**) spinodal decomposition (SD). If the phase separation path moves from stable region to the metastable region during the exchange of solvent and non-solvent NG mechanism predominates. Then a polymer-poor phase is dispersed as droplets in the polymer-rich matrix. The size of the droplets gets bigger with time if no other change is induced like change in the composition of the polymer-poor phase or thermal change in the system. If the phase separation path moves from the stable region directly into the unstable region by crossing over the critical point region then SD mechanism is favored. Concentration fluctuations that start in the initial homogeneous solution grow with increasing amplitude and two continuous phases separate. Whether NG or SD mechanism will predominate in the initial stage is explained by the phase separation theories. However, the point where the developing structure is fixed defines the starting mechanism of the phase separation. As the solvent and non-solvent

exchange proceeds the mobility of the system decreases due to the stronger polymer-polymer contacts and leads to the vitrification of the polymer concentrated phase. If the demixing by NG mechanism stops at the initial stage, then a closed cell structure is favored. At the later stage of NG while growing nuclei merge with each other an interconnected porous structure forms. The interconnected pore structure would be favorable from the beginning if a SD demixing path is followed. Since different starting paths are followed from the top surface to the bottom of the membrane, an asymmetric structure appears throughout the membrane thickness. The membrane structure can be termed as sponge-like structure or finger-like structure with macrovoids. Usually the structure can be altered by bringing changes in the membrane forming system i.e. by changing the composition and/or concentration of the membrane forming solution and the non-solvent.[43]

Since many of the membranes obtained in this work show a finger-like or macrovoid structure, their formation process is described here in brief according to the explanation of McKelvey and Koros.[53] They modeled their assumption by combination of the NG and SD demixing mechanism with a non-solvent moving front. They suggested that if the inward diffusion rate of the non-solvent into the polymer-poor phase is faster than the outward diffusion of the solvent then the formation of macrovoids is favored. The locally generated osmotic pressure drives the intrusion of the non-solvent (usually water) to the polymer-poor nuclei. The wall of the polymer-poor nuclei may rupture if their walls are fragile and will form macrovoids with unskinned walls. If the growing nuclei are in a matrix of high polymer concentration then the growth of mocrovoids can be hindered and a macrovoid free structure will be formed.[43]
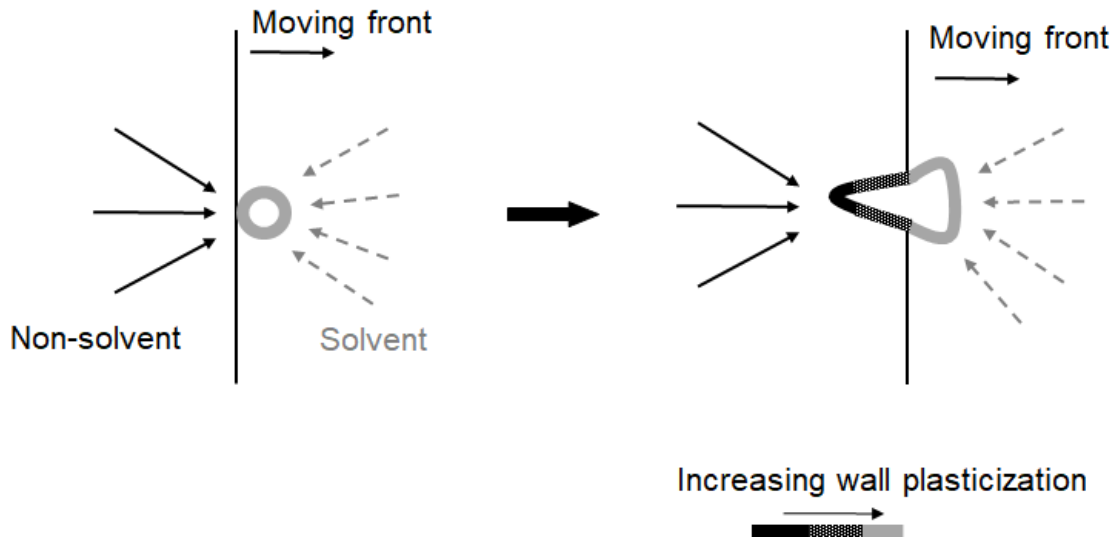
Figure 2.3 Growth of a nucleus during macrovoid formation in a membrane. This figure is adapted from reference [43] and [53].

Several measures are possible to suppress the macrovoid formation, such as- increasing the polymer concentration of the membrane forming solution or adding a solvent which can increase the viscosity of that solution, adding cross linking agents into the solution, adding non-solvent to the membrane forming solution or adding solvent to the precipitation bath to reduce the osmotic pressure between the interior of the nuclei and the non-solvent moving front.[43] In **Figure 2.4** it can be seen that the change in the solvent system shaped the membrane morphology from a finger-like structure to a sponge-like structure.
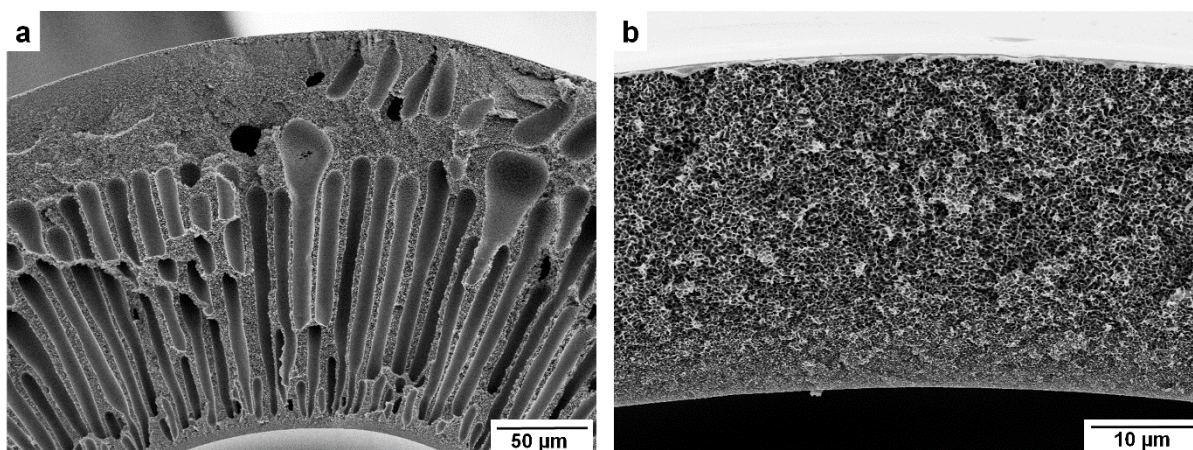
Figure 2.4 Cross sectional morphology of hollow fiber membranes which were spun by using two different solutions of polyetherimide (PEI) (ULTEM® 1000): **(a)** PEI solution in *N*-methyl-2-pyrrolidone (NMP)/γ-butyrolactone (GBL) and **(b)** PEI solution in *N,N*-dimethylformamide (DMF)/tetrahydrofuran (THF).

Some researchers explained the macrovoid formation by other terms, such as the thermodynamic phenomena of chemical potential gradient,[54-58] induced solvent and capillary flow because of the surface instability,[59-66] Marangoni effects,[59, 63] osmotic pressure,[53, 67] etc.

2.3 Block Copolymer

Block copolymers consist of usually covalently linked blocks of polymers that are different in properties. The properties of the block copolymer varies depending on the sequence and topology of the blocks, the incompatibility between the constituent blocks, and the molecular weight of the blocks. One of the fascinating features of these macromolecules is intramolecular phase separation of the blocks. This microphase separation leads to different self-assembled ordered structures in the bulk state which shows typical scattering behavior in small-angle X-ray scattering (SAXS) or in small-angle neutron scattering (SANS).[68-70]

2.3.1 Microphase Separation of Block Copolymer in Bulk

In this PhD work the block copolymer used was a diblock copolymer, polystyrene-*block*-poly(4-vinylpyridine) (PS-*b*-P4VP). So the general discussion about thermodynamics and microphase separation behavior is done for A-B diblock copolymers.

A   **B**

Scheme 2.1 Schamatic representation of a diblock copolymer consisting of A and B repeating units.

In a diblock copolymer a strong repulsion exists between the dissimilar blocks if there are repulsive interactions between the different types of repeating units. The segregation tendency between the blocks cannot result in a macroscopic phase separation because the blocks are linked together by covalent bonds. Instead microphase separation occurs when the blocks are sufficiently incompatible to each other and then microdomains rich in A and microdomains rich in B self-assemble into a crystal-like structure. The characteristic sizes of this spatially confined self-assembled structures range from about 10 to 100 nm which is on the length scale of the constituent blocks. In the case of phase separating polymer blends the incompatible polymers are macroscopolically demixed in the equilibrium which means that the critical concentration fluctuation wavelength is infinite. However, in the case of self-assembled periodic structures of block copolymers in the equilibrium state correspond to a finite length scale of the fluctuation wavelength. The two quantities that characterize the phase equilibria in molten diblock copolymers and influence the characteristic sizes and morphologies of the nanostructures are-

i. The composition *f* (the fraction of A units in the chain), and

ii. The product of χN (where, N is the degree of polymerization and χ is the Flory-Huggins segment-segment interaction parameter between A and B units).[68, 69, 71, 72]

The factors N and f are determined by the polymerization stoichiometry and affect the translational and configurational entropy. Moreover, χ influences the enthalpic contribution which is determined by the selection of the monomers (A and B).

Like all the materials at equilibrium monodisperse diblock copolymer chains arrange in a way that the free energy requirement for that configuration is minimum. Having a large number of N, while increasing the energy parameter χ or decreasing the temperature a local compositional ordering may occur in expense of translational and configurational entropy by minimizing the contact between A and B units. Moreover, a sufficient decrease of either χ or N renders in to a compositionally disordered phase while entropic factor is predominating.[69, 71-73]

χN decides the degree of segregation of A and B blocks. The degree of segregation is dependent on the combined parameter of χN which consists of three regimes: weak (WSL) and strong (SSL) segregation limits and intermediate (ISR) segregation region. For $\chi N \ll 10$ the A-B interaction is very weak and in this disordered state the individual chain statistics are considered as unperturbed or Gaussian. For a symmetric diblock copolymer ($f = 0.5$) at this state the peaks obtained from the scattering measurements correspond to a fluctuation length scale of $D \sim R_g \sim aN^{1/2}$ (where, R_g is the radius of gyration of the copolymer and a is the characteristic segment length). The WSL region covers the minuscule deviations in local composition around the stoichiometric (macroscopic) volume fraction of A (f). According to mean-field theory, this region comprises of the full disordered state and a slight portion of the

ordered region of phase space. In the case of a symmetric diblock copolymer ($f = 0.5$) lamellae form when χN value is greater than 10.5 to around 12. In this limit the microdomain (lamellar) period scales as $D \sim N^{1/2}$. In practice, with the increasing composition profile and increasing χN value a crossover from WSL behavior occurs before the order-disorder transition (ODT). This pretransitioal regime is referred as ISR and the scaling regime is characterized by $D \sim N^{0.8}$. When $\chi N >> 10$, chains are highly stretched and nearly pure A and B microdomains are well developed being separated by well-defined interfaces. In SSL region the system minimizes the total area of interface in expense of the entropic penalty of the extended chain confiormations and here the microdomain period scales as $D \sim aN^{2/3}\chi^{1/6}$. Depending on the composition (f) several ordered microphases were identified for diblock copolymers in the SSL region. **Figure 2.5** shows a theoretical representation of them in a phase diagram.[72-74]

a

b
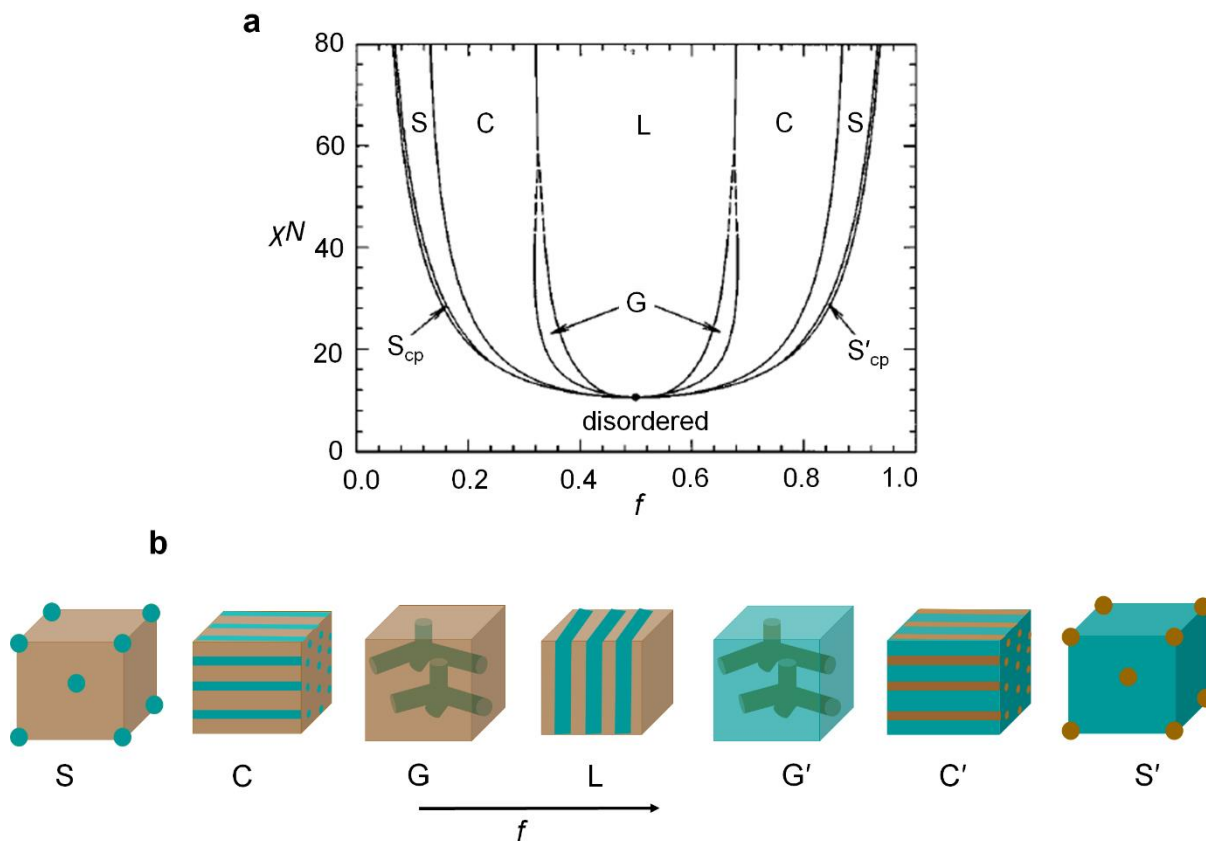
Figure 2.5 (a) Phase diagram for linear A-B diblock copolymers; **(b)** Microphase separated equilibrium morphologies for A-B type diblock copolymer melts. Equilibrium morphologies evolve depending on the composition, f and χN: spherical (S and S′), hexagonylly packed cylinders (C and C′), double gyroid (G and G′), and lamellae (L); (S_{cp} and S'_{cp} in (a) indicate closed packed spheres and are not shown in (b)). This figure is adapted from reference [27].

2.3.2 Block Copolymer Morphologies in Solution

When a block copolymer is dissolved in a solvent which is a selective solvent or thermodynamically good solvent for one of the blocks and a bad solvent or even a precipitant for the other block/s, the copolymer chains arrange in micellar or vesicular aggregates similar to low molecular weight surfactants, but larger in scale. The cores of these micelles are formed by the insoluble blocks which are surrounded by the coronal soluble blocks. The critical concentration at which the first micelle forms is called the critical micelle concentration

(CMC). For some copolymers critical micelle temperature (CMT) is an important value and the micellization of these polymers are favored with increasing temperature by the dehydration of one of the blocks (when water is used as a solvent). These micelles achieve thermodynamic equilibrium with unassociated molecules or unimers above the CMC at a fixed temperature or above the CMT at a fixed concentration.[68, 69, 75]

Generally, micelles are of spherical shapes though depending on the packing of molecules worm-like, rod-like or ellipsoidal micelles can be formed as well. Two kinds of structures can be formed in spherical shapes depending on the composition of the block copolymer and the solvent system, such as[69]

i. Starlike micelle: In this structure the core is small compared to the corona.
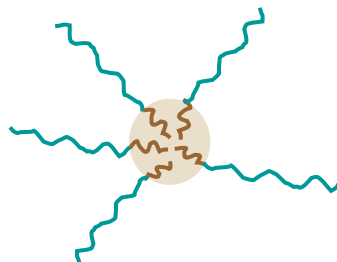
ii. Crew-cut micelle: This type of structure consists of a large core surrounded by highly stretched short chains of corona.
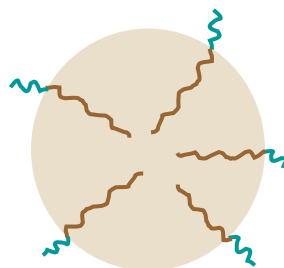
If an amphilphillic block copolymer is dissolved in an organic solvent which is selective to the hydrophobic blocks then reverse micelles form where hydrophilic cores are surrounded by the hydrophobic coronas.[69]

Some terms are frequently used to characterize the micelles, such as[69]-

- Z- the aggregation number, Z defines the process of micellization which is the number of block copolymer chains aggregate into a micelle.

- R_c - the radius of the core.

- R_m - the overall radius of the micelle.
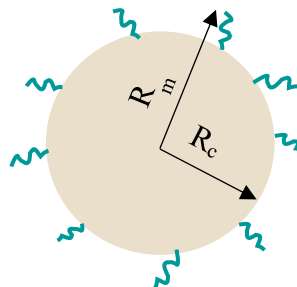
- b – grafting distance i. e. the distance between the neighboring blocks at the interface of the core and corona.

Z, R_c, R_m, b are dependent on the degree of polymerization of the blocks (N_A and N_B) and Flory-Huggins interaction parameter, χ between the segments of the different blocks.

There are other terms associated to define the size of the micelles such as their radius of gyration, R_g and the hydrodynamic radius, R_h.

2.4 Self-assembly of Block Copolymers and NIPS (SNIPS)

The process of membrane formation where the membrane morphology is the result of the self-assembly of block copolymers and the non-solvent induced phase separation (NIPS) mechanism is termed as SNIPS.

Block copolymers may form spherical, cylindrical, or other shapes of micelles in the solution when dissolved in selective solvents. Different parameters influence this micelle formation, such as block copolymer composition and molecular weight, solution concentration, solvent selectivity, etc. The block copolymer self-assembly is driven both by thermodynamic and kinetic factors which lead to the possibility of freezing the structures in a metastable state by

replacing the solvent with a non-solvent and this is the fundamental concept behind formulating a SNIPS membrane.[28, 69]

In the SNIPS process, casting of a concentrated block copolymer solution is followed by an evaporation period for the highly volatile solvent of that solution. The highly viscous block copolymer film is then immersed in a non-solvent or coagulation bath for the exchange of solvent and non-solvent as done in the fabrication of NIPS membranes. The completion of the precipitation in the non-solvent bath is followed by drying of the cast film and an integrally asymmetric membrane is formed with ordered porous structure on its surface which is supported by a highly porous substructure. The first isoporous membrane formation by SNIPS method was reported by Peinemann *et al.* in 2007 and their invention demonstrated for the first time that the integrally asymmetric isoporous membrane formation is possible in the flat sheet geometry by a one step method using block copolymer as a membrane forming material. To introduce the SNIPS membrane they had chosen a polystyrene-*block*-poly(4-vinylpyridine) (PS-*b*-P4VP) with molecular weight of 191 kg mol^{-1} where the P4VP content was of 15 wt.%. The pore density on the surface of their reported membrane was 240×10^{12} pores per m^2 with an average pore diameter of 15 nm and an average cylinder length of 250 nm. This membrane showed water flux of 20 L m^{-2} h^{-1} at a pressure of 0.5 bar. This distinguished work paved the way to a new research dimension in the field of membrane science.[28]

In this PhD work, the block copolymer used for the SNIPS membrane formation is also PS-*b*-P4VP. So the theory explained below is constrained to the SNIPS membrane formation method by PS-*b*-P4VP.

PS-*b*-P4VP is a nonionic amphiphilic block copolymer where its constituent blocks have a high segmental interaction parameter and so are strongly segregated in the bulk state and the bulk

state morphology is controlled by the volume or weight ratio of the blocks. Since for membrane application the perpendicularly aligned cylindrical morphology is of most interest the compositions of this block copolymer are chosen with the volume fraction of P4VP from 0.12 to 0.31.[28, 76]
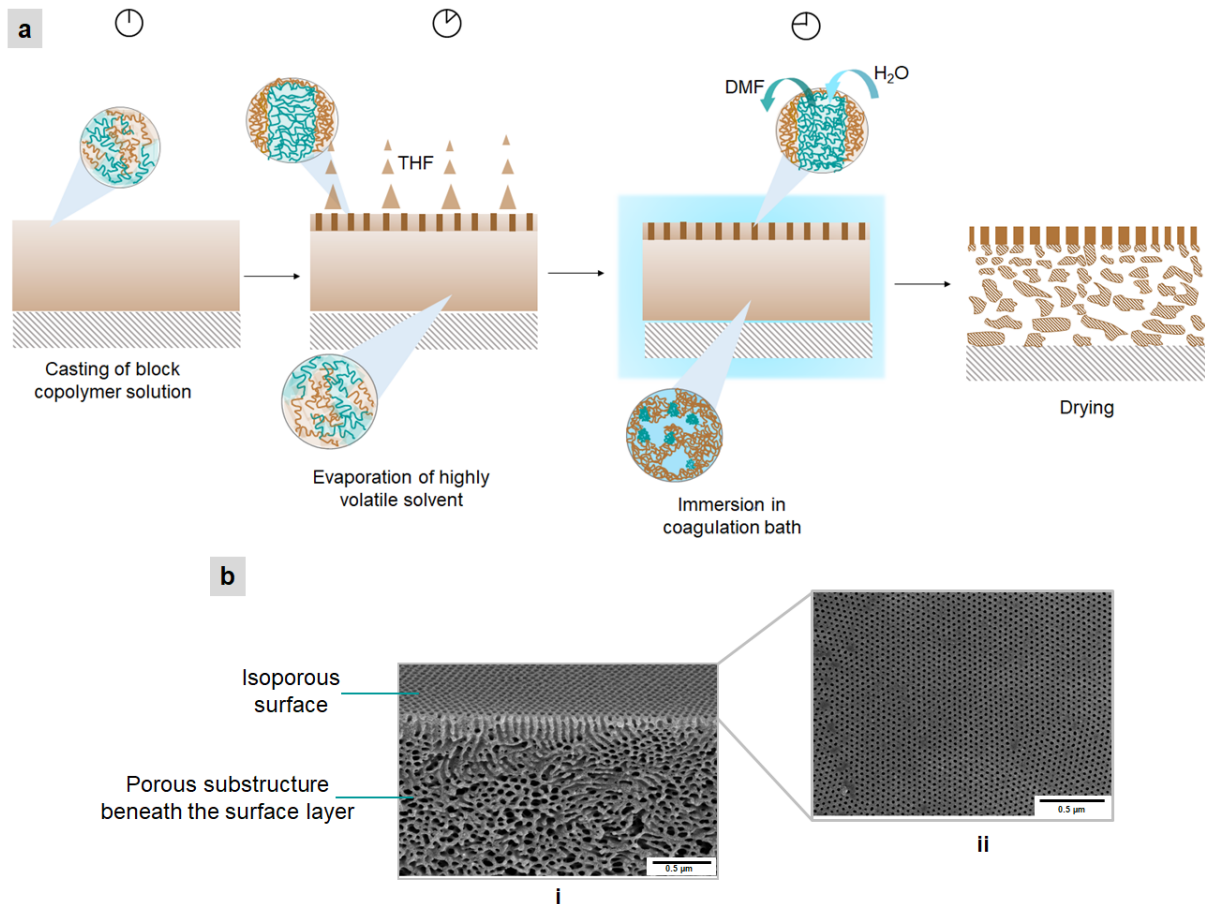
Figure 2.6 (a) Integral asymmetric isoporous membrane formation by the SNIPS method: casting of the block copolymer solution, allowing time for evaporation of the volatile solvent from the surface of the cast film, plunging of the cast film in the precipitation or water bath, and then drying of the membrane; **(b)** Scanning electron mocroscopy (SEM) image of an integral asymmetric isoporous membrane made of $PS_{77.6}$-b-$P4VP_{22.4}^{98}$ following SNIPS (subscripts and superscript denote the weight percentage of the respective blocks and the total molecular weight of the block copolymer in kg/mol, respectively); **i.** cross section of the membrane, **ii.** top surface of the membrane.

Figure 2.6 demonstrates the formation steps in a SNIPS membrane. **Figure 2.6b** represents a typical morphology of a PS-*b*-P4VP SNIPS membrane. The top layer of the membrane exhibits ordered cylindrical pores that are perpendicularly aligned to the surface. This ordered morphology is followed by a typical porous structure of a NIPS membrane underneath.

The solvent system chosen in this work to dissolve PS-*b*-P4VP is a mixture of *N,N*-dimethylformamide (DMF) and tetrahydrofuran (THF). THF is a selective solvent for PS blocks while the hydrophilic P4VP blocks dissolve better in DMF. After casting the homogeneous solution of PS-*b*-P4VP, the cast film is rested for evaporation of the volatile solvent (THF) for a period of time. The evaporation of the solvent from the surface develops a concentration gradient between the surface near air (cast film and air interface) and the bottom of the cast film. With the increasing concentration at the surface the block copolymer starts to microphase separate as the solvent evaporates and the cylindrical domains continues to grow from the surface to the still swollen layer under the surface. After immersing the highly swollen cast film in the non-solvent (water), solvent in the P4VP domains exchanges with water sooner than the solvent selective to PS since the swollen P4VP has higher compatibility with water and thus the hollow channels are formed. Moreover, the solvent from the matrix forming blocks (PS) diffuses to these channels preferentially since they occupy higher interfacial area and so the solvent-non-solvent exchange is favored. Meanwhile, the layers underneath the ordered porous layer form a sponge-like structure by the solvent and non-solvent exchange following the similar mechanism of NIPS membrane formation. SNIPS is governed by directing a microphase separating block copolymer solution into a non-solvent which is miscible with the solvent/s of the block copolymer solution and makes possible the membrane formation by the NIPS method. By this method an integral asymmetric phase inversion membrane is formed

where the selective surface is adorned by the ordered assembly of cylindrical pores which are of similar sizes.[28]

The SNIPS membrane formation mechanism is well described by the work of Phillip *et al.*[77] According to that work, the microphase separation is induced at the surface of the cast film by the evaporation of solvent and is guided to the bottom of the film. The extent to which the microphase separation proceeds is dependent on the block copolymer concentration gradient and solvent composition gradient created by the evaporation of the solvent from the surface. The variation in the compositions brings changes in the viscosity of the polymer chains and the screening effect due to the presence of solvent molecules changes effective incompatibility among the different polymer segments.[29] Since the chain relaxation (related to the viscosity of the polymer chains) and effective segmental incompatibility are not proportionally related to the composition, the ordered microphase separating domains do not grow through the full thickness of the film. The length of the ordered growth of the microdomains is limited to a few hundred nanometer from the surface and thus a random microphase separated structure is formed below the ordered cylindrical pores.[29, 77]

There have been several studies carried out on the SNIPS membrane forming block copolymer solutions. Though some studies claim that block copolymer micelles form a self-assembled ordered structure in the solution, some other studies have proven that there is no structure formation prior to casting[35] and this claim was reinforced by the explanation by Abetz.[29] The structure formation mechanism on the surface of the SNIPS membrane is described briefly in light of the previous illustration by Abetz (**Figure 2.7**).[29]
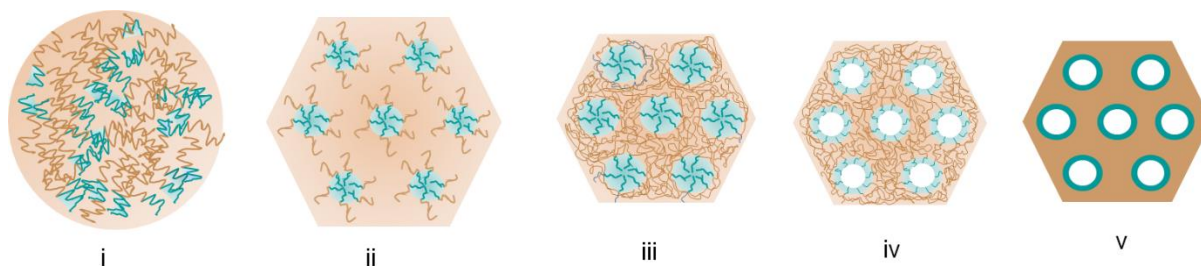
Figure 2.7 Isoporous structure evolution of a membrane from the solution: **i.** Disordered or weakly segregated diblock copolymer in mixed selective solvents (⌇ polystyrene rich domains, ⌇ poly(4-vinylpyridine) rich domains); **ii.** Microphase separation with polystyrene rich matrix after film casting; **iii.** Solidification of the matrix due to solvent evaporation; **iv.** Open pores in the poly(4-vinylpyridine) rich domains after non-solvent induced phase separation; **v.** Porous structure of dried membrane. This figure is adapted from reference [29].

From SAXS it was seen that the PS-*b*-P4VP block copolymer solutions that led to membranes with a hexagonally ordered isoporous structure were initially in the disordered or weakly segregated states. If the concentration of the casting solution was high enough to present an ordered structure in the solution then the isoporous cylindrical morphology was missing on the final membrane surface.[29, 35, 78]

In the mixture of solvents (DMF and THF) or, only in one solvent (DMF) the shorter blocks P4VP form the core of the micelle in the casting solution. This phenomenon was proved by cryo-scanning and cryo-transmission electron microscopy, and small angle neutron scattering (SANS) in previous works.[29, 79] After evaporation of the more volatile solvent THF, the matrix forming PS region shrinks and the still swollen P4VP spheres get connected and arrange into cylinders. After plunging into the non-solvent (water), this cylindrical morphology is preserved while P4VP chains collapse. And that is how the open porous structure is formed on the membrane surface.

Control over the self-assembly of the block polymer and the phase separation of the substructure tailors the porosity and the selectivity of these membranes.[80] The structure formation by the SNIPS method is dependent on several parameters such as- composition and molecular weight of the block copolymer, concentration of the casting solution, choice of solvents, composition of the solvents in the solution, evaporation time, nature of the coagulation bath etc. Only a suitable combination of all these parameters results in hexagonally ordered cylindrical pores on the surface of a membrane prepared by the SNIPS method.[28, 30]

Chapter 3

Materials and Methods

3.1 Materials and Reagents

For synthesis of PS-*b*-P4VP, tetrahydrofuran (THF) was received from Th. Geyer, Germany. Styrene was procured from Sigma-Aldrich, Netherlands. 4-vinyl pyridine (4VP) was purchased from Sigma-Aldrich, United Kingdom and *sec*-butyllithium (*sec*-BuLi) was purchased from Sigma-Aldrich, Germany. Ethylaluminium dichloride (1M in hexane) was procured from Sigma-Aldrich, USA. Dibutylmagnesium ($MgBu_2$) was purchased from Sigma-Aldrich, USA, calcium hydride (CaH_2) was purchased from Sigma-Aldrich, Germany.

Polyetherimide (PEI) (ULTEM® 1000) was purchased from General Electric Company, USA, Polyethersulfone (PESU) (Ultrason® E6020P), sulfonated polyphenylenesulfone with a sulfonation degree of around 5 mol % and 8.4 mol % (referred to as sPPSU5 and sPPSU8.4, respectively) were received from BASF, Ludwigshafen, Germany. Polyvinylidenefluoride (PVDF) (Kynar Flex®) was purchased from ARKEMA. Chlorosulfonic acid ($ClSO_3H$) (99%), poly(sodium 4-styrene sulfonate) (PSSNa) (Mw ~70,000, powder), and glycerol (anhydrous ≥99%) were purchased from Sigma-Aldrich, St. Louis, USA. *N*-methyl-2-pyrrolidone (NMP), Dichloromethane (DCM), *N,N*-dimethylformamide (DMF), tetrahydrofuran (THF), dimethyl acetamide (DMAc), γ-butyrolactone (GBL), ethylene glycol (EG) (62.07 g/mol), and poly(ethylene glycol) (PEG200) were purchased from Merck, Germany. Sodium lauryl sulfate (SDS) was procured from Carl Roth GmbH + Co. KG, Karlsruhe, Germany. Polyvinylpyrrolidone (PVP K15 Mw 10,000) was procured from Fluka, Buchs, Switzerland. Water with pH values of 2 and 11 were prepared by using Titrisol buffer concentrate which was purchased from Merck, Darmstadt, Germany. α-cyclodextrine ($C_{36}H_6O_{30}.xH_2O$) was bought from Alfa Aesar, Germany. 1,4-dioxane (anhydrous 99.8%) and poly(ethylene glycol) (PEG400) was purchased from Sigma Aldrich, Germany.

Cellulose acetate (CA 398-30 Eastman) was purchased from Eastman, USA. Styro Clear® GH 62, a star block copolymer of polystyrene-*b*-polybutadiene-*b*-polystyrene (PS-*b*-PB-*b*-PS) (StyroClear® GH 62) was procured from BASF, Ludwigshafen, Germany.

3.2 Synthesis

3.2.1 Synthesis of PS-*b*-P4VP

PS-*b*-P4VP block copolymer was synthesized by sequential anionic polymerization by following the standard method described in the references.[30, 81, 82] The block copolymers were synthesized at the department of Polymer Synthesis, Helmholtz-Zentrum Geesthacht, Germany and then were supplied for this work.[30, 81, 82]
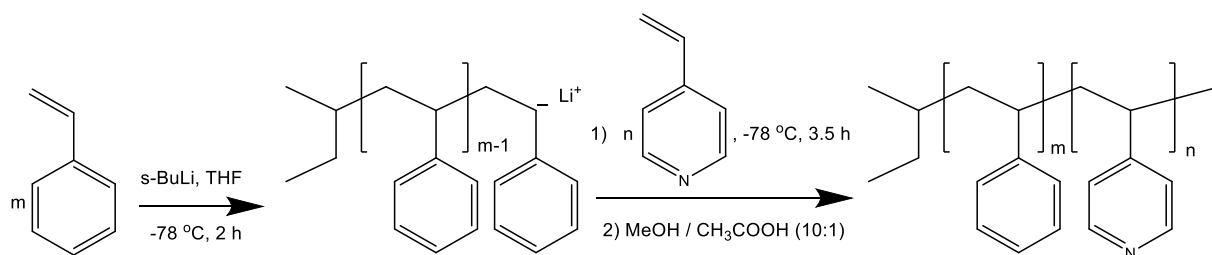
Scheme 3.1 Synthesis of PS-*b*-P4VP

Molecular weight of the precursors (PS) was determined by using gel permeation chromatography (GPC) (Waters 2410 refractive index detector) at 50 °C which was calibrated against polystyrene standards using DMAc as solvent. The compositions of the block copolymers (PS-*b*-P4VP) were determined by ^{1}H NMR spectroscopy. ^{1}H NMR spectra were recorded on a Bruker advance 300 NMR spectrometer at 300 MHz where tetramethylsilane (TMS) was used as internal standard and deuterated chloroform (CDCl$_3$) as solvent. Molecular weight of the block copolymers (PS-*b*-P4VP) was then calculated by the molecular weight of

PS and the compositions of PS and P4VP in the block copolymers determined by ^{1}H NMR spectra. Polydispersity of PS-*b*-P4VP was determined by GPC (Waters 2410 refractive index detector) at 50 ^{o}C using polystyrene as standard and DMAc as solvent.[30] The block copolymers (PS-*b*-P4VP) used in this work had polydispersity index of near 1.1.

3.2.2 Sulfonation of PESU

Polyethersulfone (PESU)[*] (Ultrason® E6020P) was sulfonated by following a procedure previously described in the literature.[83] For this reaction, dichloromethane (DCM) and 99% chlorosulfonic acid (ClSO$_3$H) were chosen as a solvent and as a sulfonating agent, respectively. PESU was dissolved in DCM in a three-neck round bottom flask and was stirred to have a homogeneous solution. Then ClSO$_3$H was added drop wise while stirring continued. Nitrogen (N$_2$) gas was purged in the reaction medium while acid was added. The amount of the sulfonating agent and the reaction time was controlled to maintain the degree of sulfonation (DS) at around 10%. After the completion of the reaction the solution was transferred into a separatory funnel and held there for 10 minutes. After that the lower solution was precipitated into ice water while stirring. The precipitate was filtered, washed off several times, and dried under air flow. The characterization spectrum and calculation to determine the DS of this polymer is shown later in **Chapter 8**. The resulting polymer is termed as sPESU10[*] in this study.[1]

Polyethersulfone (PESU)   Sulfonated polyethersulfone (sPESU)
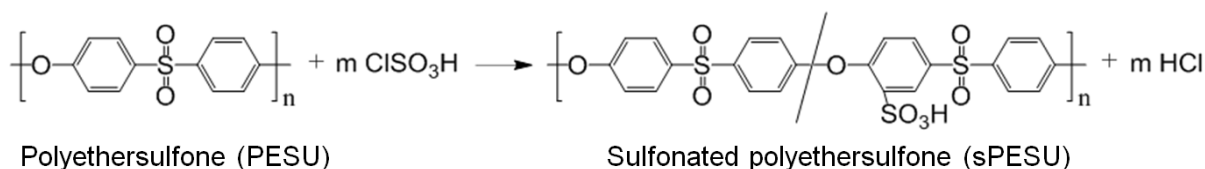
Scheme 3.2 Sulfonation of PESU

3.3 Membrane Fabrication Methods

3.3.1 Flat Sheet Membrane Casting

Hand casting
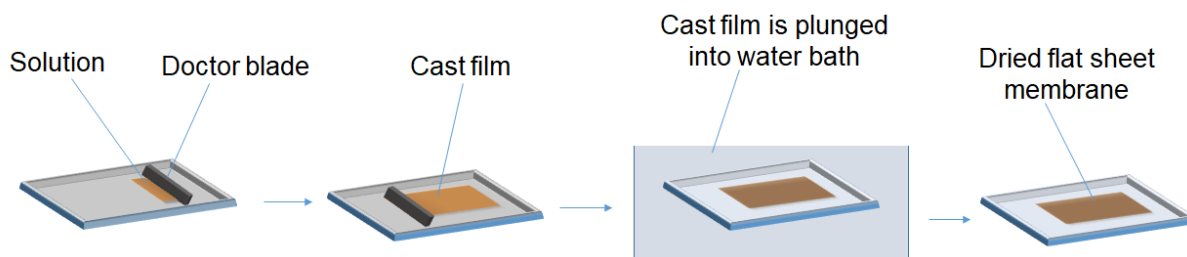
Figure 3.1 Casting of flat sheet membrane by doctor blade

Different block copolymers (PS-*b*-P4VP) were dissolved in the mixture of DMF and THF to prepare solutions of different concentrations and compositions. Flat sheet membranes were cast on non-woven support by using a doctor blade with a gap height of 200 µm. The cast films were allowed for a definite time period in air for evaporation of the solvent and then were immersed into the coagulation bath (water bath). After completion of the precipitation the membranes were dried in air or under vacuum at 40 ºC.

Machine casting

For machine casting an automated casting machine was used which was equipped with a doctor blade. The gap height for membrane casting was adjusted according to the requirements.
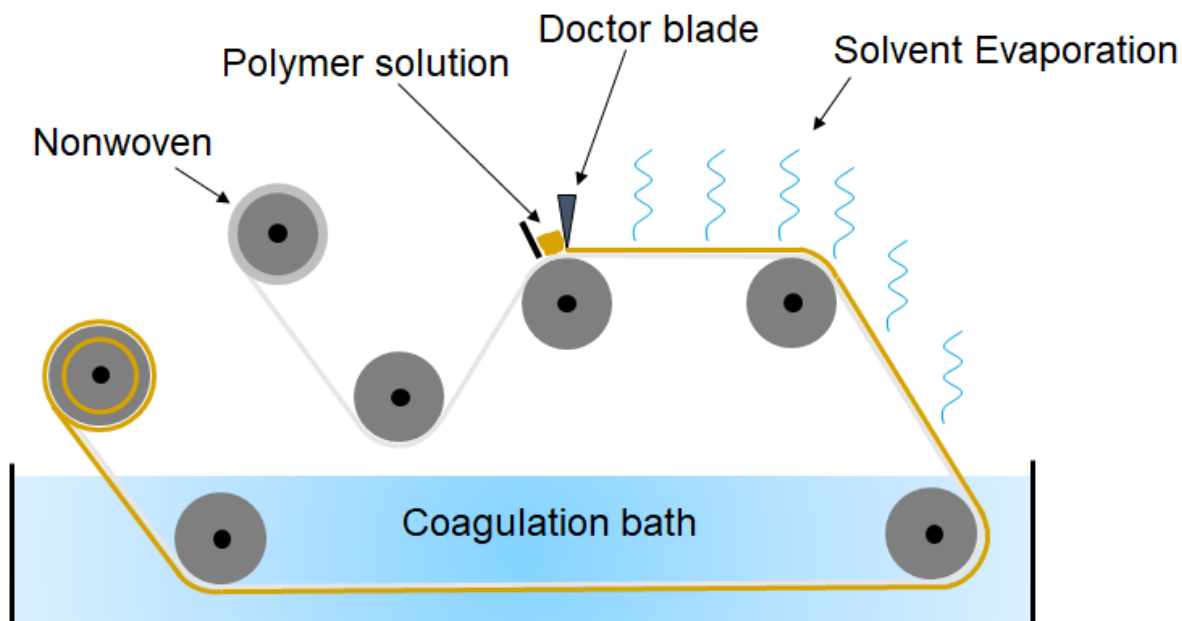
Figure 3.2 Flat sheet membrane casting by in-house built machine

3.3.2 Fabrication of Hollow Fiber Membranes

Polymer or polymers was/were dissolved in a solvent or in a mixture of solvent and additive to prepare the spinning dopes. Polymer solutions were stirred in sealed glass bottles overnight (where needed heat was applied during stirring). After complete dissolution, the solutions were left overnight without agitation to remove air bubbles. Water or water/solvent or water/additive mixture was used as a bore fluid. The water/solvent or water/additive mixture was prepared by stirring the components in capped bottles. The designated containers for polymer solutions and bore fluid were filled with the respective solutions, and then the solution/solutions and the bore fluid were pumped simultaneously to the designated orifices of the spinneret by using a gear or an infusion pump. In case of using the gear pump, the flow rates were determined in weight of the solution coming out of the pump in a minute, i.e., g/min. In case of using the infusion pump, the flow rates were determined in volume of the solution pressed through the orifice in one minute i.e., mL/min.[2]

The hollow fibers were spun by the dry-jet wet spinning method. The dope solution was extruded through the double orifice spinneret together with the bore fluid in case of single layer hollow fiber spinning.[2] In case of co-extrusion the dope solutions were extruded through the triple[1] or quadruple[3] orifice spinneret together with the bore fluid. The spun fibers entered into the coagulation bath (water) after experiencing a definite air gap distance (L_{Air}) where the solid hollow fibers formed by non-solvent induced phase separation (NIPS) (**Figure 3.3**). The schematic representation of the hollow fiber spinning method chosen (single layer, double layer, or multiple layer extrusion) and the dimensions of the spinnerets are presented in the respective Results and Discussion Chapters.
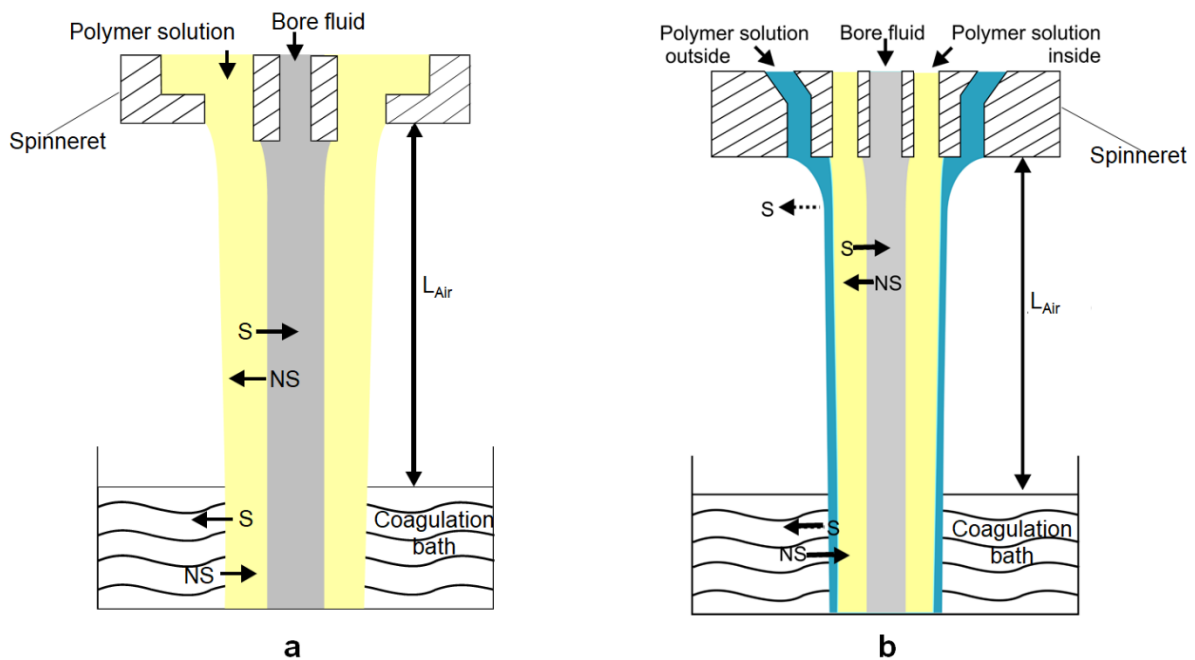
Figure 3.3 Hollow fiber spinning by dry-jet wet spinning method: **(a)** Single layer hollow fiber fabrication using a double orifice spinneret; **(b)** Double layer hollow fiber fabrication using a triple orifice spinneret. Solvent (S) and non-solvent (NS) exchange starts at the lumen side of the nascent fiber as soon as the bore fluid and the polymer solution meet at the exit of the spinneret. If volatile solvent is used in the polymer solution then phase separation is induced from the outer surface of the fiber due to evaporation of the solvent in the air gap distance

(L_{Air}). After passing L_{Air} fiber enters into the coagulation bath where solvent (S) and non-solvent (NS) exchange completes and after drying the hollow fiber membrane is obtained.

The flow behavior of the spinning solution is related to the spinneret design along with the solution properties. One of the flow instabilities or extrudate instabilities can be minimized or eliminated by considering the following factors: design of the spinneret, rheological behavior of the spinning solution and the flow rate of the solution through the channels of the spinneret, spinning temperature, air-gap distance, take-up speed.[50, 84] In all the experiments hollow fibers were spun at ambient temperature and humidity if not mentioned otherwise. The spinning was free falling means that no take-up roll was used.

3.3.2.1 Spinneret for hollow fiber spinning

Spinneret design is the first most important issue to be considered for hollow fiber spinning. Generally the spinnerets carry annular channels which have high annulus length to flow gap ratio to ensure the flow stability of the polymer solution/s. While being passed through the spinneret various stresses act upon the polymer solution influencing the macromolecular orientation and packing. Moreover, the molecular relaxation time and die swell are determined by the rheological properties of the polymeric solution after exiting from the spinneret.[50] Generally linear polymers have shorter relaxation times compared to the branched polymers since the motion is not hindered at the branch points. To reduce the flow instability caused by the very long relaxation time with the branched polymers, a modified spinneret design is necessary.[84, 85]

In all the experiments for this work, linear polymers were used so the spinnerets with straight channel design (near the exit of the spinneret) were chosen whether single, double, or multiple layer hollow fibers were spun. The polymeric solutions show non-Newtonian behavior and the highest shear stress acts along the die wall of the spinneret. Therefore different die gaps have

an influence on the stress on the solution inside the spinneret channels. Moreover, the choice of any kind of modified designed spinnerets was avoided for the experiments since the other parameters (spinning parameters, solution compositions) provide a better insight towards the aimed target of this work.

The type of spinnerets used in this study for single and double layer hollow fiber spinning is schematically shown in **Figure 3.4.**
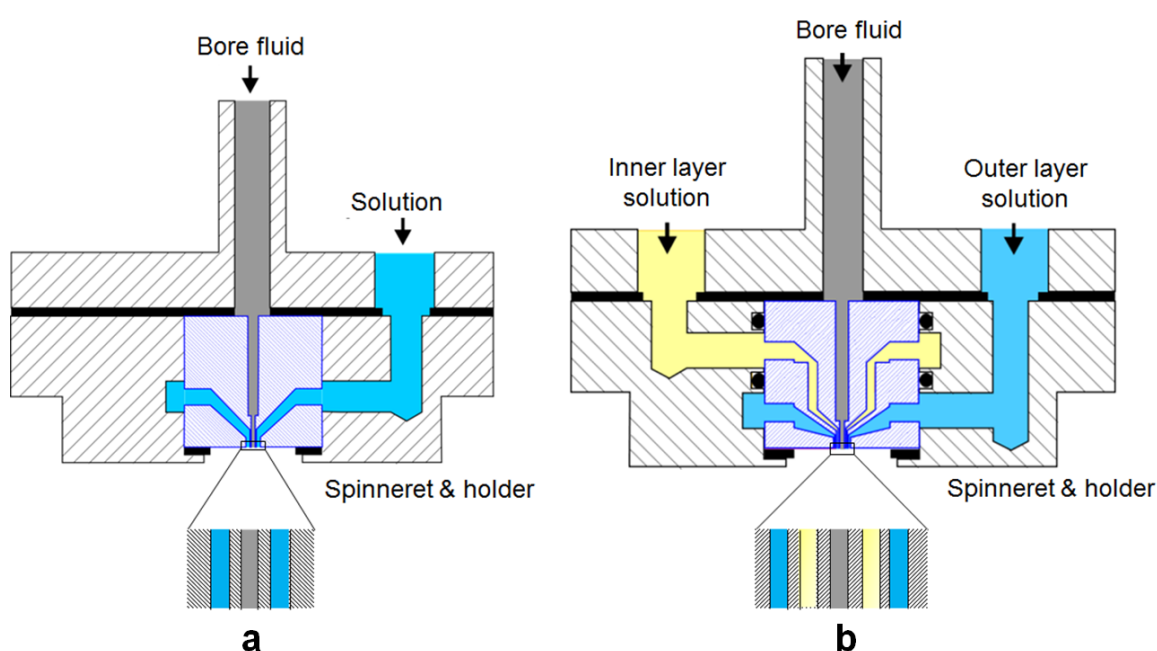
Figure 3.4 (a) Double orifice spinneret (for single layer hollow fiber spinning) and **(b)** triple orifice spinneret (for double layer hollow fiber spinning) with straight channel design near the exit of the spinnerets.

3.4 Characterization Techniques

3.4.1 Nuclear Magnetic Resonance Spectroscopy (NMR)

The polymers and hollow fibers were characterized by ^{1}H NMR spectroscopy using a Bruker AV-300 MHz spectrometer and a Bruker Avance III HD 500 MHz NMR spectrometer (Ettlingen, Germany). In every experiment tetramethylsilane (TMS) was used as an internal

standard. Deuterated dimethyl sulfoxide (d$_6$-DMSO) as a solvent to dissolve all the samples but PS-*b*-P4VP in 5 mm O.D. sample tubes. Deuterated chloroform (CDCl$_3$) was used as a solvent to dissolve PS-*b*-P4VP samples.[1, 2]

3.4.2 Thermogravimetric Analysis (TGA)

A NETZSCH TG 209F1 Iris (Selb, Germany) was used for thermo-gravimetric analysis (TGA) of the polymers and hollow fibers. The analysis was done with a ramp of 10 $^\circ$C/min at a temperature ranging from 30 $^\circ$C to 800 $^\circ$C. The experiments were done in Ar atmosphere at a flow rate of 20 mL/min.[2]

3.4.3 Differential Scanning Calorimetry (DSC)

The glass transition temperature (T$_g$) of the polymers were measured by differential scanning calorimetry (DSC) DSC1 (Star system) from Mettler Toledo in a temperature range of 30 $^\circ$C to 300 $^\circ$C at 10 $^\circ$C/min while purging N$_2$ gas stream (Flow 60 mL/min), then quenched to 30 $^\circ$C and temperature was increased over the same range in the same rate in the second run. The T$_g$ of the polymers were determined from the second heating scan. To study the spinning solutions, solutions were prepared as of the spinning dope with the same composition and concentration. Then the samples were prepared by precipitating the solutions in water followed by drying.

3.4.4 Rheological experiments

A rotational rheometer (MCR 502, Anton Paar, Graz, Austria) with a cone-plate geometry (plate diameter of 25 mm and cone angle 2°) was used for the rheological characterization of the solutions. The experiments were performed in a nitrogen environment and at the temperature of 25 $^\circ$C.

3.4.5 Scanning Electron Microscopy (SEM)

The morphology of the hollow fibers (cross-section and the inner surface of the hollow fibers) were characterized by scanning electron microscopy Leo Gemini 1550VP (Zeiss, Oberkochen, Germany) at a voltage of 3–6 kV. Cross-sections of the hollow fibers were prepared by breaking them in cryogenic condition. The hollow fibers were cut longitudinally to examine their inner surfaces. All of the samples for analysis were coated with approximately 2 nm of Pt using a coating device Bal-tec MED 020 (Bal-tec/Leica Microsystems GmbH, Wetzlar, Germany).[1, 2]

3.4.6 Elemental Analysis by Energy Dispersive Microanalysis (EDS)

For elemental analysis the double layer hollow fiber was placed in a mold and embedded in epoxy resin. After hardening, the cross section of the double layer hollow fiber was prepared by microtomy using a Leica Cryo-Ultramicrotome EM UCT FCS equipped with a diamond knife. Afterwards the hollow fiber was analyzed by secondary electron (SE) and energy disperse X-rays with a Zeiss "Merlin" scanning electron microscope equipped with an energy dispersive microanalysis (EDS) system (Oxford).[1]

3.4.7 Transmission Electron Microscopy (TEM)

Transmission electron microscopy investigation was performed using a FEI Tecnai G^2 F20 (Thermo Fisher Scientific, Eindhoven, The Netherlands) that was operated at 120 kV in bright-field mode. The hollow fibers were embedded in epoxy resin and cut into ultrathin sections of approximately 50 nm using a Leica ultramicrotome EM UCT (Leica Microsystems, Wetzlar, Germany) equipped with a diamond knife (Diatome AG, Biel, Switzerland).

3.4.8 X-ray Photoelectron Spectroscopy (XPS)

For analyzing the chemical composition of the inner or lumen side surface of the hollow fibers, XPS was carried out by using a Kratos AXIS Ultra DLD spectrometer (Kratos, Manchester, United Kingdom) with an Al-Kα X-ray source (monochromator) operated at 225 W and at vacuum of $< 2.5 \times 10^{-9}$ Torr. After degassing in the ultra-high vacuum (UHV) pre-load chamber, the hollow fibers were positioned in the UHV analytics chamber. The analyzed area was 700 µm x 300 µm. The acceleration depth was approximately 5 nm. For the scanned region the pass-energy was set to 20 eV while for survey spectra a pass-energy of 160 eV was used. All of the spectra were calibrated to 284.5 eV binding energy of the C1s signal. For all the samples charge neutralization was necessary. The evaluation and validation of the data were carried out with the software CASA-XPS version 2.3.18. For deconvolution of the region files, background subtraction (linear or Shirley) was performed before calculation.[2]

3.4.9 Surface Tension Measurement

The surface tension of the solutions, solvents, and glycerol were measured with the force tensiometer K100 from Krüss by Wilhelmy plate method. Measurements were carried out until fluctuation was within ± 0.1 mNm^{-1} for the last two readings and each sample was measured for three times.[3]

3.4.10 Pore Size Distribution

Pore size distribution of the surface of the film forming layer was determined by IMS V15Q4 (Imagic Bildverarbeitung AG, Glattbrugg, Switzerland).[3]

3.4.11 Water Flux Measurement

After spinning the hollow fibers were kept in clean water for two days to remove the residual solvents and additives. After that, the water flux was measured in dead-end mode by using an in-house built automatic testing device. For water flux measurements, one hollow fiber with an effective length of 20 cm was fitted into a module for each measurement. Deionized water was fed from the lumen side of the hollow fiber, and permeate flow was received from the shell side of the hollow fiber. During the measurement, the transmembrane pressure was kept at around 1 bar. The pressure normalized permeance (P) was calculated by the following equation:

$$P = \frac{V}{\Delta p.t.A}$$

where, P is the pressure normalized permeation flux (termed as water flux in the following discussion) in L m^{-2} h^{-1} bar^{-1} of the pure water from the hollow fiber, V is the volume of water in L, Δp is transmembrane pressure across the wall thickness of the hollow fiber in bar, A is the effective area of the inner surface of the hollow fiber in m^2, and t is the measurement time in hour.[2]

3.4.12 LASER Micrometer

The dimension of the hollow fibers during the spinning process were detected by a LASER micrometer (LASER-SCANNER from Zumbach (ODAC 16J). It was mounted near the spinning line so that the beam could cross the nascent hollow fiber in a direction perpendicular to the fiber axis.

Chapter 4

Results and Discussion

Hollow Fiber Spinning- some general phenomena

4.1 Why does Hollow Fiber Membrane Formation Differ from Flat Sheet Membrane Formation?

Hollow fiber membrane formation from the same solution differs from the flat membrane formation since several additional phenomena play a role in hollow fiber spinning, such as- the shear rate or stress may change the phase separation behavior by creating phase instability, external elongational stress occurs in the spinning process may induce the chain packing and/or alter the diffusion of coagulant and the radial outflow of the spinning solvent. All these factors may lead to a different morphology in the hollow fiber membranes in comparison to their flat sheet counterparts.[67, 86-90]

Molecular orientation is induced by different stresses during the hollow fiber spinning process. When a polymer solution is pumped through the concentric annulus of the spinneret shear stress develops within the annulus and this stress is the highest at the walls of the spinneret. Shear stress induces molecular orientation which plays a role in the final fiber morphology and in turn plays an important role in the permeation and separation behavior of the hollow fiber membranes. So, optimization of the shear rate is one of the parameters which plays a role in optimizing the performance of the hollow fiber membrane. If there is an air gap (L_{Air}) between the spinneret and the coagulation bath then the macromolecules experience die swelling and relaxation after exiting from the orifice of the spinneret and thus the shear induced orientation inside the spinneret is changed. Molecular orientation may induce again due to the elongational stress outside of the spinneret due to gravity. In case of the higher draw ratio the molecular orientation is favored due to the enhanced spin line stress. The influence of the acting stresses before the solidification of the nascent hollow fiber by the inner (bore fluid) and outer

47

(coagulation bath) coagulants affect the morphology of the hollow fibers, especially the surfaces and also the performance.[90-96]
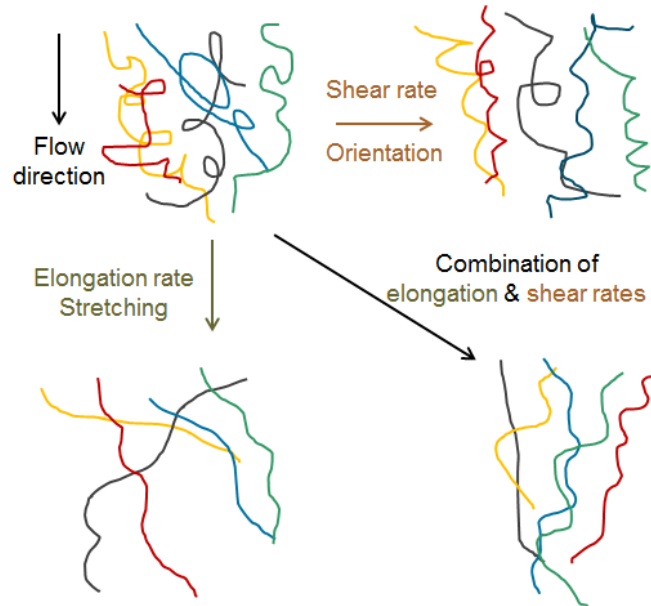
Figure 4.1 Hypothetical representation of the effect on the polymer chains due to elongation and shear rate. The illustration is inspired by the reference [96].

During the spinning of hollow fiber membranes by dry-jet wet spinning the precipitation starts from the lumen side of the nascent hollow fiber by the bore fluid which is a non-solvent for the membrane forming solution and then from the shell side in the coagulation bath. The interplay of the thermodynamics and kinetics of the precipitants (bore fluid and coagulation bath) depends on their composition.[91, 97, 98] Moreover, along the spin line the behavior of the non-Newtonian viscoelastic fluid (spinning solution) differentiates the processing of hollow fibers from that of flat sheet membranes.[50]

In short, the structure of the hollow fiber is dependent on several factors, such as[91, 97, 98]-

- Factors related to spinning solution- type of polymer, solvent, non-solvent, composition of the spinning solution and the coagulants, temperature of the spinning solution and the coagulants.

- Factors related to coagulation- air gap distance, temperature, relative humidity in the air gap, exchange of solvent and non-solvent at the inner and outer surfaces of the nascent hollow fiber.

- Spinneret design.

- Processing parameters: drawing speed, spinning speed, air gap distance, and etc.

4.2 Characterization of the *in-situ* Hollow Fiber

In the following, experimental results show the effect of two of the processing parameters on the hollow fiber (HF) dimension. A LASER micrometer (LASER-SCANNER from Zumbach (ODAC 16J) (**Figure 4.2**) is mounted near the spinning line to measure the dimension of the *in-situ* hollow fibers.
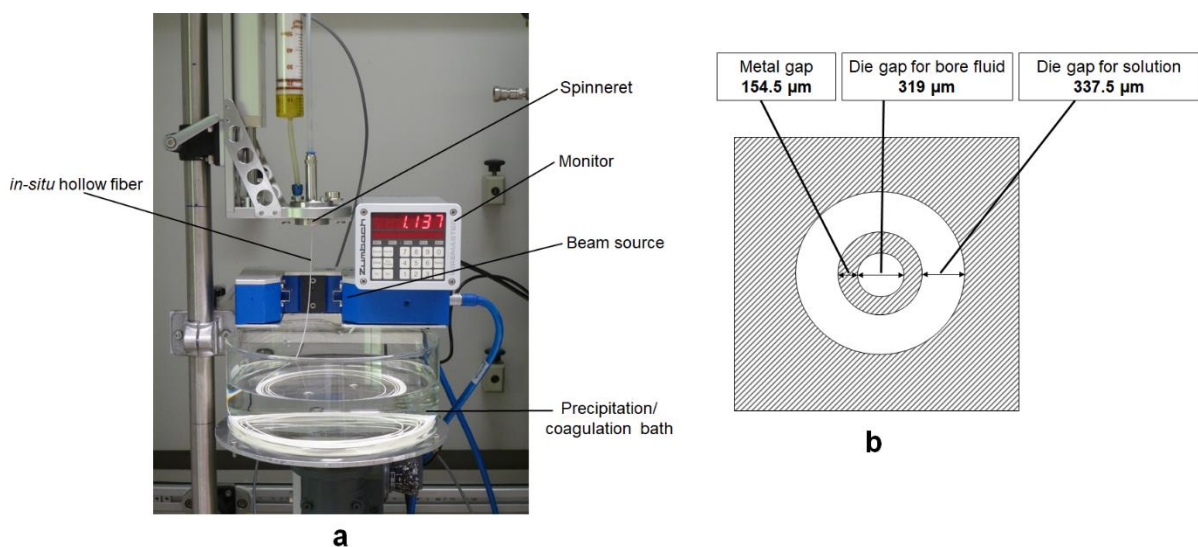
Figure 4.2 Diameter measurement of the hollow fiber during spinning by LASER micrometer:

(**a**) Experimental set-up for measuring the outer diameter of *in-situ* hollow fiber and (**b**) schematic representation of the cross section of the end of the spinneret used for hollow fiber spinning.

For demonstration the solutions of PEI were chosen due to the ease of spinning and so for the ease of the measurement. The results are categorized in two experimental set-ups.

i. Effect of change in flow rates

The effect of the change in polymer solution flow rate (Q_P) and bore fluid flow rate (Q_B) on the diameter of the hollow fiber was measured *in-situ*. The air gap distance (L_{Air}) was set to 20 cm and the LASER was targeted at the position of 5 mm below the spinneret exit. While spinning, the outer diameter of the *in-situ* hollow fiber was recorded for different flow rates of the polymer solution and bore fluid.

For this category 25 wt.% of PEI solution in a mixture of NMP and GBL (NMP/GBL: 73/27 (wt./wt.)) was taken as a spinning dope solution and water was taken as bore fluid and coagulation bath.
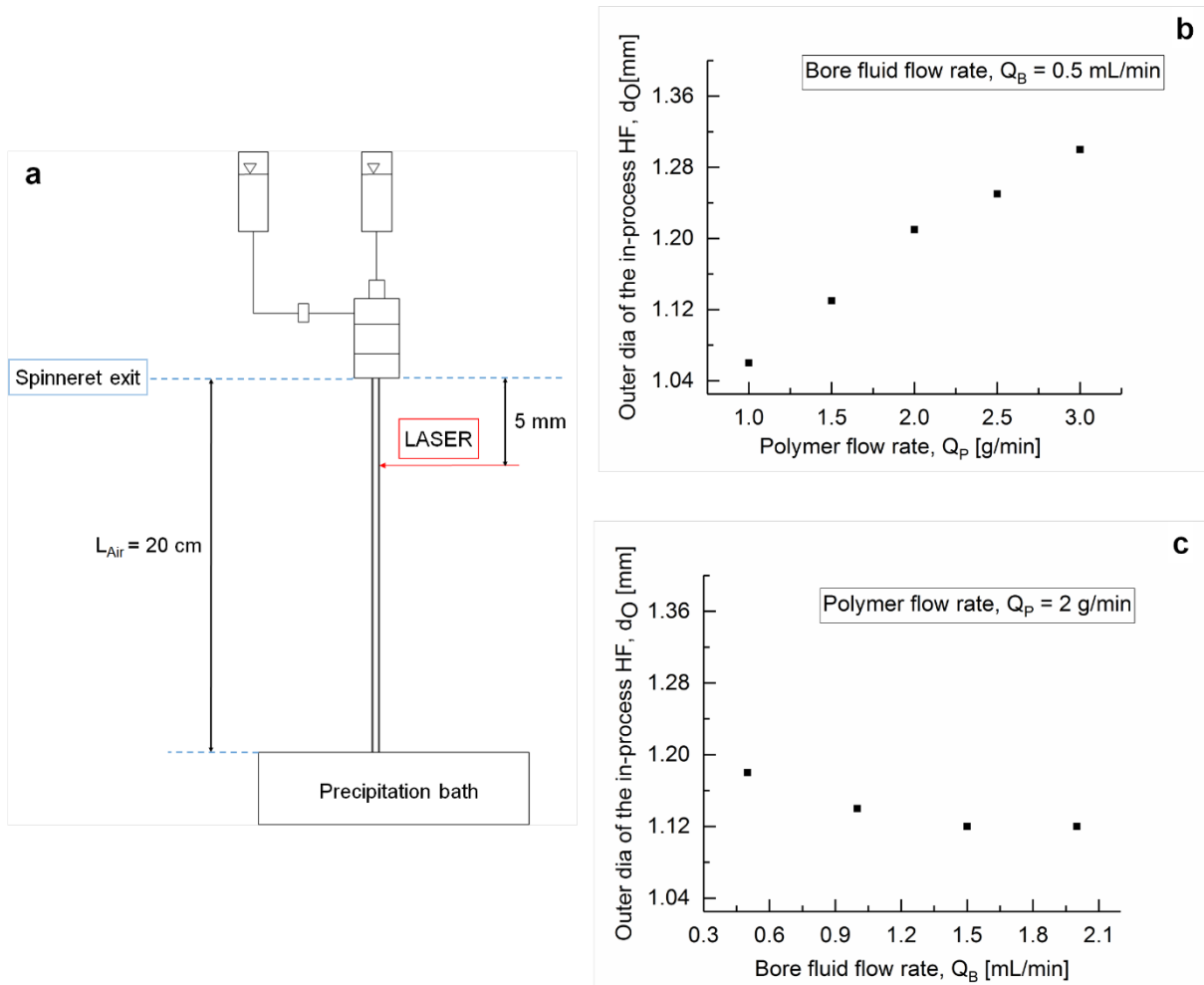
Figure 4.3 Diameter measurement of the *in-situ* hollow fiber during spinning by the LASER micrometer. (**a**) Instrumental set-up for the measurement; (**b**) Change in the outer diameter (d_O) of the *in-situ* hollow fiber with change in Q_P when L_{Air} (20 cm) and Q_B (0.5 mL/min) was constant; (**c**) Change in the outer diameter (d_O) of the *in-situ* hollow fiber with change in Q_B when L_{Air} (20 cm) and Q_P (2 g/min) was constant. Spinning dope solution consisted of 25 wt.% PEI in NMP/GBL: 73/27 (wt./wt.).

From **Figure 4.3b** it is seen that with constant bore fluid flow rate ($Q_B = 0.5$ mL/min) and air gap distance ($L_{Air} = 20$ cm) the outer diameter of the *in-situ* hollow fiber increased as the polymer flow rate (Q_P) increased. On the other hand, keeping other parameters constant ($Q_P = 2$ g/min and $L_{Air} = 20$ cm) if the bore fluid flow rate (Q_B) was increased the diameter of the

hollow fiber decreased. After crossing a certain value for Q_B, the diameter of the hollow fiber did not change with the increase in Q_B value. After exiting from the spinneret the lumen side of the hollow fiber was immediately coagulated by the bore fluid (water) and the lumen side skin was solidified. This phenomenon can be compared to the freezing of the as-spun hollow fiber morphology into the solidified structure by a wet spinning process.[91] However, the layers beyond the inner surface or lumen side surface were still to solidify and got time for relaxation while passing the distance in air (L_{Air}). As Q_B increased the intrusion of the coagulant from the lumen side to the outer edge of the hollow fiber was faster and therefore after crossing a value for Q_B the solidification length scale extended towards the outer edge and the outer diameter of the *in-situ* hollow fiber decreased. Consequently for high enough Q_B the *in-situ* hollow fiber was solidified right below the spinneret exit and so for further increase in Q_B no more change in the outer diameter of the *in-situ* hollow fiber was detectable.

The outer diameters of the *in-situ* hollow fibers were detected for two other PEI solutions where DMF and THF were used as solvents- 25 wt.% of PEI solution in DMF/THF: 60/40 (wt./wt.) and 25 wt.% of PEI solution in DMF/THF: 80/20 (wt./wt.).

The bore fluid flow rate (Q_B = 0.5 mL/min) and air gap distance (L_{Air} = 20 cm) were kept constant whereas the polymer flow rate (Q_P) was changed. From **Figure 4.4** it is seen that the hollow fibers that were spun from the PEI solutions in DMF/THF were smaller in diameter compared to the hollow fibers which were spun from the PEI solution in NMP/GBL. THF is a highly volatile solvent. As the solution of PEI in DMF/THF exited from the spinneret THF started to evaporate. So when solutions in THF were spun solidification did not only start from the lumen side by the strong precipitant but the evaporation of highly volatile solvent facilitated the solidification as well from the outer surface of the hollow fiber. That is why as the THF

content increased in the solutions the diameter of the *in-situ* hollow fiber decreased for the same set of processing parameters.
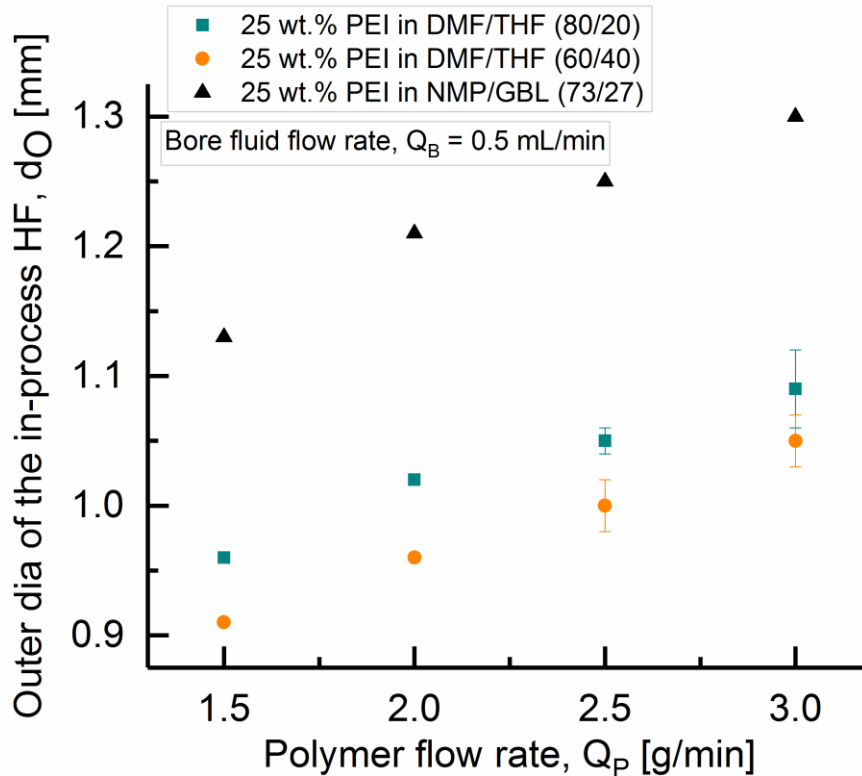
Figure 4.4 Diameter measurement of the *in-situ* hollow fiber during spinning by LASER micrometer. Change in the outer diameter (d_O) of the *in-situ* hollow fiber with change in Q_P is shown when L_{Air} (20 cm) and Q_B (0.5 mL/min) was constant. Hollow fibers were spun from three different solutions- ■ 25 wt.% PEI in DMF/THF: 80/20 (wt./wt.), ● 25 wt.% PEI in DMF/THF: 60/40 (wt./wt.), ▲ 25 wt.% PEI in NMP/GBL: 73/27 (wt./wt.).

ii. Effect of change in air gap distance, L_{Air}

The effect of the change in air gap distance, L_{Air} on the diameter of the hollow fibers was measured *in-situ*. For this category of experiments a solution of 25 wt.% of PEI in a mixture of NMP and GBL (NMP/GBL: 73/27 (wt./wt.)) was taken as a spinning dope solution and water was taken as bore fluid and coagulation bath.

The polymer flow rate (Q_P) and bore fluid flow rate (Q_B) were set to 2 g/min and 0.5 mL/min, respectively. L_{Air} was changed from 10 to 40 cm. The LASER was targeted at the position of 5 cm above the surface of the coagulant (it was the lowest possible point where the LASER micrometer could be set with the existing instrumental set-up) (**Figure 4.5**). While spinning, the outer diameter of the *in-situ* hollow fibers was recorded before entering the coagulation bath. Hollow fibers spun with different L_{Air} were collected, dried, and the outer diameter of the dried hollow fibers was measured by optical microscope.
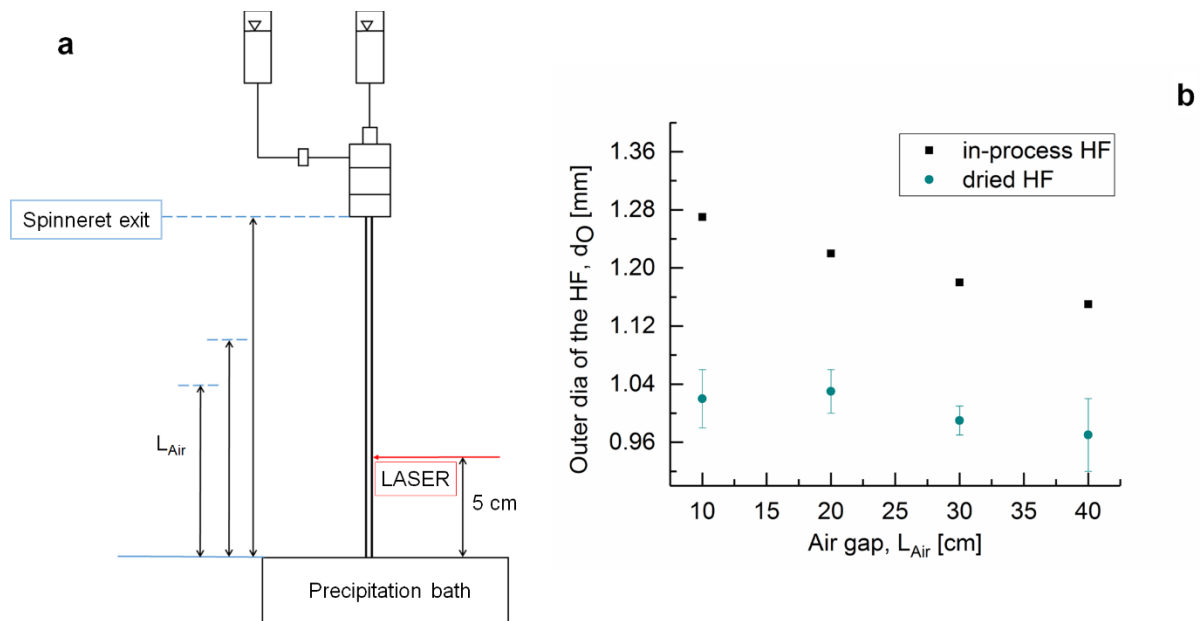
Figure 4.5 Diameter measurement of the *in-situ* hollow fiber during spinning by LASER micrometer: **(a)** Instrumental set-up for the measurement; **(b)** Change in the outer diameter (d_O) of the *in-situ* and dried hollow fibers with change in L_{Air} when Q_P (2 g/min) and Q_B (0.5 mL/min) was constant. Spinning dope solution consisted of 25 wt.% PEI in NMP/GBL: 73/27 (wt./wt.).

From **Figure 4.5** it is seen that the outer diameter of the hollow fiber (HF) decreased as L_{Air} increased. With increase in L_{Air} the hollow fiber was stretched due to the gravity induced elongation. Therefore elongational stress was induced and so the diameter of the hollow fiber decreased.[91]

Chapter 5

Results and Discussion

Double Layer Hollow Fiber Spinning by Co-extrusion with Commercial Polymers

The aim of this work was to spin double layer hollow fiber membranes where the outer layer or the selective layer would consist of PS-*b*-P4VP and the inner layer or the support layer would consist of commercially available polymers. The idea was that by this strategy one may save some of the expensive block copolymer and also improve the mechanical robustness of the fiber. So the co-extrusion method was first tested with the existing instrumentation and the processing arrangement was optimized by using commercial polymers for both inner and outer layer solutions before implementing the tailor-made expensive PS-*b*-P4VP diblock copolymer.

5.1 Co-extrusion of Double Layer Hollow Fiber

The hollow fibers were spun by the dry-jet wet spinning method by using a triple orifice spinneret. The dimensions of the spinneret used for the results of this chapter are shown in **Figure 5.1**.
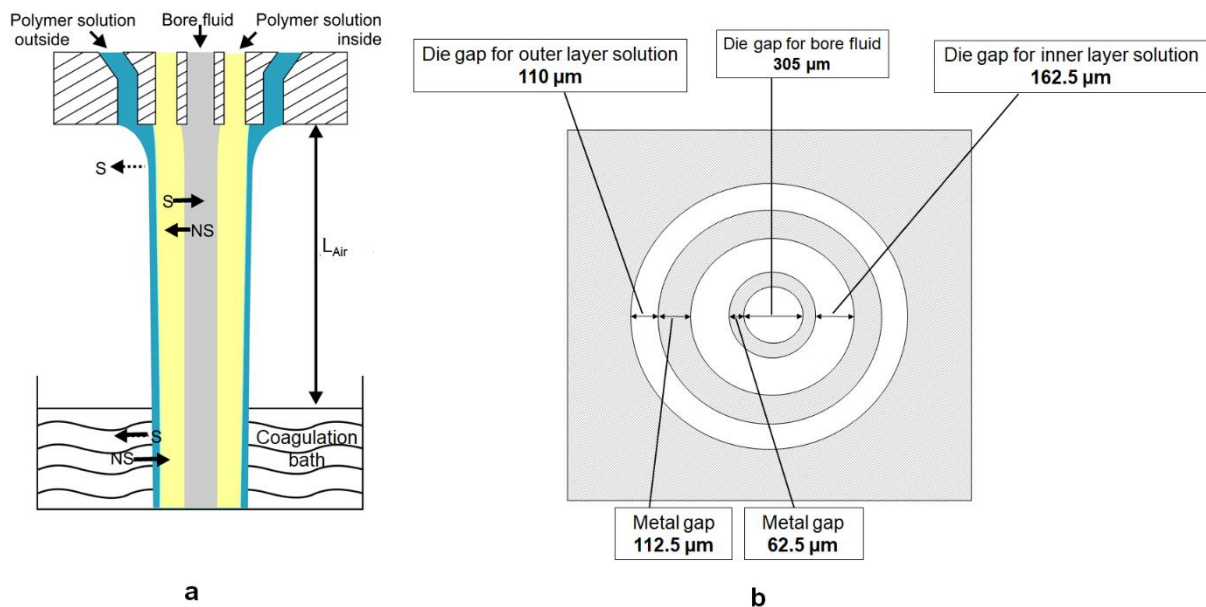
Figure 5.1 (a) Double layer hollow fiber preparation by dry-jet wet spinning. Two polymer solutions and bore fluid are extruded simultaneously through a triple-orifice spinneret. Spun

hollow fiber enters into the coagulation bath following a definite air gap distance, L_{Air};[1] (**b**) Schematic representation of the exit of the spinneret used in the experiments of this chapter.

5.2 Double Layer Hollow Fiber spinning with PEI Solutions

Two compatible PEI solutions were selected to fabricate double layer hollow fibers by co-extrusion. Solution compositions are listed in **Table 5.1** and the spinning parameters are listed in **Table 5.2**. The obtained hollow fibers from this experiment are shown in **Figure 5.2** and **Figure 5.3**.

Table 5.1 Compositions of the spinning solutions

Inner layer solution		Outer layer solution		Bore fluid	Coagulation bath
Polymer concentration (in wt.%)	Solvent concentration[a] (in wt.%)	Polymer concentration (in wt.%)	Solvent concentration[a] (in wt.%)	concentration (in wt.%)	concentration (in wt.%)
25% PEI	75% NMP/GBL (73/27)	17.5 % PEI	82.5% NMP/GBL (73/27)	100% Water	100% Water

[a]Solvent concentration and composition is expressed as x% A/B (y/z), where x is the total solvent concentration in weight% in the solution, and y and z are the weight percentage of solvent A and B, respectively, in the solvent mixture.

Table 5.2 Spinning parameters of the hollow fibers

Hollow fiber	Bore fluid flow rate, Q_B [mL/min]	Inner solution flow rate, Q_I [g/min]	Outer solution flow rate, Q_O [g/min]	Air gap, L_{Air} [cm]
Figure 5.2a	1.5	1.15	1.94	90
Figure 5.2b	1.5	2.31	1.94	90
Figure 5.3a	1.5	1.15	0.45	90
Figure 5.3b	1.5	1.15	1.15	90
Figure 5.3c	1.5	1.15	1.94	90
Figure 5.3d	1.5	1.15	2.93	90
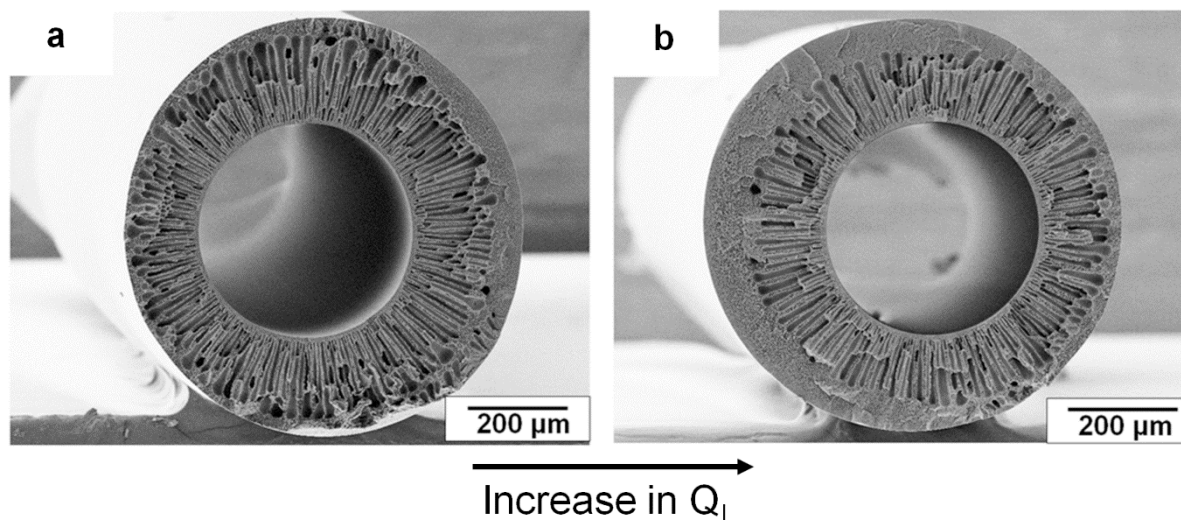
Figure 5.2 SEM images of the double layer hollow fibers; Inner layer solution: 25 wt.% PEI in NMP and GBL (NMP/GBL: 73/27 (wt./wt.)); Outer layer solution: 17.5 wt.% PEI in NMP and GBL (NMP/GBL: 73/27 (wt./wt.)). Spinning parameters: Q_B = 1.5 mL/min, Q_O = 1.94 g/min, L_{Air} = 90 cm, and Q_I = 1.15 g/min (**a**), 2.31 g/min (**b**).
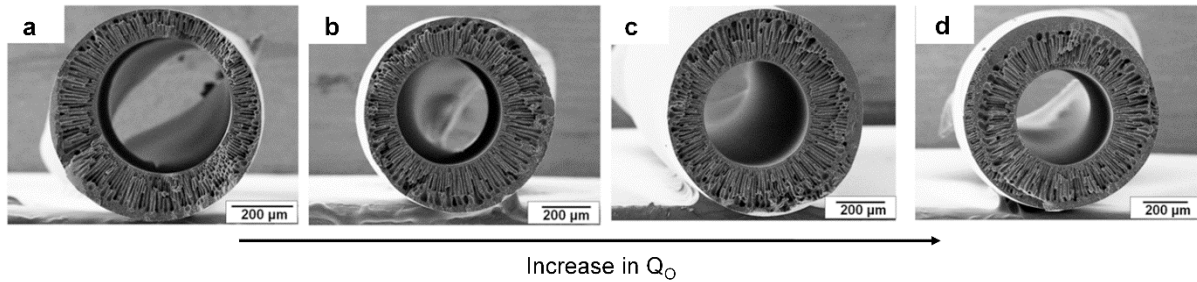
Figure 5.3 SEM images of the double layer hollow fibers: Inner layer solution: 25 wt.% PEI in NMP and GBL (NMP/GBL: 73/27 (wt./wt.)); Outer layer solution: 17.5 wt.% PEI in NMP and GBL (NMP/GBL: 73/27 (wt./wt.)). Spinning parameters: Q_B = 1.5 mL/min, Q_I = 1.15 g/min, L_{Air} = 90 cm, and Q_O = 0.45 g/min (**a**), 1.15 g/min (**b**), 1.94 g/min (**c**), 2.93 g/min (**d**).

From **Figure 5.2** it is seen that while keeping the bore fluid flow rate, Q_B, the outer layer solution flow rate, Q_O, and the air gap distance, L_{Air} constant, a change in the flow rate of the inner layer solution, Q_I did not bring any significant change in the morphology of the hollow fibers. The same statement is true in case of change in Q_O while keeping the other parameters constant (**Figure 5.3**). **Figure 5.2** and **5.3** show that the interface between the two layers is not detectable in the cross section of the hollow fibers. Different concentrations of PEI were used for both inner and outer layer solutions but since they were completely miscible with each other there was no detectable boundary line between the layers in the hollow fibers. In a co-extrusion process the interface between the layers must not be interrupted by the intrusion of coagulant from the bore fluid side in the air gap distance before plunging in to the coagulation bath.[39, 99, 100] As these solutions were miscible their interface immediately disappeared below the spinneret and therefore was not even disturbed in a long distance (90 cm of L_{Air}) although a strong coagulant (water) was used as a bore fluid. The precipitation was fast and created finger like structure along the thickness of the hollow fibers which extended from the bore fluid side to the outer edge of the hollow fiber.

5.3 Double Layer Hollow Fiber from Solutions of PEI and GH 62

When two different kinds of polymer solutions are used for inner and outer layers interfacial adherence is not guaranteed. Moreover, for some pairs of solutions for the inner and outer layers the interfacial attachment may not be attained with any sets of parameters. Since the aim of this work was to co-extrude PS-*b*-P4VP block copolymer with a support layer, a commercial block copolymer which has polystyrene (PS) as its major component was chosen as an outer layer material for screening suitable conditions before using the tailor-made PS-*b*-P4VP diblock copolymer.

Solution compositions are listed in **Table 5.3** and the spinning parameters are listed in **Table 5.4**. The hollow fibers obtained from this experiment are shown in **Figure 5.4**.

Table 5.3 Compositions of the spinning solutions

Inner layer solution		Outer layer solution		Bore fluid	Coagulation bath
Polymer concentration (in wt.%)	Solvent concentration[a] (in wt.%)	Polymer concentration (in wt.%)	Solvent concentration[a] (in wt.%)	concentration (in wt.%)	concentration (in wt.%)
25% PEI	75% NMP/GBL (73/27)	28 % GH 62	72% NMP/THF (70/30)	100% Water (**Figure 5.4a-d**) and 80% Water 20% NMP (**Figure 5.4e**)	100% Water

[a]Solvent concentration and composition are expressed as x% A/B (y/z), where x is the total solvent concentration in weight% in the solution, and y and z are the weight percentage of solvent A and B, respectively, in the solvent mixture.

Table 5.4 Spinning parameters of the hollow fibers

Hollow fiber	Bore fluid flow rate, Q_B [mL/min]	Inner solution flow rate, Q_I [g/min]	Outer solution flow rate, Q_O [g/min]	Air gap, L_{Air} [cm]
Figure 5.4a	1.5	1.15	0.45	90
Figure 5.4b	1.5	1.15	0.45	50
Figure 5.4c	1.5	1.15	0.45	20
Figure 5.4d	1.5	1.15	0.45	5
Figure 5.4e	1.5	1.15	0.45	90

Decrease in L_{Air}

Solvent in bore fluid
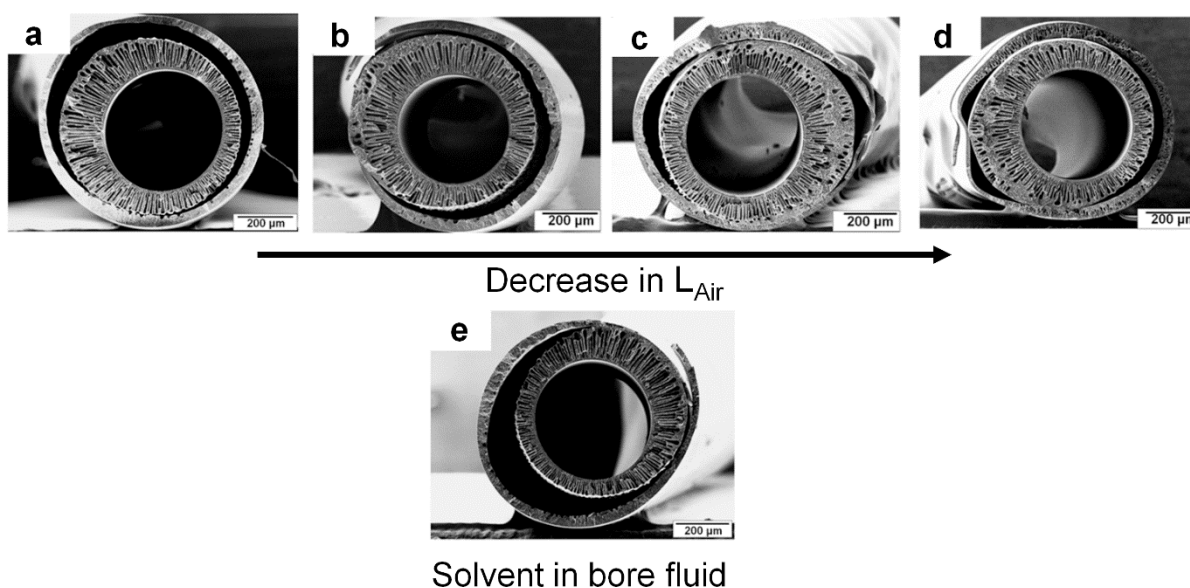
Figure 5.4 SEM images of the double layer hollow fibers: Inner layer solution: 25 wt.% PEI in NMP and GBL (NMP/GBL: 73/27 (wt./wt.)); Outer layer solution: 28 wt.% GH 62 in NMP and THF (NMP/THF: 70/30 (wt./wt.)); Bore fluid: water (**a-d**) and water/NMP (80/20) (**e**); Spinning parameters: Q_B = 1.5 mL/min, Q_I = 1.15 g/min, Q_O= 0.45 g/min, and L_{Air} = 90 cm (**a & e**), 50 cm (**b**), 20 cm (**c**), and 5 cm (**d**).

While PEI solutions for both layers showed interfacial miscibility in the double layer hollow fibers, a completely opposite phenomenon was observed when using PEI and GH 62 solutions

for the two different layers. The same spinning parameters which were applied to spin the hollow fibers shown in **Figure 5.3a** resulted in delamination between the PEI and GH 62 layers (**Figure 5.4a**). The effect of L_{Air} on delamination was studied by decreasing L_{Air} and even with decreased L_{Air} the two layers became separated from each other (**Figure 5.4b, c, d**). Non-solvent intrusion from the bore fluid side was slowed down by using a mixture of water and NMP but the double layer hollow fiber still showed delamination between the layers (**Figure 5.4e**). Here it is to be noticed that the morphology of the inner layer did not show any significant change with the addition of solvent in the bore fluid. Moreover, the extended finger like structure indicates that precipitation occurred fast enough even if a water-solvent mixture (water/solvent: 80/20 (wt.wt.)) was used as a bore fluid.

Since a slower exchange of the solvent-non-solvent pair could help to retain the interfacial interaction, DMF was added as a solvent to the inner layer solution in order to slow down the precipitation rate. Moreover, to increase the interdiffusion[101] among the components of the two layers, the same solvent system was used for both layers (DMF/THF). Solution compositions are listed in **Table 5.5** and the spinning parameters are listed in **Table 5.6**. The hollow fibers obtained from this experiment are shown in **Figure 5.5**.

Table 5.5 Compositions of the spinning solutions

Inner layer solution		Outer layer solution		Bore fluid	Coagulation bath
Polymer concentration (in wt.%)	Solvent concentration[a)] (in wt.%)	Polymer concentration (in wt.%)	Solvent concentration[a)] (in wt.%)	concentration (in wt.%)	concentration (in wt.%)
25% PEI	75% DMF/THF (60/40)	28 % GH 62	72% DMF/THF (60/40)	100% Water	100% Water

[a)]Solvent concentration and composition are expressed as x% A/B (y/z), where x is the total solvent concentration in weight% in the solution, and y and z are the weight percentage of solvent A and B, respectively, in the solvent mixture.

Table 5.6 Spinning parameters of the hollow fibers

Hollow fiber	Bore fluid flow rate, Q_B [mL/min]	Inner solution flow rate, Q_I [g/min]	Outer solution flow rate, Q_O [g/min]	Air gap, L_{Air} [cm]
Figure 5.5a	1.5	1.15	0.45	90
Figure 5.5b	1.5	2.31	0.45	90
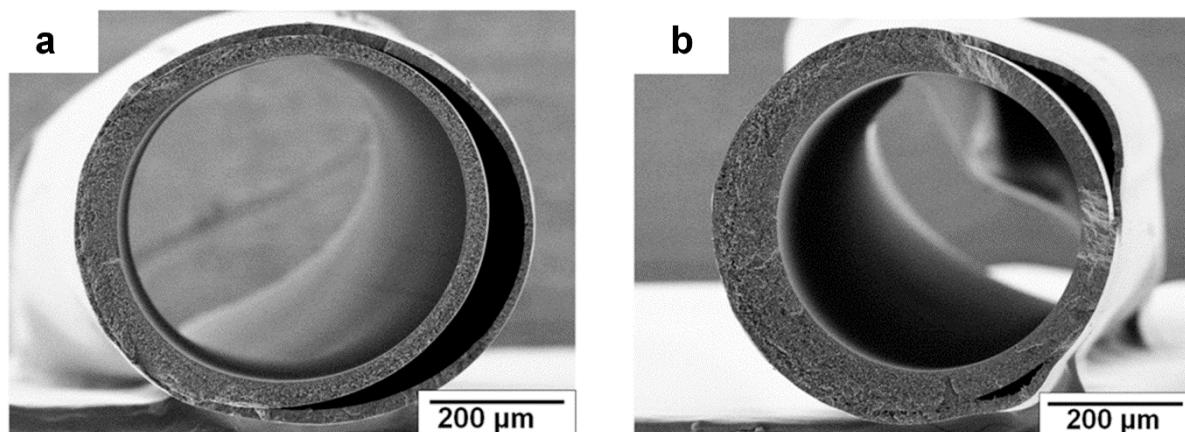
Figure 5.5 SEM images of the double layer hollow fibers: Inner layer solution: 25 wt.% PEI in DMF and THF (DMF/THF: 60/40 (wt./wt.)), Outer layer solution: 28 wt.% GH 62 in DMF and THF (DMF/THF: 60/40 (wt./wt.)); Spinning parameters: Q_B = 1.5 mL/min, Q_O = 0.45 g/min, L_{Air} = 90 cm, Q_I = 1.15 g/min (**a**) and 2.31 g/min (**b**).

Slower precipitation from the bore fluid side is evident from the spongy structure and the absence of macrovoids in the inner layer (**Figure 5.5**). But the detachment of layers was unavoidable (at least by the combination of these tested spinning parameters) by choosing solvents for the solutions which have a slower exchange rate with water. A same solvent or solvent mixture for both layer forming solutions often help to exclude the delamination problem between layers by facilitating interpenetration of the solutions.[101] But the polymers chosen here were too different from each other in their properties and they are incompatible what played the vital role in causing delamination between PEI and GH 62 layers.

When L_{Air} was kept decreasing the adhesion between the layers was observed (**Figure 5.6**). Solution compositions were the same as those listed in **Table 5.5** and the spinning parameters are listed in **Table 5.7**.

Table 5.7 Spinning parameters of the hollow fibers

Hollow fiber	Bore fluid flow rate, Q_B [mL/min]	Inner solution flow rate, Q_I [g/min]	Outer solution flow rate, Q_O [g/min]	Air gap, L_{Air} [cm]
Figure 5.6a	1.5	2.31	0.45	50
Figure 5.6b	1.5	1.15	0.45	20
Figure 5.6c	1.5	1.15	0.45	5
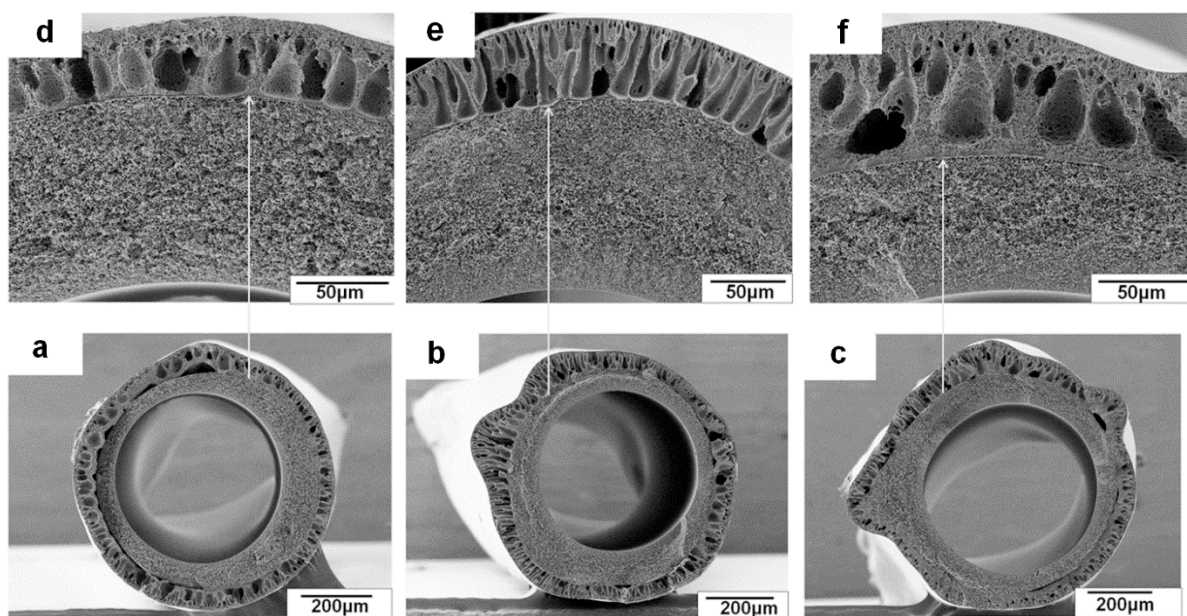
Figure 5.6 SEM images of the double layer hollow fibers: Inner layer solution: 25 wt.% PEI in DMF and THF (DMF/THF: 60/40 (wt./wt.)); Outer layer solution: 28 wt.% GH 62 in DMF and THF (DMF/THF: 60/40 (wt./wt.)); Spinning parameters: Q_B = 1.5 mL/min, Q_I = 2.31 g/min, Q_O = 0.45 g/min, and L_{Air} = 50 cm **(a)**, 20 cm **(b)**, 5 cm **(c)**. **a**, **b**, **c** are the cross sections of the hollow fibers and **d**, **e**, **f** are their magnified images, respectively taken near the interfacial regions of two layers.

In the previous works it was seen that an increase in L_{Air} facilitated the adhesion between two layers. Since with increased L_{Air} the gravity induced elongation accelerates the spinning

process and so the thinning down of the fiber dimension and wall thickness was observed which tightened the gap between the layers.[102] But in our case the decrease in L_{Air} from 90 cm (**Figure 5.5**) to 5 cm (**Figure 5.6**) showed a better interaction between layers. This phenomenon can be explained by the presence of highly volatile THF in the dope solutions. After exiting from the spinneret THF started to evaporate which introduced faster precipitation of the solutions preferably of the outer layer solution. And it helped to tighten the outer layer and as the L_{Air} decreased the possibility of creating disturbance at the interface between the layers by the bore fluid intrusion before entering the coagulation bath was minimized.

The solutions used for spinning experiments shown in this chapter show a shear thinning behavior and this rheological behavior is shown in the Appendix (section 13.2) of this dissertation.

Chapter 6

Results and Discussion

Isoporous Structure Formation in Flat Sheet Geometry by the SNIPS Method

6.1 Structure Formation in SNIPS membranes from PS-*b*-P4VP

To administer the solutions of the tailor-made block copolymer, polystyrene-*block*-poly(4-vinylpyridine) (PS-*b*-P4VP) as an outer layer forming solution in co-extrusion, the solutions of PS-*b*-P4VP were cast as flat films beforehand to determine the right solution composition to obtain the isoporous structure on the membrane surface within an acceptable processing window. Different PS-*b*-P4VP were chosen considering their composition. This was especially essential as the spinning process required large amounts of polymer. Although the high shear stress and elongational stress during spinning have an effect on the structure formation in hollow fiber geometry,[35] optimization of the solution concentration and the composition in flat sheet geometry beforehand was required to minimize the wastage of the block copolymer during spinning. The selection procedure is summarized in **Figure 6.1** below.
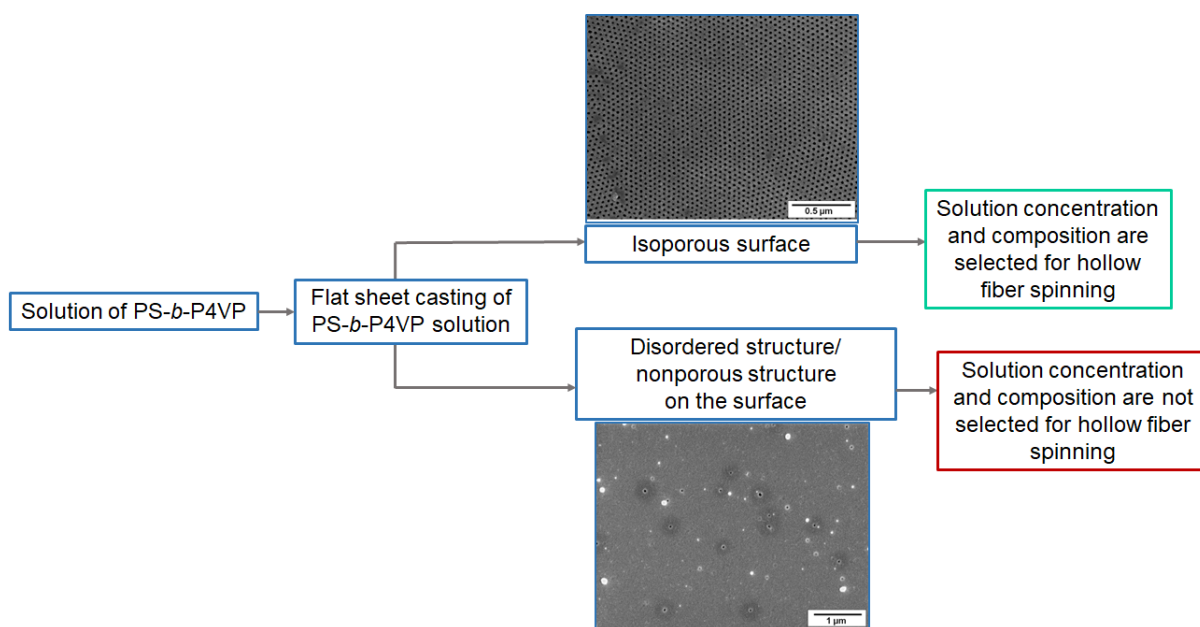
Figure 6.1 Selection strategy of PS-*b*-P4VP solution for spinning

In the previous work published in 2014 the development and optimization procedure to have isoporous surface forming PS-*b*-P4VP casting solutions were discussed elaborately.[30] The work provided a guidance in the selection of the composition of PS-*b*-P4VP for isoporous membrane forming solutions and it was suggested to choose a composition where PS-*b*-P4VP is predicted to show spherical or cylindrical domains in the bulk. Moreover, the concentrations and compositions of the PS-*b*-P4VP solutions were analyzed and chosen in a way so that they would render into the isoporous surface forming membranes.

Several solutions with different compositions of PS-*b*-P4VP were studied and among them some of the representative results are chosen here to demonstrate their isoporous surface formation. The block copolymer is termed as PS_x-*b*-$P4VP_y^z$ where, subscripts and superscript denote the weight percentage of the respective blocks and the total molecular weight of the block copolymer in kg/mol, respectively. This naming method is followed throughout this dissertation where block copolymer identification is required to be mentioned. The membranes were cast at ambient condition (temperature at around 20 °C and humidity of around 30-40%) and water was used as the coagulation medium.

6.1.1 Structure formation of $PS_{79.8}$-*b*-$P4VP_{20.2}^{95}$

Solutions of two different concentrations of $PS_{79.8}$-*b*-$P4VP_{20.2}^{95}$ (29 wt.% and 30 wt.%) were prepared in the solvent mixture of DMF and THF where they were mixed in equal wt.% i.e. DMF/THF: 50/50 (wt./wt.). Membranes were cast with three different evaporation times for each of the solutions.

Solution composition and the casting parameters are listed in **Table 6.1** and the final surface structure is shown in **Figure 6.2.**

Table 6.1 Solution composition and the membrane casting parameters

Polymer concentration (in wt.%)	Solvent Concentration[a] (in wt.%)	Gate height (in µm)	Evaporation time (in sec)	
29 % $PS_{79.8}$-b-$P4VP_{20.2}^{95}$	71 wt.% DMF/THF (50/50)			
30 % $PS_{79.8}$-b-$P4VP_{20.2}^{95}$	70 wt.% DMF/THF (50/50)	200	5	10

[a]Solvent concentration and composition are expressed as x% A/B (y/z), where x is the total solvent concentration in weight% in the solution, and y and z are the weight percentage of solvent A and B, respectively, in the solvent mixture.
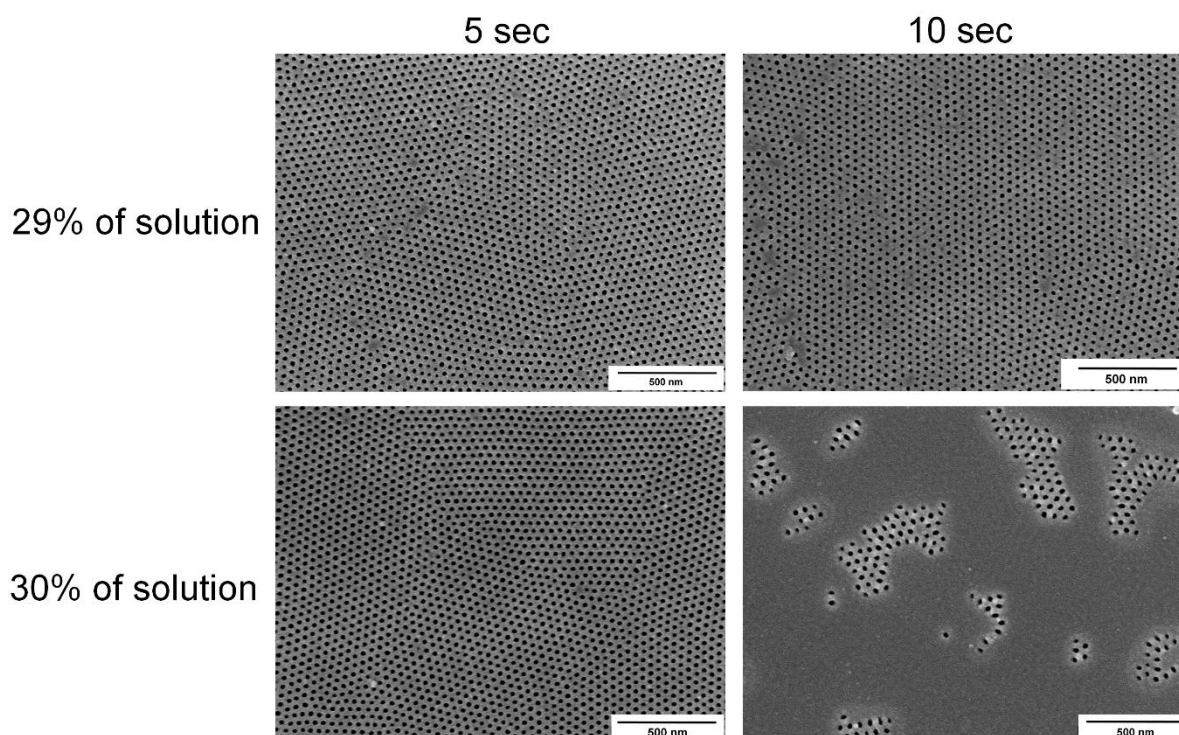
Figure 6.2 SEM images of the membrane surfaces. Membranes were cast from 29% and 30 % solution of $PS_{79.8}$-b-$P4VP_{20.2}^{95}$ in DMF/THF: 50/50 (wt./wt.). Time prior to precipitation or evaporation time was 5 sec and 10 sec.

The surface structure of the membrane is a combined result of the solution concentration, solvent composition, and evaporation time.[30] Both concentrations of 29 wt.% and 30 wt.% of block copolymer led to membranes with uniform isoporous structure on the surface for the shorter evaporation time (5 sec). Although an evaporation time of 10 seconds led to a uniform structure all over the surface for the 29 wt.% of solution of $PS_{79.8}$-b-$P4VP_{20.2}^{95}$, the structure formed by the 30 wt.% of solution was discrete. Moreover, from the experiment it was found that with increased evaporation time (more than 10 sec) the solution of 29% resulted in a membrane with discontinuity in the surface structure. To achieve the required polymer density to form an isoporous structure on the membrane surface the less concentrated solution would require longer evaporation time. However, in case of higher concentration of the solution the longer evaporation time diminishes the concentration gradient along the cast film thickness and so the discontinuity in the surface structure appears. Since even small changes in the concentration of the block copolymer solution affect the mobility of the chains due to the change in viscosity, the isoporous structure controlling window is altered.[30]

If this block copolymer would have been implemented in the spinning process then the spinning solution of 29% or 30% with the solvent composition of DMF/THF: 50/50 (wt./wt.) would be the potential isoporous structure forming solution. Since the viscosity of the solution is an important factor to be selected as a spinning solution, it is also a selection criterion to be included.

6.1.2 Structure formation with PS$_{81}$-*b*-P4VP$_{19}$[287]

Another example of isoporous structure formation is presented here where a block copolymer with higher molecular weight is used. The solution concentration, composition and the casting parameters are listed in the **Table 6.2** and the obtained membrane surface structure is shown in **Figure 6.3.**

Table 6.2 Solution composition and the membrane casting parameters

Sample no.	Polymer concentration (in wt.%)	Solvent Concentration[a] (in wt.%)	Gap height (in μm)	Evaporation time (in sec)
a	17% PS$_{81}$-*b*-P4VP$_{19}$[287]	83% DMF/THF (60/40)		
b	18% PS$_{81}$-*b*-P4VP$_{19}$[287]	82% DMF/THF (60/40)		
c	19% PS$_{81}$-*b*-P4VP$_{19}$[287]	81% DMF/THF (60/40)	200	5
d	20% PS$_{81}$-*b*-P4VP$_{19}$[287]	80% DMF/THF (50/50)		
e	21% PS$_{81}$-*b*-P4VP$_{19}$[287]	79% DMF/THF (60/40)		

[a]Solvent concentration and composition are expressed as x% A/B (y/z), where x is the total solvent concentration in weight% in the solution, and y and z are the weight percentage of solvent A and B, respectively, in the solvent mixture.
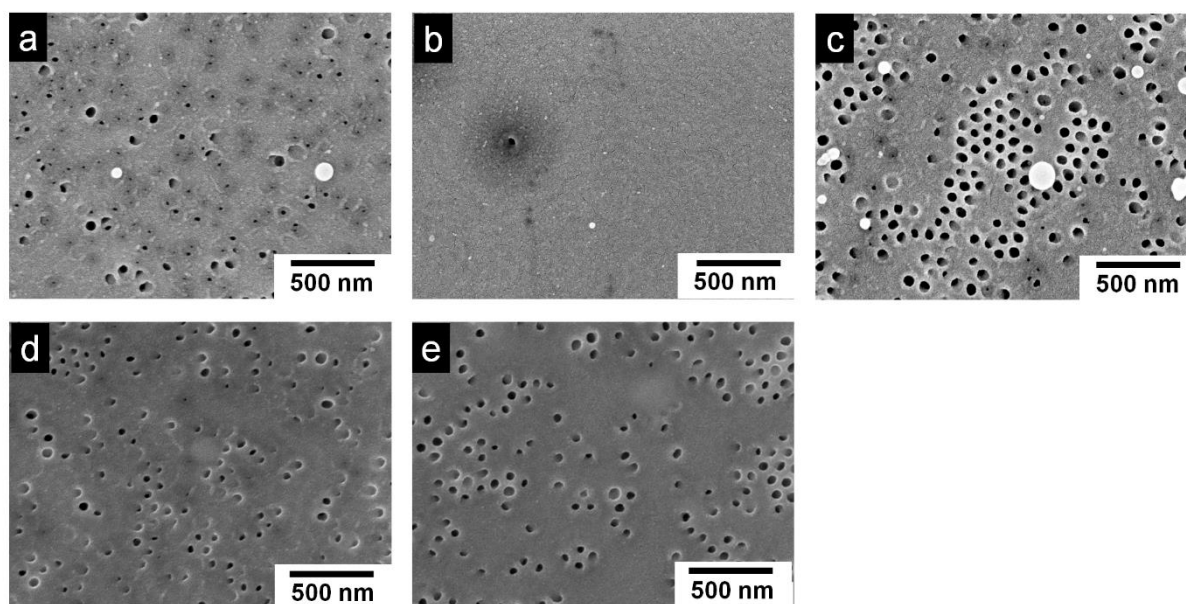
Figure 6.3 SEM images of the membrane surfaces. Membranes were cast from 17 wt.% **(a)**, 18 wt.% **(b)**, 19 wt.% **(c)**, 20 wt.% **(d)**, 21 wt.% **(e)** solution of PS_{81}-b-$P4VP_{19}^{287}$ in DMF/THF: 60/40 (wt./wt.).

Figure 6.3 shows that the polymer solutions of PS_{81}-b-$P4VP_{19}^{287}$ with a concentration ranging from 17 wt.% to 21 wt.% do not show a hexagonally oriented porous structure all over the membrane surface. Several factors influence the isoporous structure formation on the membrane surface. In this case, the absence of order or continuity of order on the surface may arise from the limitation of the polymer chains to self-assemble into a microphase separated structure within 5 seconds of evaporation time in the chosen solvent composition. The increase in evaporation time for all the five concentrations of these solutions did not lead to any ordered structure on the surface as well. So, the absence of the ordered structure on the surface may be due to the lack of compositional balance in the block copolymer which is essential for isoporous structure formation on the surface. If the composition does not facilitate segregation, the ordered structure might not be formed. Moreover, the viscosity of the solution plays a vital role in the formation of micellar aggregates.[30]

Since the taken concentrations of the solutions of PS_{81}-b-$P4VP_{19}^{287}$ with the chosen solvent composition did not lead to hexagonally ordered cylindrical pore formation all over the membrane surface, none of these solutions was considered for hollow fiber spinning.

In the previous studies it was shown that the isoporous structure formation can be induced by the incorporation of different additives into the block copolymer solution. For example, supramolecular interaction between the additive molecules (complex forming metal ions or sugar) and the pyridine units of PS-b-P4VP diblock copolymer facilitated stabilizing micellar aggregates and so the isoporous structure formation.[103-105]

A solution of PS_{81}-b-$P4VP_{19}^{287}$ was prepared by the addition of α-cyclodextrine and the solution composition and the membrane casting parameters are listed in **Table 6.3.** The obtained membrane surface structure is shown in **Figure 6.4**.

Table 6.3 Solution composition and the membrane casting parameters

Polymer concentration (in wt.%)	Additive concentration (in wt.%)	Solvent Concentration[a] (in wt.%)	Evaporation time (in sec)	
			a	b
16% PS_{81}-b-$P4VP_{19}^{287}$	1% α-cyclodextrine	83% DMF/THF (60/40)	5	10

[a]Solvent concentration and composition are expressed as x% A/B (y/z), where x is the total solvent concentration in weight% in the solution, and y and z are the weight percentage of solvent A and B, respectively, in the solvent mixture.
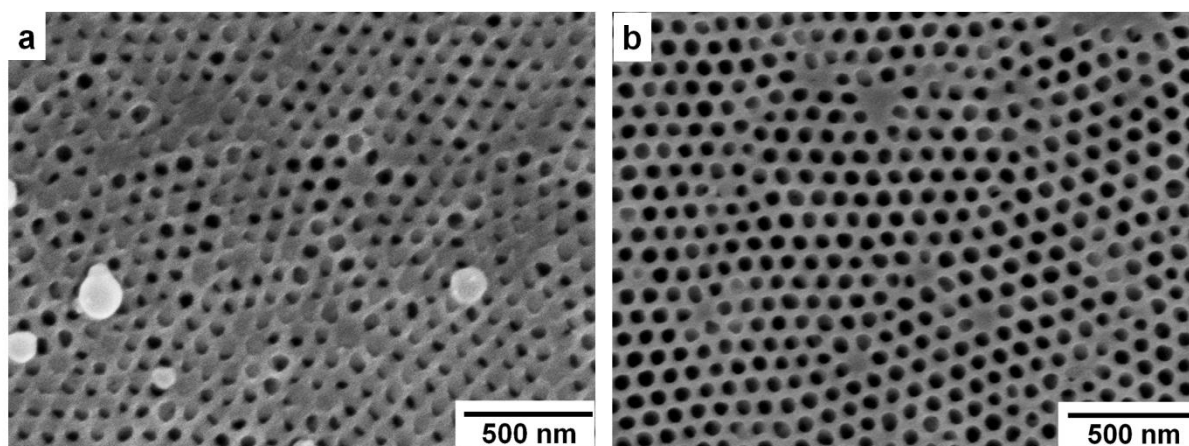
Figure 6.4 SEM images of the membrane surfaces. Membranes were cast from the solution of 16 wt.% PS_{81}-b-$P4VP_{19}^{287}$ with α-cyclodextrine in DMF/THF: 60/40 (wt./wt.). Evaporation time prior to precipitation was 5 sec **(a)** and 10 sec **(b)**.

From **Figure 6.4** it is seen that in presence of α-cyclodextrine the solution of PS_{81}-b-$P4VP_{19}^{287}$ formed an isoporous structure all over the membrane surface with less polymer concentration. The structure got improved when the evaporation time was increased from 5 to 10 seconds.

The multifunctionality of the added carbohydrate (α-cyclodextrine) formed hydrogen bonds with PS-b-P4VP molecules and connected different block copolymer chains together which is reflected in a higher solution viscosity and the micelle stabilization. The carbohydrate associated P4VP blocks formed the cylinders in the microphase separated structure and the carbohydrate later was washed off when the cast film was immersed into water bath.[105]

So, if PS_{81}-b-$P4VP_{19}^{287}$ had to be employed for the spinning experiments, a carbohydrate containing block copolymer solution would be used in order to recover the isoporous structure on the surface of the hollow fiber geometry as well.

Chapter 7

Results and Discussion

**Double Layer Hollow Fiber Spinning by Co-extrusion
with PS-*b*-P4VP as the Outer Layer Forming Material**

Chapter 7: Results and Discussion
Double Layer Hollow Fiber Spinning by Co-extrusion
with PS-*b*-P4VP as the Outer Layer Forming Material

7.1 Why Co-extrusion was Chosen?

PS-*b*-P4VP is a high cost tailor-made polymer. The reason to choose it as a selective layer material is because it can form highly ordered pores with narrow size distribution on the membrane surface. If a support layer can be inserted underneath the selective layer of PS-*b*-P4VP by co-extrusion it may turn out to be advantageous for several reasons, such as-

    i.   The membrane will possess mechanical stability for real life implication,

    ii.   It will save the material cost of PS-*b*-P4VP.

    iii.   Co-extrusion method makes possible the insertion of a support layer beneath the selective layer in a single step and so makes the processing of composite hollow fiber membrane much easier compared to other methods e.g. dip coating.[106]

To check the potential of the dip coating method a PESU containing hollow fiber membrane was coated with a solution of $PS_{83.3}$-*b*-$P4VP_{16.7}$[198]. The solution was composed of 25 wt.% of $PS_{83.3}$-*b*-$P4VP_{16.7}$[198] in a mixture of DMF and THF (DMF/THF: 60/40 (wt./wt.)). The procedure is explained in **Figure 7.1.**

Chapter 7: Results and Discussion
Double Layer Hollow Fiber Spinning by Co-extrusion
with PS-*b*-P4VP as the Outer Layer Forming Material
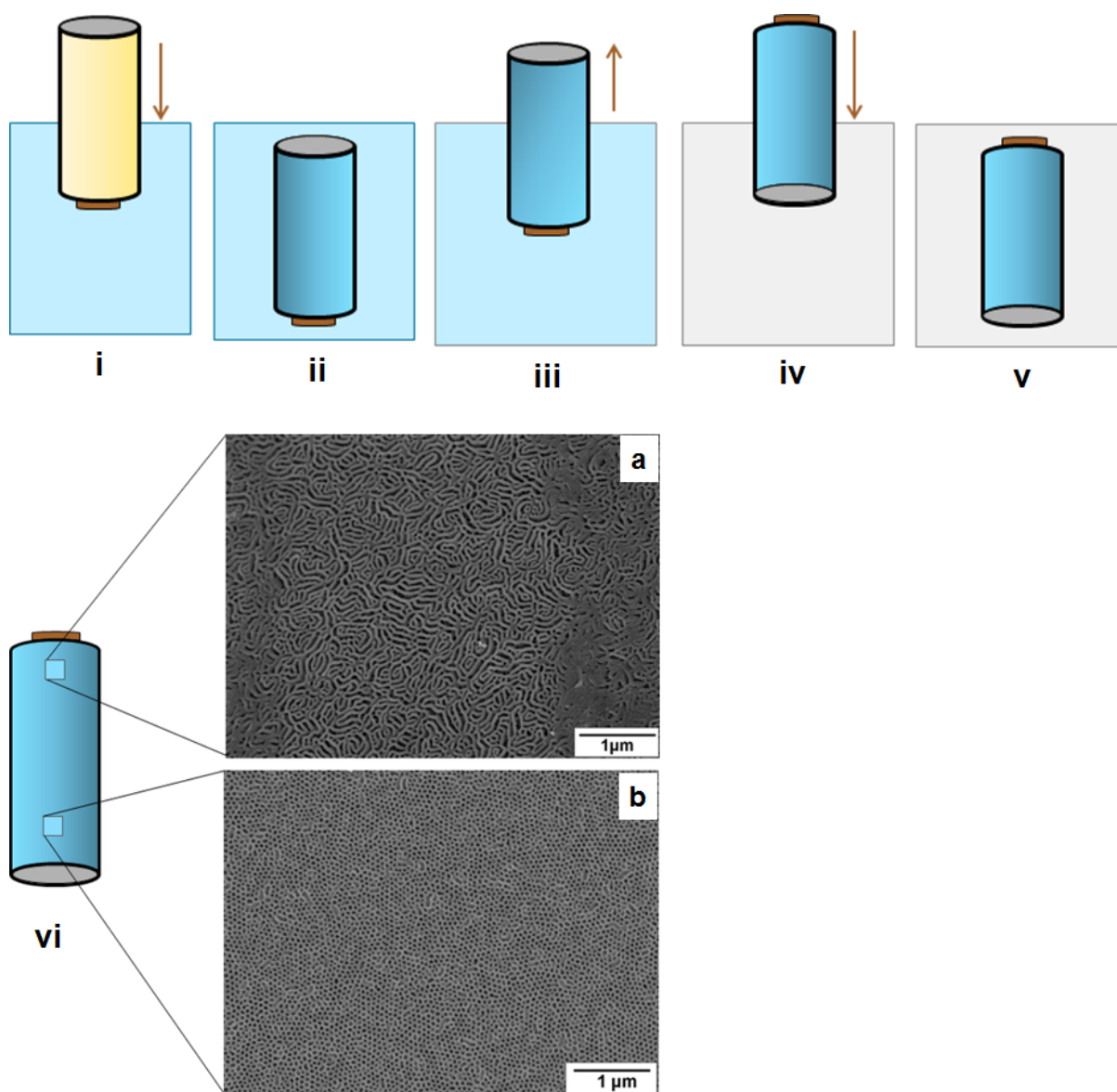
Figure 7.1 Dip coating of a hollow fiber by PS-*b*-P4VP solution: **i.** PESU hollow fiber was plunged into the solution of 25 wt.% of $PS_{83.3}$-*b*-$P4VP_{16.7}$[198] in a mixture of DMF and THF (DMF/THF: 60/40 (wt./wt.)); **ii.** Coating of the hollow fiber in the solution of $PS_{83.3}$-*b*-$P4VP_{16.7}$[198]; **iii.** The hollow fiber was pulled upward through the $PS_{83.3}$-*b*-$P4VP_{16.7}$[198] solution and the hollow fiber was allowed to stay in air for a definite time period for the evaporation of the solvent; **iv.** Plunging of the coated hollow fiber into the water bath; **v.** Keeping the coated hollow fiber in the water bath for the completion of the precipitation; **vi.** Surface structure analysis of the dried hollow fiber by SEM shows that the different regions of the hollow fiber show different microstructure such as- parallelly aligned cylinder **(a)** and perpendicularly

Chapter 7: Results and Discussion
Double Layer Hollow Fiber Spinning by Co-extrusion
with PS-*b*-P4VP as the Outer Layer Forming Material

aligned cylindrical pores **(b)**, respectively. One end of the hollow fiber is marked in brown to indicate the plunging and drawing direction.

The isoporous structure formation by SNIPS method is time dependent. The edge of the hollow fiber that passed out of the coating solution earlier would experience longer evaporation time compared to the other end of the hollow fiber that came out of the coating solution later. So, to ensure the constant evaporation time on all over the coated hollow fiber the direction of the plunging into the water bath was followed in a way so that the edge of the hollow fiber that came out earlier from the coating solution was plunged into the water bath first and then was followed by the rest of the length of the hollow fiber. Even though this experiment was done with a short length of a hollow fiber, it was not possible to maintain a constant evaporation time all along the coated hollow fiber. So, it was unmanageable to bring out the intended feature of perpendicularly aligned cylindrical pores on all over the surface of the hollow fiber by using the solution of PS-*b*-P4VP by dip coating (**Figure 7.1a** and **b**). If PS-*b*-P4VP would be used to dip coat a support layer hollow fiber then the control over the isoporous structure along the hollow fiber length could not be assured by the described procedure since there exists a narrow window of processing parameters for the structure formation on PS-*b*-P4VP by the SNIPS mechanism. There are some works published on the fabrication of isoporous structure on hollow fiber membranes by dip coating method[107, 108] but for the longer or applicable length of hollow fibers the desirable structure formation by this method would be more tedious and would require a sophisticated controlling device.

Chapter 7: Results and Discussion
Double Layer Hollow Fiber Spinning by Co-extrusion
with PS-*b*-P4VP as the Outer Layer Forming Material

7.2 Co-extrusion of Double Layer Hollow Fiber with PS-*b*-P4VP

The hollow fibers were spun by dry-jet wet spinning using a triple orifice spinneret. The dimension of the spinneret used for the results of this chapter is shown in **Figure 7.2**.
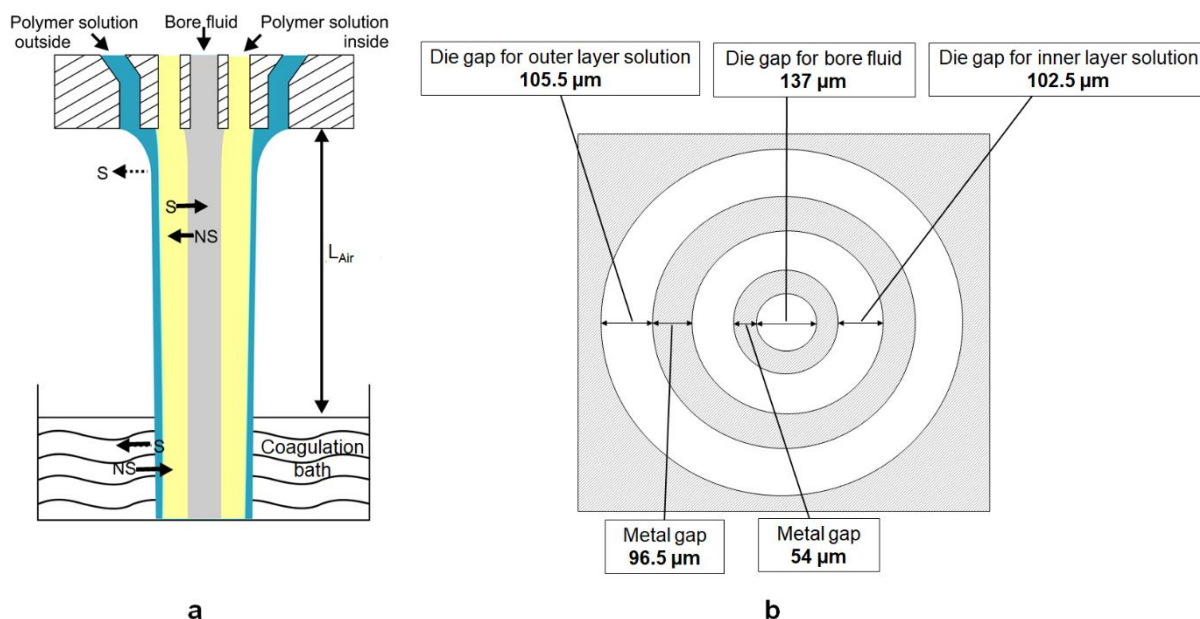
Figure 7.2 (a) Spinning of double layer hollow fibers by co-extrusion: Polymer solutions are extruded simultaneously along with bore fluid from a triple-orifice spinneret. After passing a definite distance in air (air gap distance, L_{Air}), nascent fiber is coagulated in non-solvent or coagulation bath;[1] **(b)** Schematic sketch of the cross section of the exit of the triple-orifice spinneret used in the experiments.

In these experiments PS-*b*-P4VP diblock copolymer solution was used as the outer layer dope and solutions of different commercial polymers were used for the inner layer dope. Since a volatile solvent THF was used to prepare the PS-*b*-P4VP solutions, due to its evaporation from the PS-*b*-P4VP solution in the air gap, a concentration gradient evolved along the wall thickness of the outer layer in the direction perpendicular to the hollow fiber axis which led to develop the self-assembled structure on the surface of the hollow fiber. This ordered structure

Chapter 7: Results and Discussion
Double Layer Hollow Fiber Spinning by Co-extrusion
with PS-*b*-P4VP as the Outer Layer Forming Material

on the surface was trapped in the coagulation bath where pores were created by the exchange of solvent (responsible for swelling of minority blocks) with the non-solvent (water in this case).[1, 30, 35] Different combinations of spinning parameters were examined and the results are presented below.

Polyetherimide (PEI), polyethersulfone (PESU), and polyvinylidenefluoride (PVDF) were used as the support layer materials because of their well accepted mechanical properties in membranes formed by non-solvent induced phase separation (NIPS) and good processibility for fiber spinning.[1, 96, 109, 110]

7.2.1 Support Layer of PEI Solution

In these experiments the inner layer solution was made of PEI and the outer layer solution was made of PS-*b*-P4VP. The experiments are divided in three categories-

i. PEI was dissolved in the same solvents as of the block copolymer solution i.e. DMF and THF to increase the possibility of interdiffusion of the components between the layers. The block copolymer had a high molecular weight, $PS_{83.3}$-*b*-$P4VP_{16.7}^{198}$.

ii. PEI was dissolved in the mixture of NMP and GBL to prepare the inner layer solution. The block copolymer used for outer layer solution was $PS_{82.7}$-*b*-$P4VP_{17.3}^{154}$.

iii. PEI was dissolved in the mixture of NMP and GBL to prepare the inner layer solution. The block copolymer used had a low molecular weight, $PS_{79.8}$-*b*-$P4VP_{20.2}^{95}$.

Chapter 7: Results and Discussion
Double Layer Hollow Fiber Spinning by Co-extrusion
with PS-*b*-P4VP as the Outer Layer Forming Material

The solution composition of the block copolymer solutions were optimized in flat sheet geometry beforehand as described in **Chapter 6**. In the spinning experiments, processing parameters were chosen so as to keep the self-assembled isoporous structure on the PS-*b*-P4VP surface which is the prerequisite to go for this type of membrane fabrication. To get an isoporous structure on the surface it is required to maintain a certain ratio of inner to outer layer dope flow rates. For spinning with different support layer solutions this ratio was different every time which turned into non uniformity of the lumen side contour and uneven thickness of the inner layer (**Figure 7.3, 7.6** and **7.7**). Overlooking other features of the hollow fiber, it was aimed to resolve the problem of delamination of the two layers by varying the flow rate of the bore fluid (Q_B), flow rate of dope solutions for the inner layer (Q_I) and outer layer (Q_O), the air gap distance between spinneret and coagulation bath (L_{Air}) over a wide range.[1] The solution compositions and spinning parameters are listed in **Table 7.1** and **7.2**, respectively. The corresponding results are shown in **Figure 7.3, 7.4, 7.5**.

Chapter 7: Results and Discussion
Double Layer Hollow Fiber Spinning by Co-extrusion
with PS-*b*-P4VP as the Outer Layer Forming Material

Table 7.1 Compositions of the spinning solutions

Hollow fiber	Inner layer solution		Outer layer solution		Bore fluid conc. (in wt.%)	Coagul-ation bath conc. (in wt.%)
	Polymer concentration (in wt.%)	Solvent concentration[a] (in wt.%)	Polymer concentration (in wt.%)	Solvent concentration[a] (in wt.%)		
Figure 7.3	25% PEI	75% DMF/THF (60/40)	25% $PS_{83.3}$-*b*-$P4VP_{16.7}$ [198]	75% DMF/THF (50/50)	100% Water	100% Water
Figure 7.4	25% PEI	75% NMP/GBL (73/27)	27% $PS_{82.7}$-*b*-$P4VP_{17.3}$ [154]	73% DMF/THF (60/40)		
Figure 7.5[1]	25% PEI	75% NMP/GBL (73/27)	30% $PS_{79.8}$-*b*-$P4VP_{20.2}$ [95]	70% DMF/THF (50/50)		

[a]Solvent concentration and composition are expressed as x% A/B (y/z), where x is the total solvent concentration in weight% in the solution, and y and z are the weight percentage of solvent A and B, respectively, in the solvent mixture.

Table 7.2 Spinning parameters of the hollow fibers

Hollow fiber	Bore fluid flow rate, Q_B [mL/min]	Inner solution flow rate, Q_I [g/min]	Outer solution flow rate, Q_O [mL/min]	Air gap, L_{Air} [cm]
Figure 7.3	0.7	1.45	0.5	10
Figure 7.4a	0.7	1.1	0.5	5
Figure 7.4b	0.7	1.1	0.5	10
Figure 7.4c	0.7	1.5	0.5	5
Figure 7.4d	0.7	1.5	0.5	10
Figure 7.5a[1]	0.7	1.1	1.1	10
Figure 7.5b	0.7	1.5	1.5	10
Figure 7.5c	0.7	1.5	0.9	10

Chapter 7: Results and Discussion
Double Layer Hollow Fiber Spinning by Co-extrusion
with PS-*b*-P4VP as the Outer Layer Forming Material
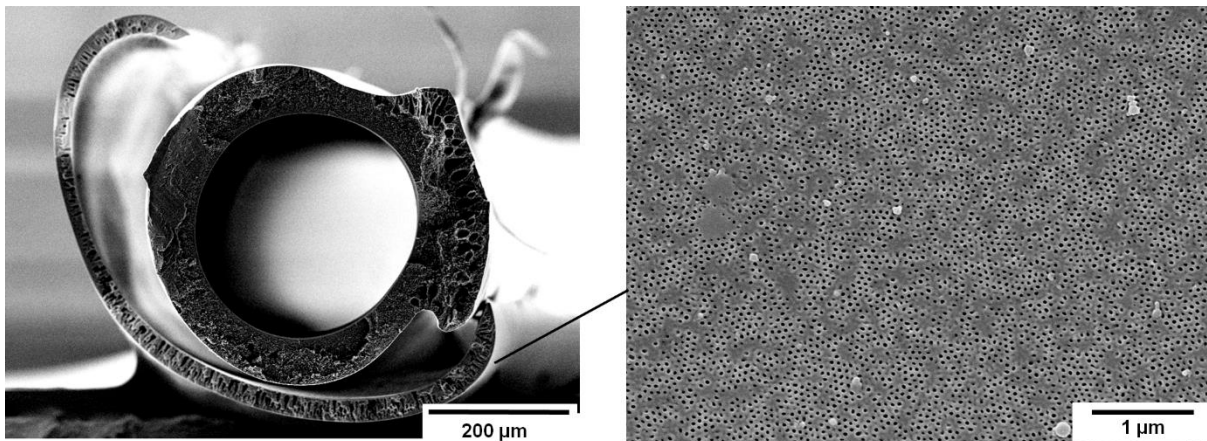
Figure 7.3 SEM micrographs of the cross section and the outer surface of the outer layer of the double layer hollow fiber where 25 wt.% PEI in a mixture of DMF and THF (DMF/THF: 60/40 (wt./wt.)) was used for the inner layer solution and 25 wt.% $PS_{83.3}$-*b*-$P4VP_{16.7}$[198] solution in a mixture of DMF and THF (DMF/THF: 50/50 (wt./wt.)) was used for the outer layer solution.
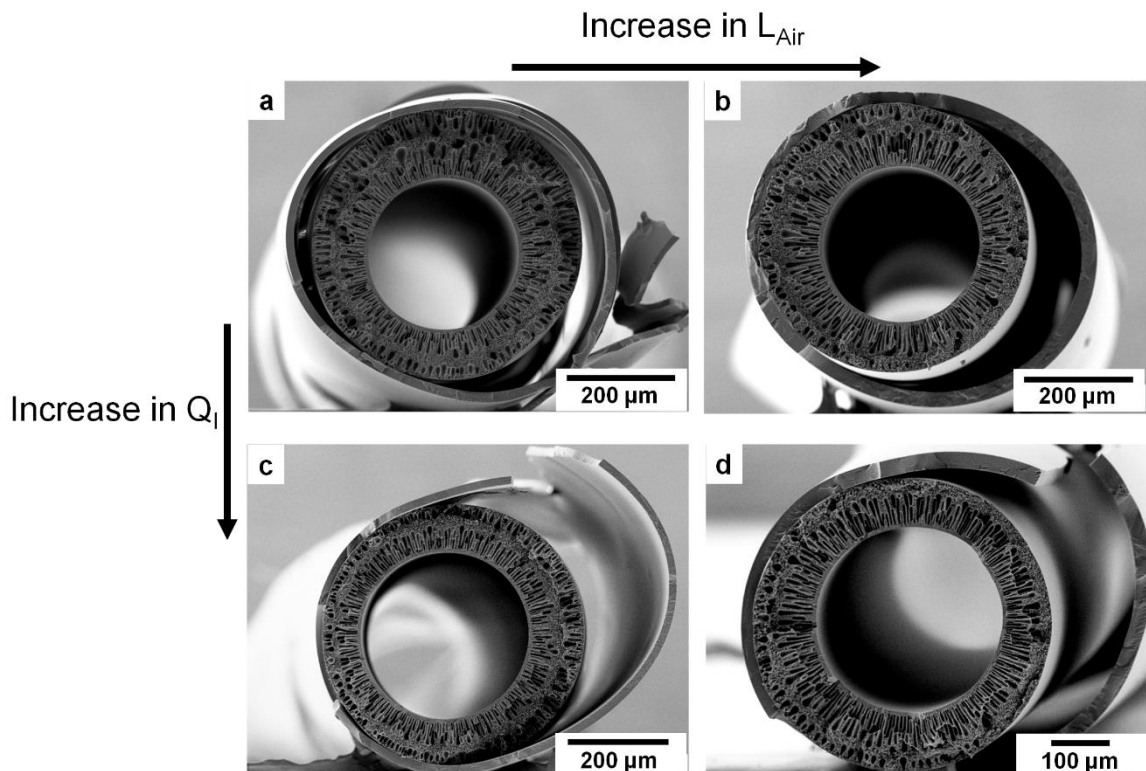
Figure 7.4 SEM micrographs of the cross sections of the double layer hollow fibers where 25 wt.% PEI in a mixture of NMP and GBL (NMP/GBL: 73/27 (wt./wt.)) was used for the inner

Chapter 7: Results and Discussion
Double Layer Hollow Fiber Spinning by Co-extrusion
with PS-*b*-P4VP as the Outer Layer Forming Material

layer solution and 27 wt.% $PS_{82.7}$-*b*-$P4VP_{17.3}$[154] in a mixture of DMF and THF (DMF/THF: 60/40 (wt./wt.)) was used for the outer layer solution.
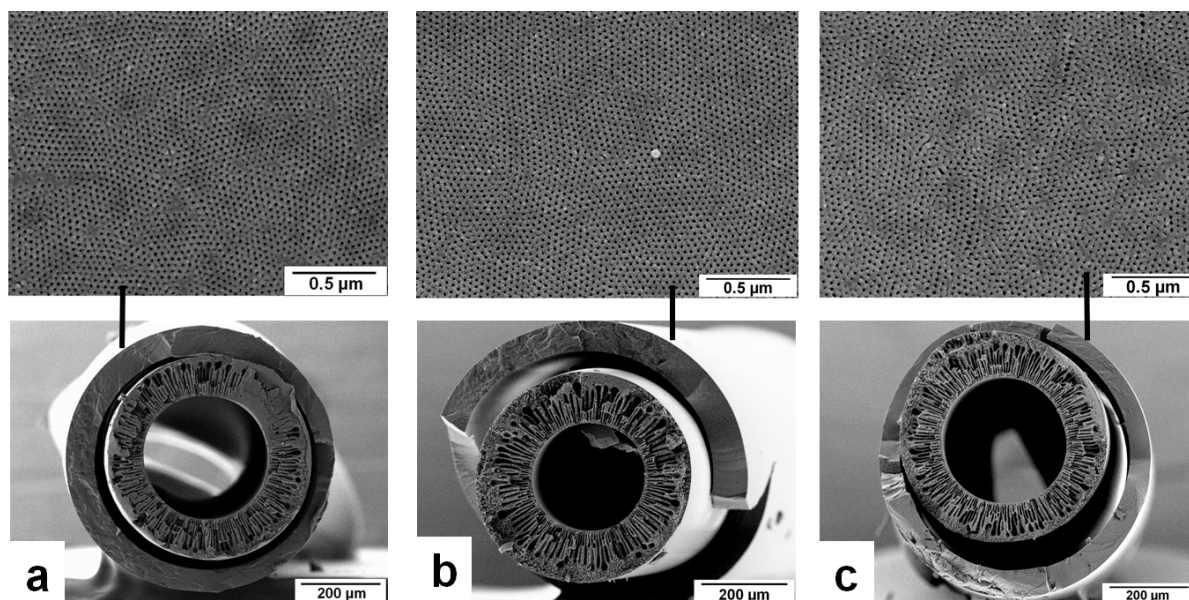
Figure 7.5 SEM micrographs of cross sections and outer surfaces of the outer layer of the double layer hollow fibers where 25 wt.% PEI in a mixture of NMP and GBL (NMP/GBL: 73/27 (wt./wt.)) was used for the inner layer solution and 30 wt.% $PS_{79.8}$-*b*-$P4VP_{20.2}$[95] in a mixture of DMF and THF (DMF/THF: 50/50 (wt./wt.)) was used for the outer layer solution.[1]

Although the processing parameters could be adjusted to achieve an isoporous structure on the outer surface of the PS-*b*-P4VP layer, the two layers always delaminated for any combination of the processing parameters over a wide range. Every combination of the processing parameters ended up with a non-adherence between the layers. The reason for splitting apart of the layers is mainly the incompatibility and uneven shrinkage of the block copolymer and the homopolymer solutions used as the outer and inner layers, respectively.[1]

Chapter 7: Results and Discussion
Double Layer Hollow Fiber Spinning by Co-extrusion
with PS-*b*-P4VP as the Outer Layer Forming Material

7.2.2 Support Layer of PESU Solution

PESU was dissolved in the mixture of NMP and GBL to prepare the inner layer solution. The block copolymer used for this category of experiment was of low molecular weight, $PS_{79.8}$-*b*-$P4VP_{20.2}^{95}$. The solution compositions and spinning parameters are listed in **Table 7.3** and **7.4**, respectively. The corresponding results are shown in **Figure 7.6.**

Table 7.3 Compositions of the spinning solutions[1]

Hollow fiber	Inner layer solution		Outer layer solution		Bore fluid conc.	Coagu-lation bath conc.
	Polymer conc. (in wt.%)	Solvent/non solvent conc.**a)** (in wt.%)	Polymer conc. (in wt.%)	Solvent conc.**a)** (in wt.%)	(in wt.%)	(in wt.%)
Figure 7.6	25% PESU	75% NMP/GBL/SDS (42.5/57/0.5)	30% $PS_{79.8}$-*b*-$P4VP_{20.2}^{95}$	70% DMF/THF (50/50)	100% Water	100% Water

a) Solvent/non-solvent or solvent concentration and composition are expressed as x% A/B/C (w/y/z) and x% A/B (y/z), respectively, where x is the total solvent/non-solvent or solvent concentration in weight% in the solution, and w, y, and z are the weight percentage of the components in the solvent mixture.

Table 7.4 Spinning parameters of the hollow fibers

Hollow fiber	Bore fluid flow rate, Q_B [mL/min]	Inner solution flow rate, Q_I [g/min]	Outer solution flow rate, Q_O [mL/min]	Air gap, L_{Air} [cm]
Figure 7.6a	0.7	2.2	1.1	10
Figure 7.6b[1]	0.5	2.2	1.1	10
Figure 7.6c	0.7	2.2	1.1	5

Chapter 7: Results and Discussion
Double Layer Hollow Fiber Spinning by Co-extrusion
with PS-*b*-P4VP as the Outer Layer Forming Material
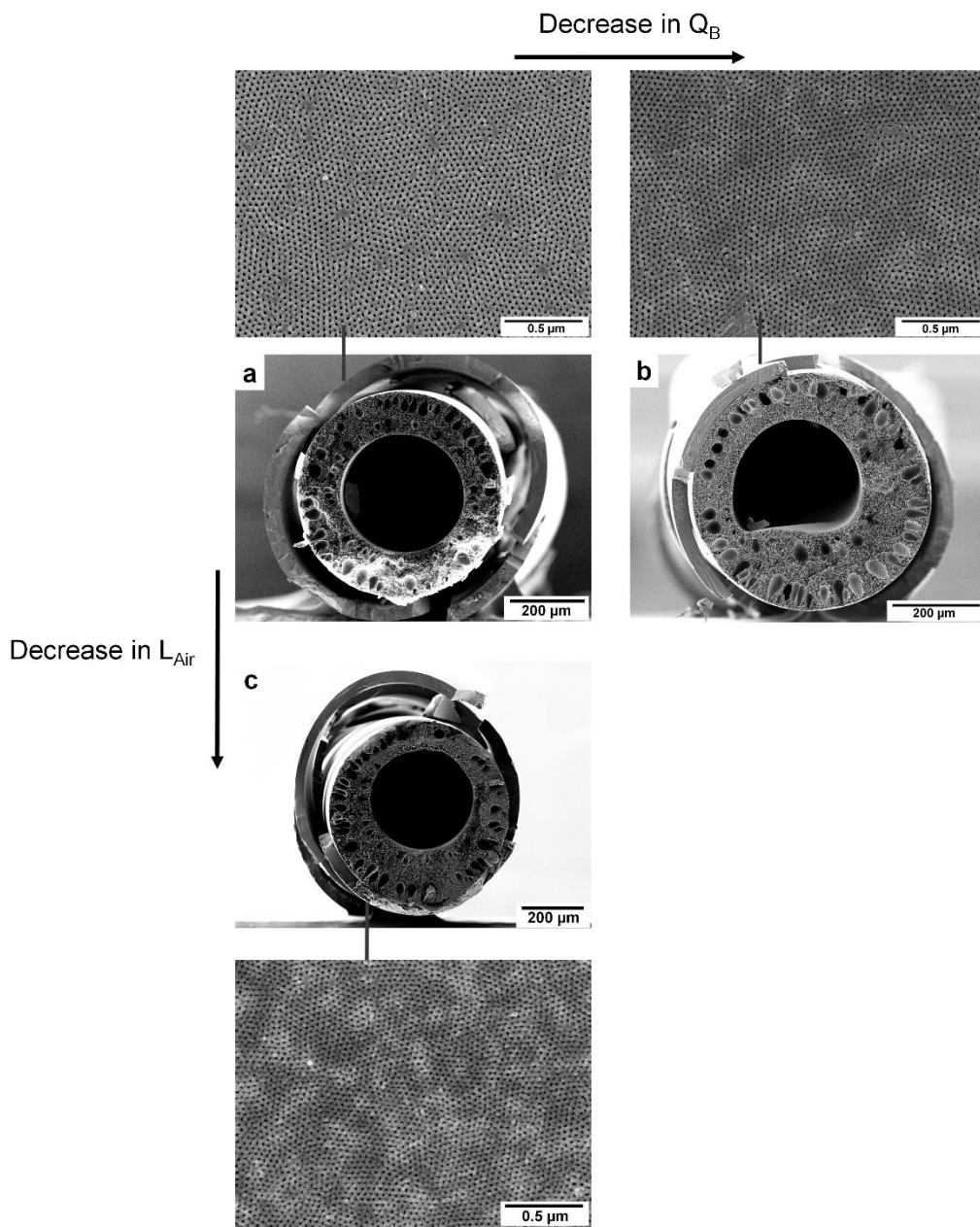
Figure 7.6 SEM micrographs of cross sections and outer surfaces of the outer layer of the double layer hollow fibers where 25 wt.% PESU in a mixture of NMP, GBL, and SDS (NMP/GBL/SDS: 42.5/57/0.5 (wt./wt./wt.)) was used for the inner layer solution and 30 wt.% PS$_{79.8}$-*b*-P4VP$_{20.2}$[95] in a mixture of DMF and THF (DMF/THF: 50/50 (wt./wt.)) was used for the outer layer solution.[1]

Although it was possible to tune the isoporous structure formation on the outer surface of the hollow fibers (**Figure 7.6**), none of the combinations of the processing parameters resulted in

Chapter 7: Results and Discussion
Double Layer Hollow Fiber Spinning by Co-extrusion
with PS-*b*-P4VP as the Outer Layer Forming Material

delamination free hollow fibers. As for example, slowing down the intrusion of non-solvent from the bore fluid side (decrease in Q_B) or plunging the nascent hollow fiber earlier into the coagulation bath (decrease in L_{Air}) could not maintain the integration between the layers at the interfacial region (**Figure 7.6**).

7.2.3 Support Layer of PVDF Solution

PVDF was dissolved in NMP to prepare the inner layer solution. The block copolymer used for this category of experiment was of low molecular weight, $PS_{79.8}$-*b*-$P4VP_{20.2}^{95}$. The solution compositions and spinning parameters are listed in **Table 7.5** and **7.6**, respectively. The corresponding results are shown in **Figure 7.7.**

Table 7.5 Compositions of the spinning solutions[1]

Hollow fiber	Inner layer solution		Outer layer solution		Bore fluid conc.	Coagulation bath conc.
	Polymer conc. (in wt.%)	Solvent conc.**a)** (in wt.%)	Polymer conc. (in wt.%)	Solvent conc.**a)** (in wt.%)	(in wt%)	(in wt.%)
Figure 7.7	25% PVDF	75% NMP (100)	30% $PS_{79.8}$-*b*-$P4VP_{20.2}^{95}$	70% DMF/THF (50/50)	100% Water	100% Water

a)Solvent concentration and composition are expressed as x% A (y) or x% A/B (y/z), where x is the total solvent concentration in weight% in the solution, and y and z are the weight percentage of solvent A and B, respectively, in the solvent mixture.

Chapter 7: Results and Discussion
Double Layer Hollow Fiber Spinning by Co-extrusion
with PS-*b*-P4VP as the Outer Layer Forming Material

Table 7.6 Spinning parameters of the hollow fibers

Hollow fiber	Bore fluid flow rate, Q_B [mL/min]	Inner solution flow rate, Q_I [g/min]	Outer solution flow rate, Q_O [mL/min]	Air gap, L_{Air} [cm]
Figure 7.7a[1]	0.7	1.1	1.1	10
Figure 7.7b	0.7	0.9	1.1	10
Figure 7.7c	0.7	1.1	0.5	10
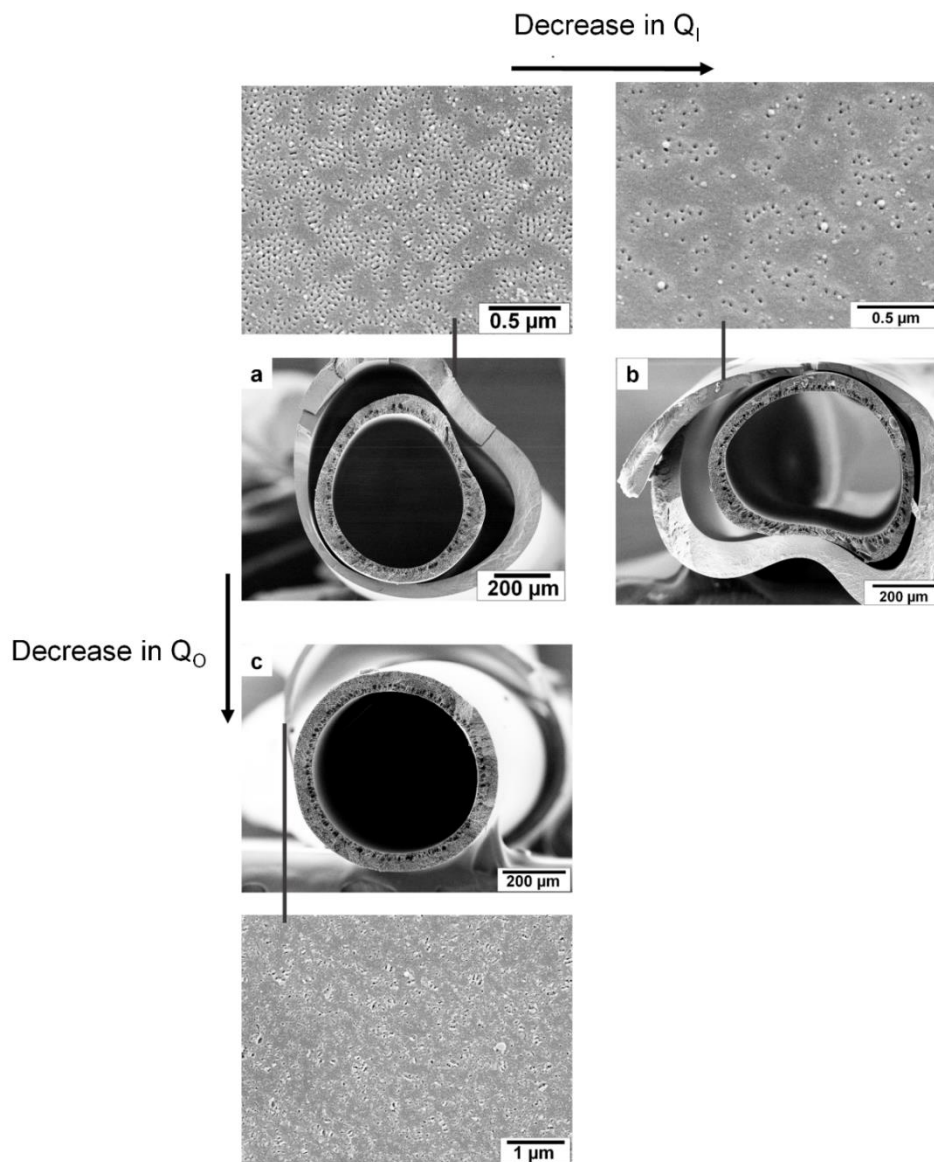
Figure 7.7 SEM micrographs of the cross sections and the outer surfaces of the outer layer of the double layer hollow fibers where 25 wt.% PVDF in NMP was used for the inner layer

Chapter 7: Results and Discussion
Double Layer Hollow Fiber Spinning by Co-extrusion
with PS-*b*-P4VP as the Outer Layer Forming Material

solution and 30 wt.% $PS_{79.8}$-*b*-$P4VP_{20.2}$[95] in a mixture of DMF and THF (DMF/THF: 50/50 (wt./wt.)) was used for the outer layer solution.

As seen before for the use of PEI and PESU, the use of PVDF as the support layer material also did not lead to any solution of the problem of delamination between the support layer and the PS-*b*-P4VP layer (**Figure 7.7**). Whether the combinations of processing parameters resulted in isoporous structure on the outer surface of the outer layer or not, none of the above mentioned experiments led to the amalgamation of the layers at the interface.

Some mechanisms highly contribute to the adhesion between the layers, such as- relative energy difference (RED), the control over precipitation rate of the two layers, diffusion of components through the layers. In previous studies these mechanisms were directed in an optimum path to ensure the adherence of the layers at their interface.[99, 111-114] But in the case of using PS-*b*-P4VP for one of the layers in co-extrusion the compatibility factor prevails over other factors and therefore no optimum combination of solution and spinning parameters were found to eliminate the non-adherence between the layers.

Besides optimizing the processing parameters there are several other methods reported in the literatures to eliminate the delamination between outer and inner layers. One of the techniques is the heat treatment of the double layer hollow fiber where the two layers are formed of two different polymers with a vast difference in their glass transition temperature, T_g (outer layer of lower T_g polymer). In the previous works it was shown that if the double layer hollow fiber was annealed at a temperature above the T_g of the outer layer forming polymer it helped eliminating delamination between the layers because of the relaxation of the polymer chains and so the release of the stress.[115] This technique was facilitated by the incorporation of the

Chapter 7: Results and Discussion
Double Layer Hollow Fiber Spinning by Co-extrusion
with PS-*b*-P4VP as the Outer Layer Forming Material

nanoparticles into the inner layer dope solution to reduce its densification.[116, 117] This kind of heat treatment cannot be applied to the hollow fiber membranes where PS-*b*-P4VP is used since the ordered structure formed on its surface by SNIPS process will not be intact afterwards and the reason to employ the block copolymers for isoporous membrane formation will be overruled.

The problem of disintegration between the layers of a double layer hollow fiber membrane where the outer layer was formed by PS-*b*-P4VP was solved by Hilke *et al.* by using PS as support layer material which was chemically similar to the continuous phase of the selective layer (PS-*b*-P4VP).[40] But using PS as a support layer kept the problem of brittleness since PS itself is responsible for the poor mechanical properties of the membranes. Moreover, selecting materials for support layer on the basis of miscibility narrow the scope of material selection for the support layer.[1]

In this PhD work an approach was followed for the first time to develop an isoporous double layer hollow fiber of improved mechanical stability by solving the problem of delamination *in-situ* without increasing the number of processing steps and the procedure is described in the next chapter.

Chapter 8

Results and Discussion

Double Layer Isoporous Hollow Fiber Membrane by
***In-situ* Hydrogen Bond Formation in the Spinning Line**

The basic pyridine groups of PS-*b*-P4VP can form hydrogen bonds with hydrogen donor organic molecules. By using this feature of the P4VP block, works have been reported on modification of the self-assembled structure of such block copolymers[118, 119] and the change of pore sizes in membranes of such block copolymers.[120] Therefore, an attempt was taken to utilize the hydrogen bonding acceptor nature of P4VP block of the block copolymer at the interface of two layers by introducing acidic groups in the support layer material.[1] The experiment and their results are discussed in the following sections.

8.1 Co-extrusion of Double Layer Hollow Fiber

The hollow fibers were spun by the dry-jet wet spinning method by using a triple orifice spinneret and the dimension of the spinneret used for the experiments of this chapter is shown in **Figure 8.1**. In these experiments PS-*b*-P4VP diblock copolymer solution was used for outer layer dope and blend solution of homopolymer and random copolymer (PESU and functionalized PESU) was used for inner layer dope.[1]

The membrane formation by NIPS method and the isoporous structure formation on the outer surface were directed as the same way as is described in the previous chapters.
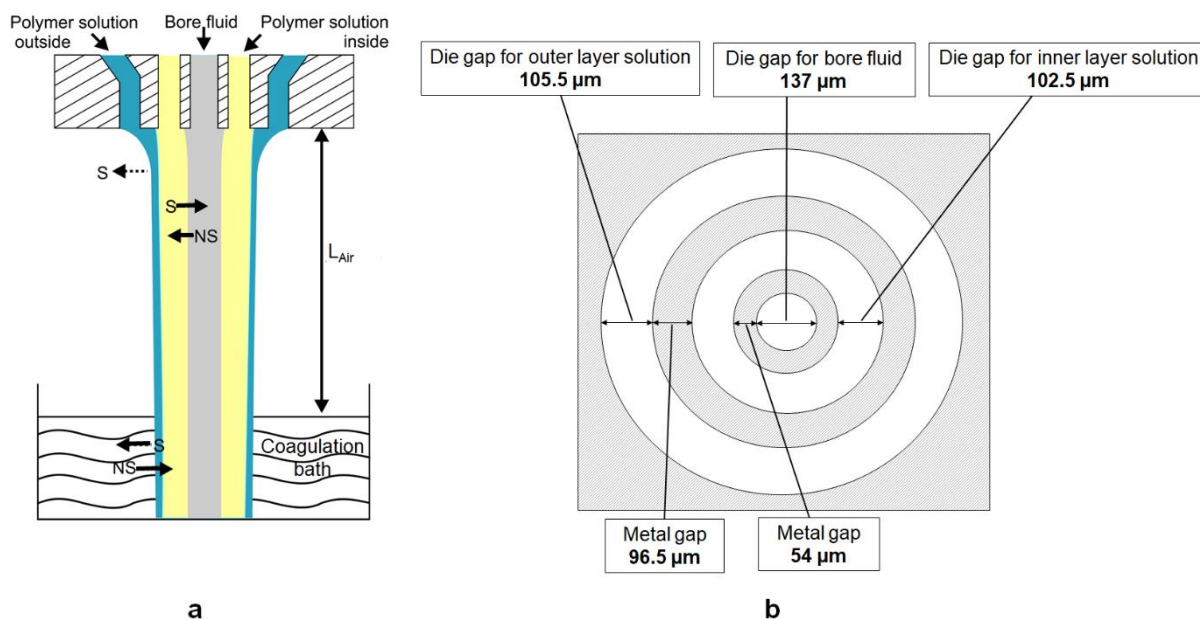
Figure 8.1 (a) Spinning of double layer hollow fiber by co-extrusion: Polymer solutions are extruded simultaneously along with bore fluid from a triple-orifice spinneret. After passing a definite distance in air (air gap distance, L_{Air}), nascent hollow fiber is coagulated in non-solvent bath; **(b)** Schematic sketch of the cross section of the exit of the triple-orifice spinneret used in the experiments.[1]

8.2 Functionalization of the Support Layer Material

For the formation of the support layer a commercially available polymer PESU (Ultrason® E6020P) was chosen and was sulfonated by using chlorosulfonic acid (ClSO$_3$H) as sulfonating agent and dichloromethane (CH$_2$Cl$_2$) as solvent by following the previously reported procedure in the reference[1, 121] which is described in **Chapter 3**.

It was preferential to keep a low degree of sulfonation of PESU as higher degrees of conversion would compromise the mechanical and thermal properties of the membranes and render the problem of precipitation of sulfonated PESU (sPESU) in water during fiber formation.[7, 39, 122]

Therefore the degree of sulfonation (DS) was maintained at around 10% by controlling the reaction time and the amount of acid.[1] ^{1}H NMR results are shown in the next section.

8.2.1 ^{1}H NMR of the Polymers

PESU and sPESU were characterized by ^{1}H NMR spectroscopy by recording spectra on a Bruker advance 500 NMR spectrometer at 500 MHz where tetramethylsilane (TMS) was used as internal standard and deuterated dimethyl sulfoxide (d_6-DMSO) as solvent.

Degree of sulfonation (DS) was measured by using equation (8.1).

$$\frac{I_b}{4I_{a1}} = \frac{1-DS}{DS} \qquad (8.1)$$

where, I_b and I_{a1} are the integral area of peak b and a1 respectively.[1]
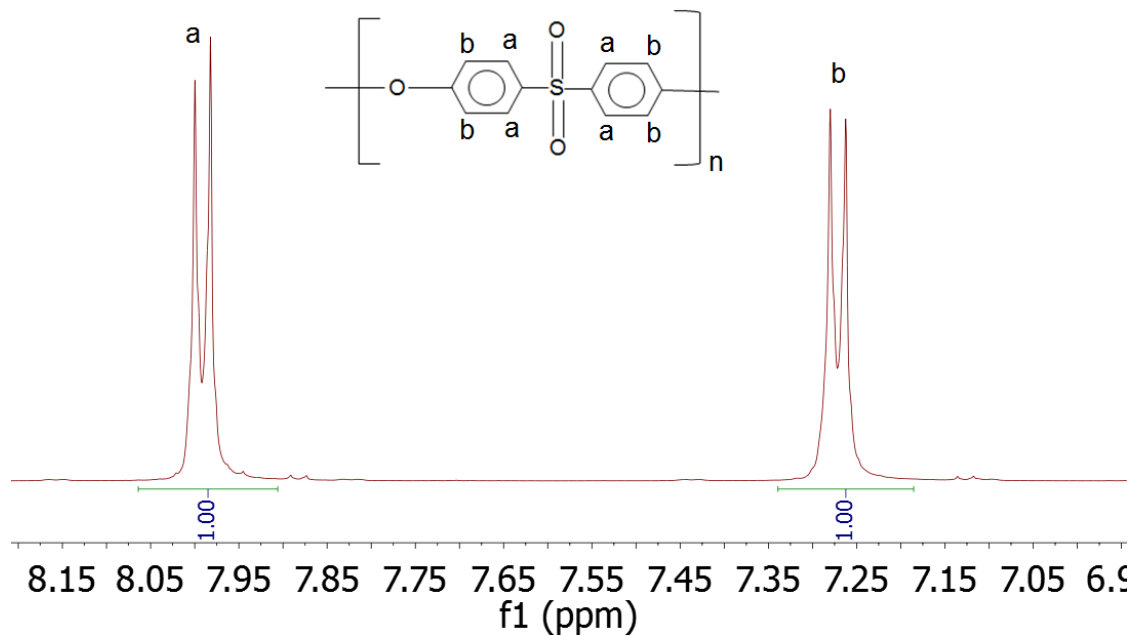
Figure 8.2 ¹H NMR spectra of PESU[1]
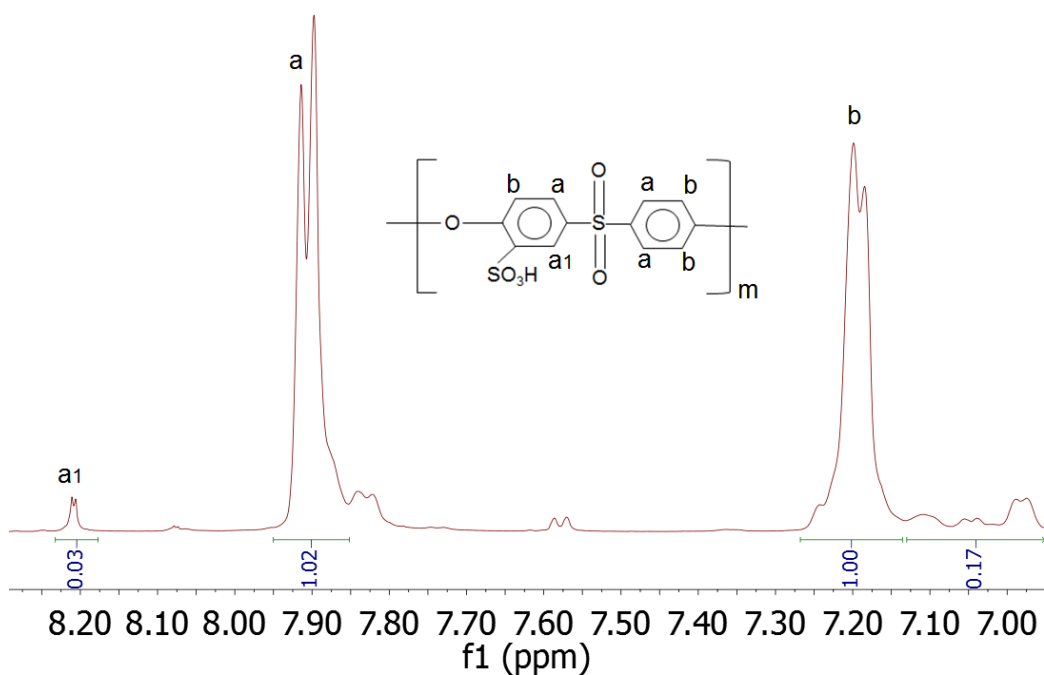
Figure 8.3 ¹H NMR spectra of sPESU[1]

From equation 8.1 the calculated value of DS is 10.7%. In the following discussion this sulfonated PESU (sPESU) is denoted as sPESU10.

8.3 Fabrication of Double Layer Hollow Fiber by using sPESU10 and PS-*b*-P4VP

sPESU10 was taken as a blend partner with PESU for preparing the support layer dope solution. 25 wt.% polymer solution was prepared in 1-methyl-2-pyrrolidone (NMP) by using 40 wt.% sPESU10 of the total polymer concentration (DSC thermogram of this blend is shown in Appendix). For the outer layer, 25 wt.% of $PS_{82.8}$-*b*-$P4VP_{17.2}$[166] was dissolved in a solvent mixture of DMF and THF (DMF/THF: 60/40 (wt./wt.)). Water was used as bore fluid or internal coagulant with the flow rate (Q_B) of 0.7 mL/min. The hollow fiber was spun by keeping the ratio of dope flow rates (Q_I/Q_O) of 1 and after passing 10 cm distance in air (L_{Air}) nascent hollow fibers were coagulated in water. This spinning process was performed at 21°C and the hollow fibers were dried in air at 21°C.[1] **Table 8.1** and **8.2** enlist the spinning solution compositions and the processing parameters, respectively. **Figure 8.4** shows the cross section and surface morphology of the hollow fiber which was spun by using the aforementioned solutions and parameters.

Table 8.1 Compositions of the spinning solutions[1]

Hollow fiber	Composition of inner layer solution		Composition of outer layer solution		Bore fluid conc.	Coagul-ation bath conc.
	Polymer conc.**a)**	Solvent conc.	Polymer conc.	Solvent conc.**b)**		
	(in wt.%)	(in wt.%)	(in wt.%)	(in wt.%)	(in wt.%)	(in wt.%)
Figure 8.4	25% PESU/sPESU10 (60/40)	75% NMP	25% of $PS_{82.8}$-*b*-$P4VP_{17.2}$[166]	75% DMF/THF (60/40)	100% Water	100% Water

a)Polymer concentration and composition are expressed as x% A/B (y/z), where x is the total polymer concentration in weight% in the solution, and y and z are the weight percentage of polymer A and B, respectively, in the polymer blend. **b)**Solvent concentration and composition is expressed as w% C/D (u/v), where w is the total solvent concentration in weight% in the solution, and u and v are the weight percentage of solvent C and D, respectively, in the solvent mixture.

Table 8.2 Spinning parameters of the hollow fibers[1]

Hollow fiber	Bore fluid flow rate, Q_B [mL/min]	Inner solution flow rate, Q_I [mL/min]	Outer solution flow rate, Q_O [mL/min]	Air gap, L_{Air} [cm]
Figure 8.4	0.7	1	1	10
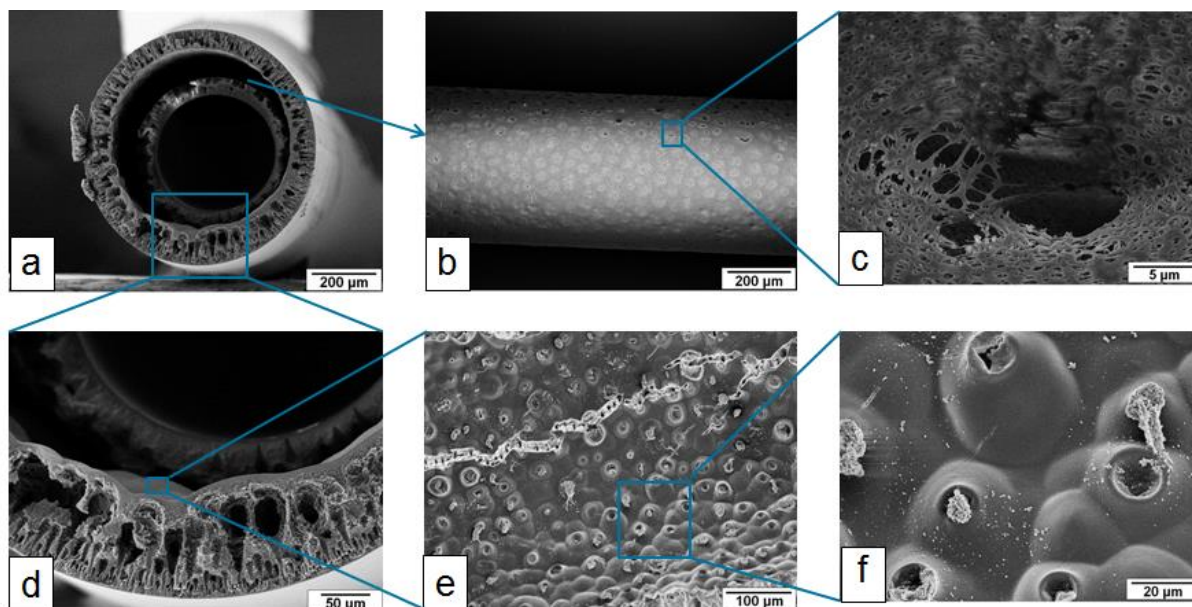
Figure 8.4 SEM micrographs of the double layer hollow fiber spun by using 25 wt.% polymer blend (PESU/sPESU10: 60/40 (wt./wt.)) in NMP as inner layer dope solution and 25 wt.% $PS_{82.8}$-*b*-$P4VP_{17.2}$[166] in a mixture of DMF and THF (DMF/THF: 60/40 (wt./wt.)) as outer layer dope solution, water as both bore fluid and external coagulant. **(a)** Cross section of the double layer hollow fiber; **(b)** Outer surface of the inner layer; **(c)** Grooves in the outer surface of the inner layer in magnified view; **(d)** Part of the cross section shown in (a); **(e)** Inner surface of the outer layer; **(f)** Magnified view of the inner surface of the outer layer.[1]

Figure 8.4a indicates the presence of delamination of layers even after using sPESU10 in the inner layer dope solution. To study the interfacial surface morphology, the layers of the double layer hollow fiber were separated mechanically. **Figure 8.4b** shows the outer surface of the inner layer along the length of the hollow fiber. Small ruptured cavities were present all over the surface which is more clearly illustrated in **Figure 8.4c** in a magnified view. The interfacial surface of PS-*b*-P4VP layer (that is the inner surface of outer layer) showed a protruded or bulge structure throughout its surface (**Figure 8.4e** and **8.4f**). The surface feature at the interface led to the assumption that after interacting with each other these layers got separated because of high interfacial tension. This could happen if the formation of interactions of the

chains of the inner layer with the chains of the outer layer was suppressed by the fast intrusion of coagulant from the lumen side. This might result in chains which were folded back to the layer they belonged to. To check this hypothesis the interfacial region was analyzed by elemental mapping.[1]

8.3.1 Elemental Analysis by Energy Dispersive Microanalysis (EDS)

Figure 8.5a shows the SEM micrograph of the hollow fiber which was filled with epoxy resin. The constituent material for the inner layer was PESU blended with sPESU10 and for the outer layer it was PS-*b*-P4VP. So both layers were rich in carbon (C) and this is clearly visible from the C-mapping (**Figure 8.5b**). Since there was sulfur (S) in the constituent polymer of the inner layer it is not surprising that a sulfur rich area in the inner layer was observed (**Figure 8.5c**). Moreover, a fine line of sulfur (S) is clearly visible along the inner edge of the outer layer. The surface morphology of the interface found in **Figure 8.4** can be explained more clearly by the presence of sulfur at the PS-*b*-P4VP layer. Since basic groups of the block copolymer are able to form hydrogen bonds with the acid groups of sPESU10, PS-*b*-P4VP and sPESU10 of the inner layer interacted with each other after the two layers got into contact with each other outside the spinneret. But since a strong coagulant (water) was used as the bore fluid, the precipitation front from the lumen side reached the interface through the wall thickness of the hollow fiber in a shorter time than the time required for the formation of the attractive interactions between basic groups and acid groups of the layers (illustrated in **Figure 8.6**). Therefore the shallow interaction between the layers was destroyed because of high tension created at the interface region and the two layers lost adherence between them. But the sPESU10 chains which formed hydrogen bonds with the PS-*b*-P4VP chains were pulled out to the outer layer side and this may explain the presence of sulfur at the outer layer of the hollow fiber (**Figure 8.5c**). Thus the surface of the inner layer got ruptured and this is the reason of

the presence of grooves and ridges at the opposing sides of the interfacial surfaces (**Figure 8.4**). But different solubility parameters of different components present at the interface and different phase inversion mechanism of two different solution systems might also be responsible for the inconsistent morphology at the interfacial surfaces. From this observation the supposition of the interfacial interaction at the interface was strengthened and the next target was to extend the time of interaction between the two layers prior to the coagulation. The hypothesis here about delamination and the approach to remove delamination are in accordance with the previous works which were focused on the delamination of layers both in flat or hollow fiber geometry.[1, 39, 99, 100]
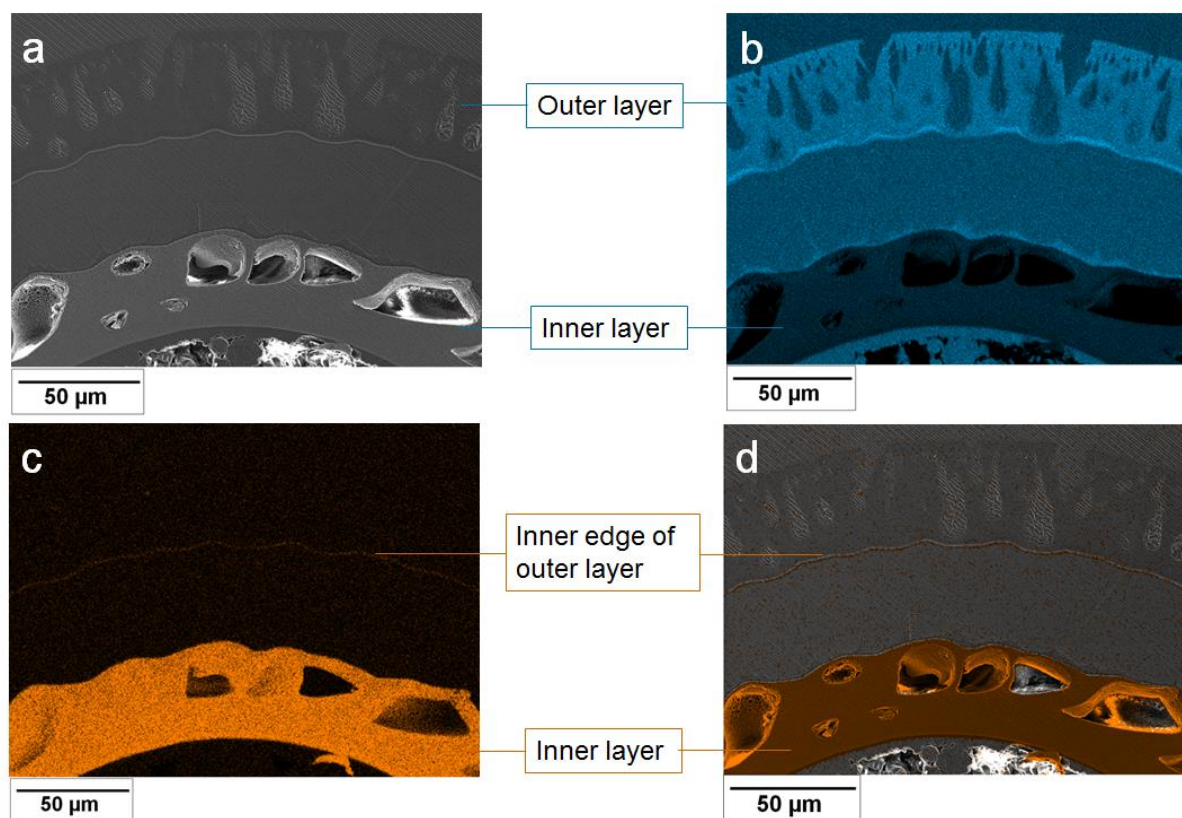
Figure 8.5 Double layer hollow fiber spun by using solution of 25 wt.% polymer blend (PESU/sPESU10: 60/40 (wt./wt.)) in NMP as inner layer dope and 25 wt.% $PS_{82.8}$-*b*-$P4VP_{17.2}$[166] solution in a mixture of DMF and THF (DMF/THF: 60/40 (wt./wt.)) as outer layer dope, water as both bore fluid and external coagulant. **(a)** Secondary electron (SE) image of a

cross section of the double layer hollow fiber embedded in epoxy resin; **(b)** Elemental mapping of carbon (C) by EDS; **(c)** Elemental mapping of sulfur (S) by EDS; **(d)** Overlay of sulfur (S) distribution by EDS on secondary electron (SE) image.[1]
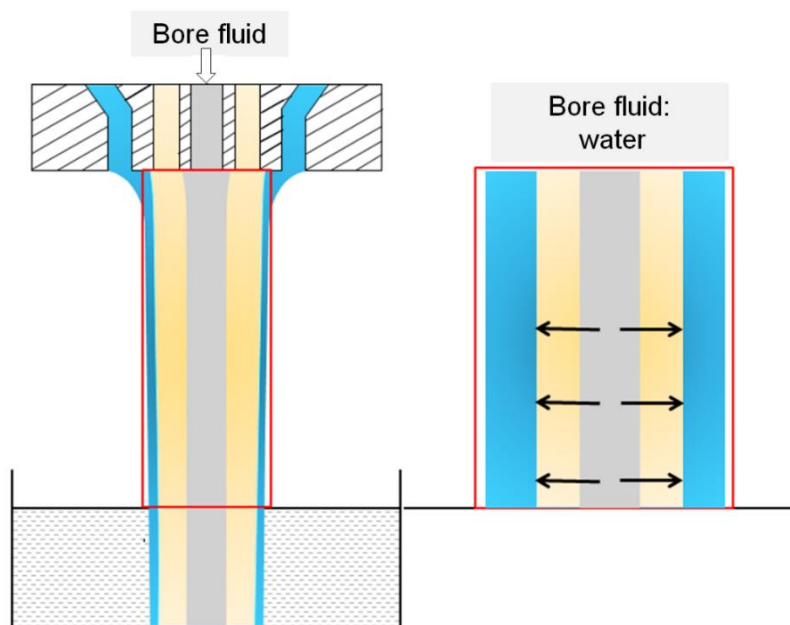
Figure 8.6 Illustration of the intrusion of water towards the interface when water was used as the bore fluid to spin hollow fiber. ⟶ Indicates the faster intrusion of water from the lumen side disturbs the interface between the layers before the hollow fiber is plunged into the coagulation bath.

8.3.2 Co-extrusion of Double Layer Hollow Fiber by using Bore Fluid of Solvent and Water

To decelerate the intrusion of coagulant from the lumen side to the interface of the two layers a solvent-water mixture was used as the bore fluid instead of pure water. A water/NMP mixture of 80/20 (wt./wt.) was used as an internal coagulant. The dope solution for the inner layer was prepared by keeping the same composition of PESU, sPESU10, and NMP as mentioned before

in the **section 8.3**. And for the outer layer dope solution 26 wt.% of $PS_{83.3}$-*b*-$P4VP_{16.7}$[168] was

dissolved in a solvent mixture of DMF and THF (DMF/THF: 60/40 (wt./wt.)). Water was

chosen as the external coagulant. The hollow fibers were spun at a constant flow rate of the

bore fluid (Q_B= 0.7 mL/min) and a constant air gap distance (L_{Air} = 10 cm). The solution

compositions and the spinning parameters are listed in **Table 8.3** and **8.4**, respectively.[1]

Table 8.3 Compositions of the spinning solutions[1]

| Hollow fiber | Inner layer solution | | Outer layer solution | | Bore fluid conc. | Coag-ulation bath conc. |
	Polymer conc.[a] (in wt.%)	Solvent conc. (in wt.%)	Polymer conc. (in wt.%)	Solvent conc.[b] (in wt.%)	(in wt.%)	(in wt.%)
Figure 8.7	25% PESU/sPESU10 (60/40)	75% NMP	26% of $PS_{83.3}$-*b*-$P4VP_{16.7}$[168]	74% DMF/THF (60/40)	100% Water/NMP (80/20)	100% Water

[a]Polymer concentration and composition are expressed as x% A/B (y/z), where x is the total polymer concentration in weight% in the solution, and y and z are the weight percentage of polymer A and B, respectively, in the polymer blend. [b]Solvent concentration and composition is expressed as w% C/D (u/v), where w is the total solvent concentration in weight% in the solution, and u and v are the weight percentage of solvent C and D, respectively, in the solvent mixture.

Table 8.4 Spinning parameters of the hollow fibers[1]

Hollow fiber	Bore fluid flow rate, Q_B [mL/min]	Inner solution flow rate, Q_I [mL/min]	Outer solution flow rate, Q_O [mL/min]	Air gap, L_{Air} [cm]
Figure 8.7a	0.7	1	1	10
Figure 8.7b	0.7	1.2	1	10
Figure 8.7c	0.7	1.5	1	10

For the dope solution flow rate ratio of 1 ($Q_I/Q_O = 1$), the double layer hollow fiber showed good adhesion in some parts and delamination in some other parts (**Figure 8.7a**). With the increase in dope flow rate ratio the interfacial adhesion was improved (**Figure 8.7b**) and finally with the dope solution flow rate ratio of 1.5, a delamination free double layer hollow fiber was obtained (**Figure 8.7c**).[1]
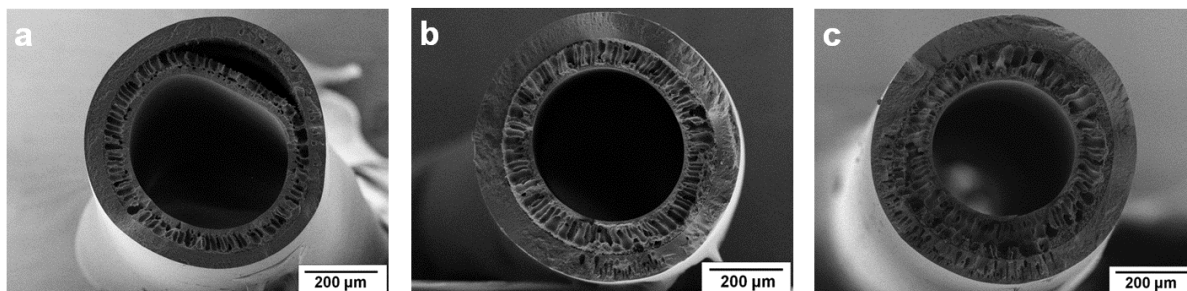
Figure 8.7 Cross section of double layer hollow fibers spun by using solution of 25 wt.% polymer blend (PESU/sPESU10: 60/40 (wt./wt.)) in NMP as inner layer dope, 26 wt.% PS$_{83.3}$-*b*-P4VP$_{16.7}$[168] solution in a mixture of DMF and THF (DMF/THF: 60/40 (wt./wt.)) as outer layer dope, water/NMP mixture (water/NMP: 80/20 (wt./wt.)) as bore fluid, and water as external coagulant. **(a)** Ratio of flow rates, $Q_I/Q_O = 1$; **(b)** Ratio of flow rates, $Q_I/Q_O = 1.2$; **(c)** Ratio of flow rates, $Q_I/Q_O = 1.5$.[1]

The analysis of the interfacial region of the hollow fiber shown in **Figure 8.7c** is shown in **Figure 8.8**. The interface of the hollow fiber illustrates good interconnection between the two layers and a defect free interface all over the cross section (**Figure 8.8b**). So by decreasing the rate of non-solvent intrusion to the interface sufficient time was given for interfacial hydrogen bond formation.[1] Moreover, when using water/NMP (80/20) as the bore fluid instead of water the solidification rate of the inner layer solution was slower. And when the solidification rates of the inner and outer layer are closer to each other then this helps to distribute the stresses more evenly at the interface and this minimizes the occurrence of delamination between the two layers.[123] (The rheological properties of these inner and outer layer solution are shown in Appendix (section 13.2).

It is presumed that the nascent hollow fibers entered into the coagulation bath without getting separated from each other in air or in the spinning line which is a recognized requirement for adhesion of two layers (**Figure 8.9**). The spinning parameters set for this experiment were in accordance to the required time for self-assembling PS-*b*-P4VP into an ordered microphase separated structure. **Figure 8.8c** illustrates the self-assembled surface morphology of the PS-*b*-P4VP layer. But there is room for fine tuning of molecular and process parameters during hollow fiber spinning so that the outer surface forms a well ordered hexagonally packed morphology of uniform pores while keeping a good adherence of both layers.[1]
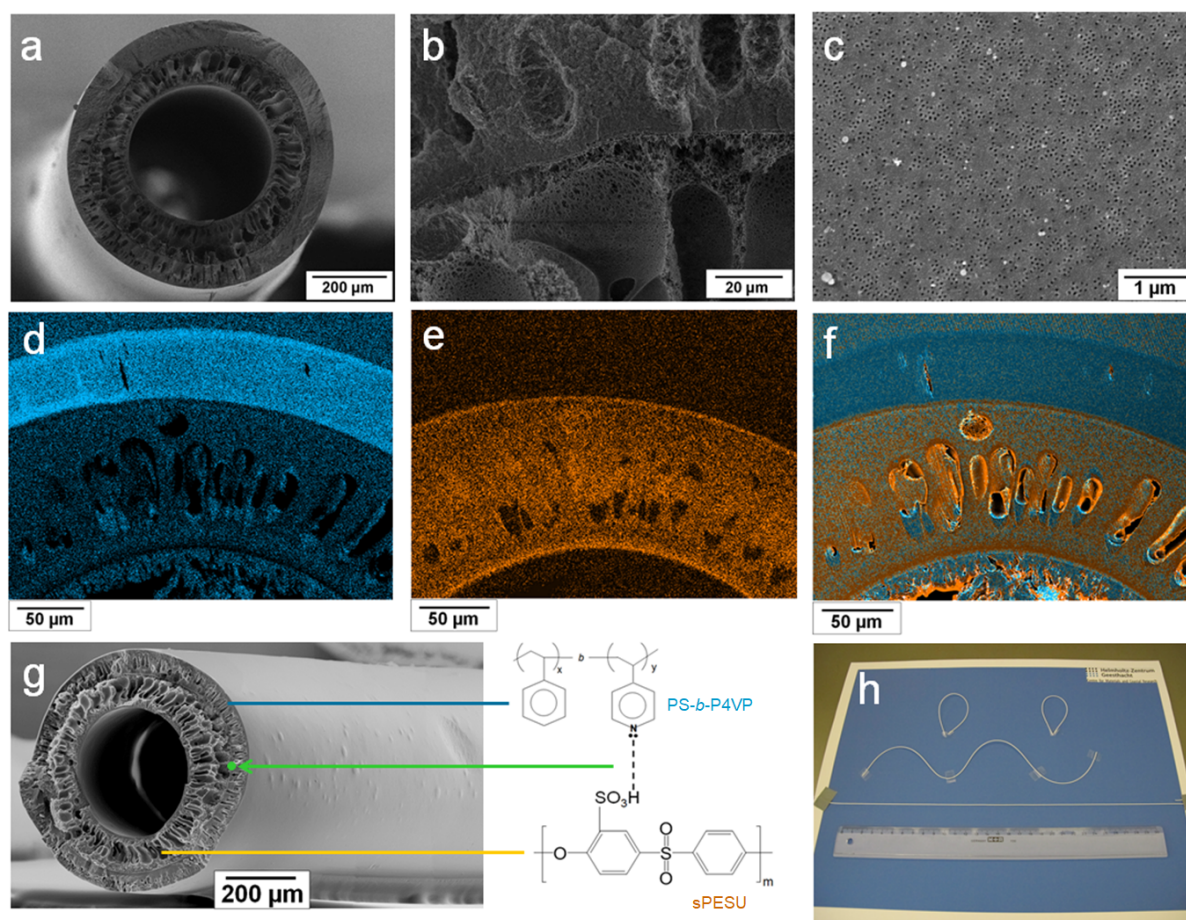
Figure 8.8 Double layer hollow fiber spun by using solution of 25 wt.% polymer blend (PESU/sPESU10: 60/40 (wt./wt.)) in NMP as the inner layer dope, 26 wt.% $PS_{83.3}$-*b*-$P4VP_{16.7}$[168] solution in a mixture of DMF and THF (DMF/THF: 60/40 (wt./wt.)) as the outer layer dope, water-NMP mixture (water/NMP: 80/20 (wt./wt.)) as the bore fluid, and water as the external coagulant. **(a)** Cross section of the double layer hollow fiber; **(b)** Delamination

free interface; **(c)** Outer surface of the outer layer; **(d)** Carbon (C) mapping of the double layer hollow fiber by EDS; **(e)** Sulfur (S) mapping of the double layer hollow fiber by EDS; **(f)** Overlay of carbon (C) and sulfur (S) distribution by EDS on secondary electron (SE) image; **(g)** Good interfacial integrity between the layers along the hollow fiber because of H-bond formation; **(h)** Mechanically stable and bendable PS-*b*-P4VP hollow fiber.[1]

The double layer hollow fiber with seamless interface was analyzed by EDS in the same way as described before (**section 8.3.1**). **Figure 8.8d**, **e**, and **f** show mappings of carbon (C), sulfur (S), and the overlay of the carbon and sulfur distributions on the secondary electron (SE) image of the hollow fiber, respectively. Because of the interfacial bond formation between block copolymer and blend (depicted in **Figure 8.8g**), a double layer hollow fiber with a PS-*b*-P4VP outer layer manifests far better mechanical stability compared to a single layer PS-*b*-P4VP hollow fiber. A visual demonstration of bendability is presented in **Figure 8.8h**.
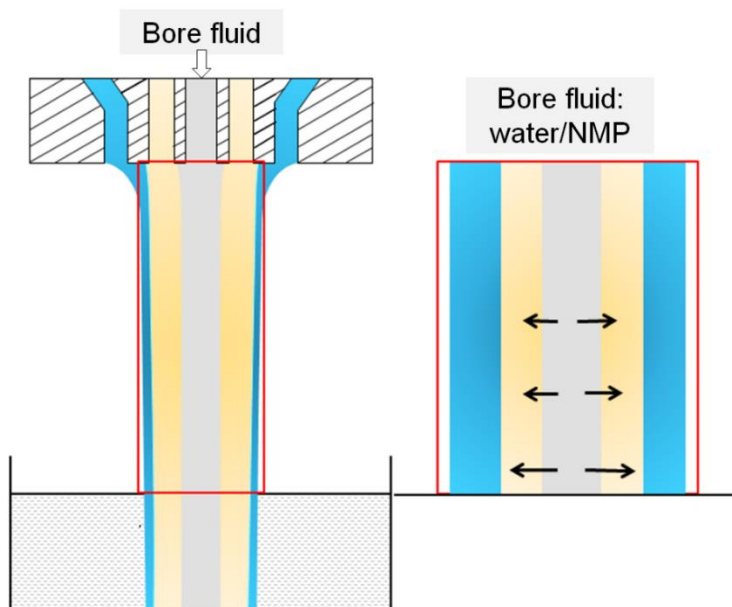
Figure 8.9 Illustration of the intrusion of the bore fluid (mixture of solvent and water) towards

the interface of the nascent hollow fiber. ⟶ Indicates that the interface of the nascent hollow fiber is not disturbed in the air gap by the intrusion of the bore fluid in the air gap.

Finding a commercial polymer suitable as a support layer for NIPS process which makes an isoporous hollow fiber membrane mechanically stable after being spun by co-extrusion was not successful until a blend solution consisting of PESU and sulfonated PESU (sPESU) was employed for this purpose. However, better mechanical properties of this composite membrane comes along with much higher resistance (**Figure 8.10**) due to the substructure than it would be the case of a single layer PS-*b*-P4VP hollow fiber membrane. Therefore, it is necessary to study and modify the PESU/sPESU blend hollow fiber membrane that would provide less resistance and can be engaged as a support layer material for the composite membrane formation by the co-extrusion method in future.
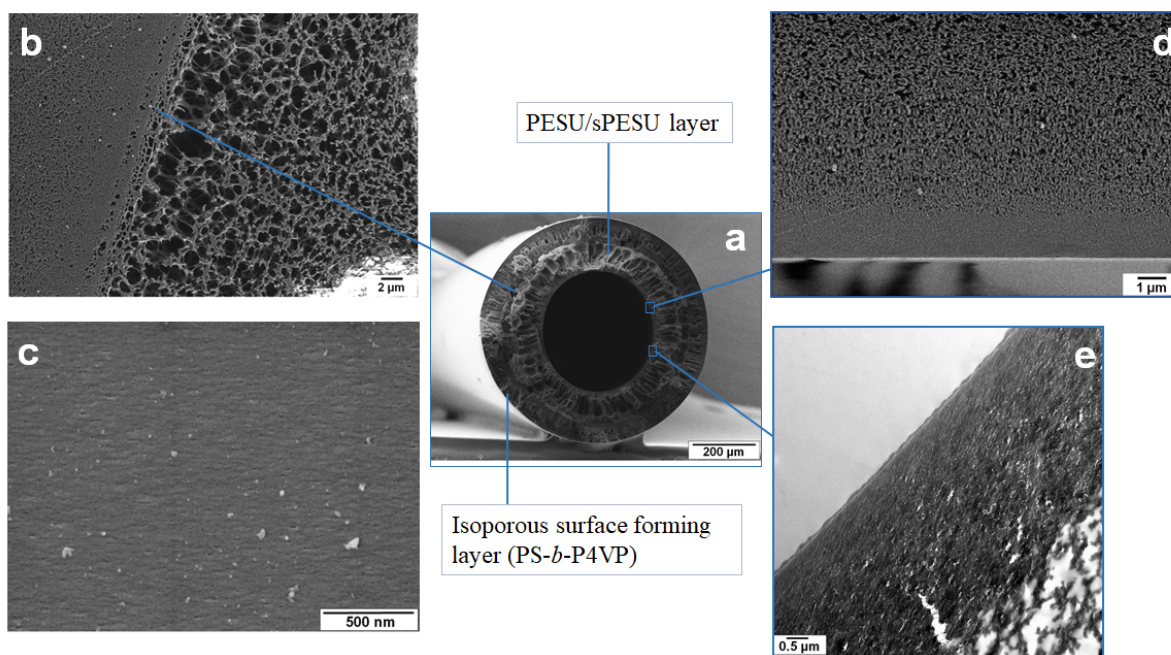
Figure 8.10 Double layer hollow fiber spun by using a solution of 25 wt.% polymer blend (PESU/sPESU10: 60/40 (wt./wt.)) in NMP as the inner layer or support layer dope, 26 wt% PS$_{83.3}$-*b*-P4VP$_{16.7}$[168] solution in a mixture of DMF and THF (DMF/THF: 60/40 (wt./wt.)) as the outer layer dope, water-NMP mixture (water/NMP: 80/20 (wt./wt.)) as the bore fluid, and water as an external coagulant. **(a)** SEM image of the cross section of the double layer hollow fiber;

(b) SEM image of the cross section of the hollow fiber near the interfacial region between the two layers; **(c)** SEM image of the lumen side surface or inner surface of the hollow fiber; **(d)** SEM image of the cross section near the lumen side surface; **(e)** TEM image of the cross sectional area near the lumen side surface.

Chapter 9

Results and Discussion

Characterization and Modification of PESU/Sulfonated Polymer Blends Hollow Fiber Membranes

In this chapter, the characterization and analysis of the single layer hollow fiber membranes which are made from the blend of PESU and sPESU are presented. Membranes spun with different spinning dope compositions and different bore fluids are studied along with their water permeance. The characterization and performance of these membranes are compared also with the hollow fiber membranes made up of commercially available sulfonated polymers, sulfonated polyphenylenesulfone (sPPSU) as a blend partner in the spinning dope solutions.

9.1 Hollow Fiber Spinning by Double Orifice Spinneret

The hollow fibers were spun by the dry-jet wet spinning method by using a double orifice spinneret. The dimensions of the spinneret used for the experiments of this chapter are shown in **Figure 9.1**.
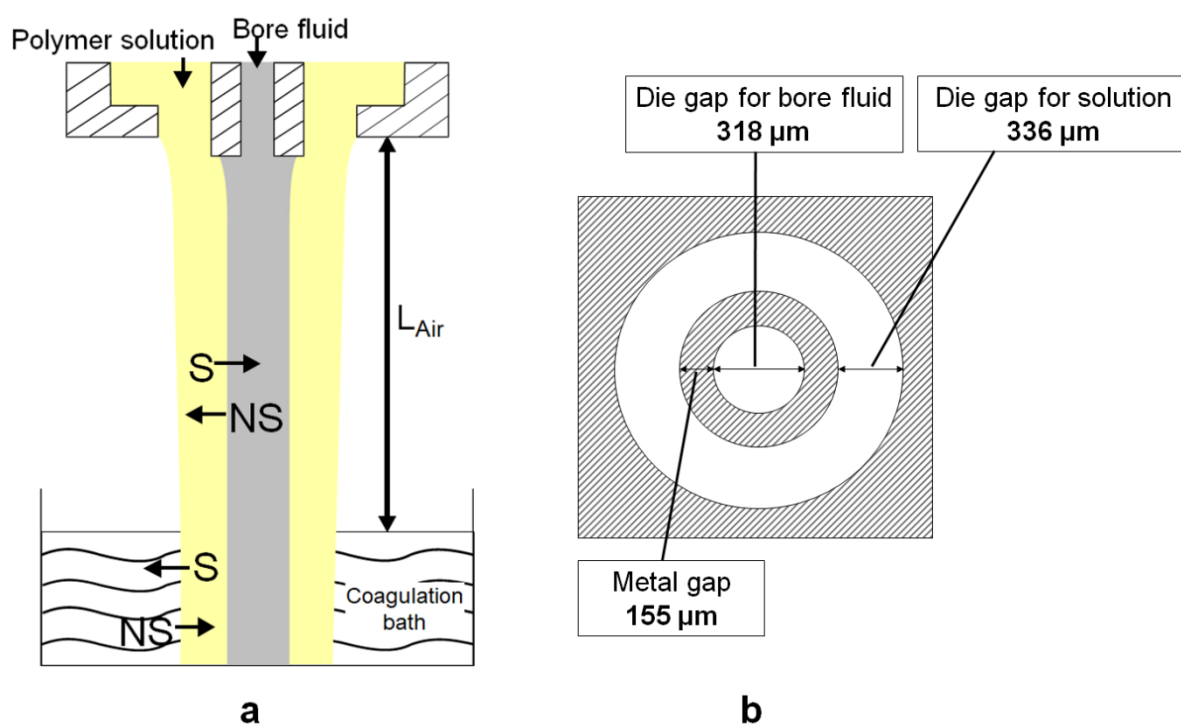
Figure 9.1 (a) Spinning of hollow fiber membrane by NIPS. Polymer solution and bore fluid are extruded simultaneously from a double-orifice spinneret. Nascent hollow fiber enters into

the coagulation bath following a definite air gap distance, L_{Air}; **(b)** Schematic representation of the cross section of the exit of the spinneret used in the experiments.[2]

9.2 Dope Solution with Common Additives

In this section, the effect of the commonly used additives on hollow fibers (**Table 9.1**) is studied. The spinning parameters are listed in **Table 9.2**. The morphology of these hollow fibers is shown in **Figure 9.2**. The spinning dope solution was prepared by keeping a constant blend ratio for PESU and sPESU10 (60 wt.% PESU and 40 wt.% sPESU10). GBL, PVP, and PEG200 were used as additives in the spinning solutions of hollow fibers HF-Ad 01, HF-Ad 02, and HF-Ad 03, respectively.

Table 9.1 Compositions of the spinning solutions and
water flux of the hollow fibers[2]

Membrane code	Polymer concentration & composition[a]	Solvent and additive concentration	Bore fluid composition[b]	Water flux [L m^{-2} h^{-1} bar^{-1}]
HF-Ad 01	25% PESU/sPESU10 (60/40)	54.75% NMP 20.25% GBL	Water/NMP (80/20)	
HF-Ad 02	25% PESU/sPESU10 (60/40)	45% NMP 22.5% GBL 7.5% PVP	Water/NMP (80/20)	Too little to be measured
HF-Ad 03	25% PESU/sPESU10 (60/40)	67.5% NMP 7.5% PEG200	Water/NMP (80/20)	

[a]Polymer concentration and composition are expressed as x% A/B (y/z), where x is the total polymer concentration in weight% in the solution, and y and z are the weight percentage of polymer A and B, respectively, in the polymer blend; [b] bore fluid composition is expressed as C/D (v/w), where v and w are the concentration of C and D, respectively, in weight% in the total bore fluid content.

Table 9.2 Spinning parameters of the hollow fibers shown in **Figure 9.2**[2]

Membrane ID	Flow rate of bore fluid	Flow rate of polymer solution	Air gap, L_{Air}
HF-Ad 01	1.5 g/min	2.5 mL/min	10 cm
HF-Ad 02	1.5 g/min	2 mL/min	10 cm
HF-Ad 03	1.5 mL/min	2 mL/min	10 cm
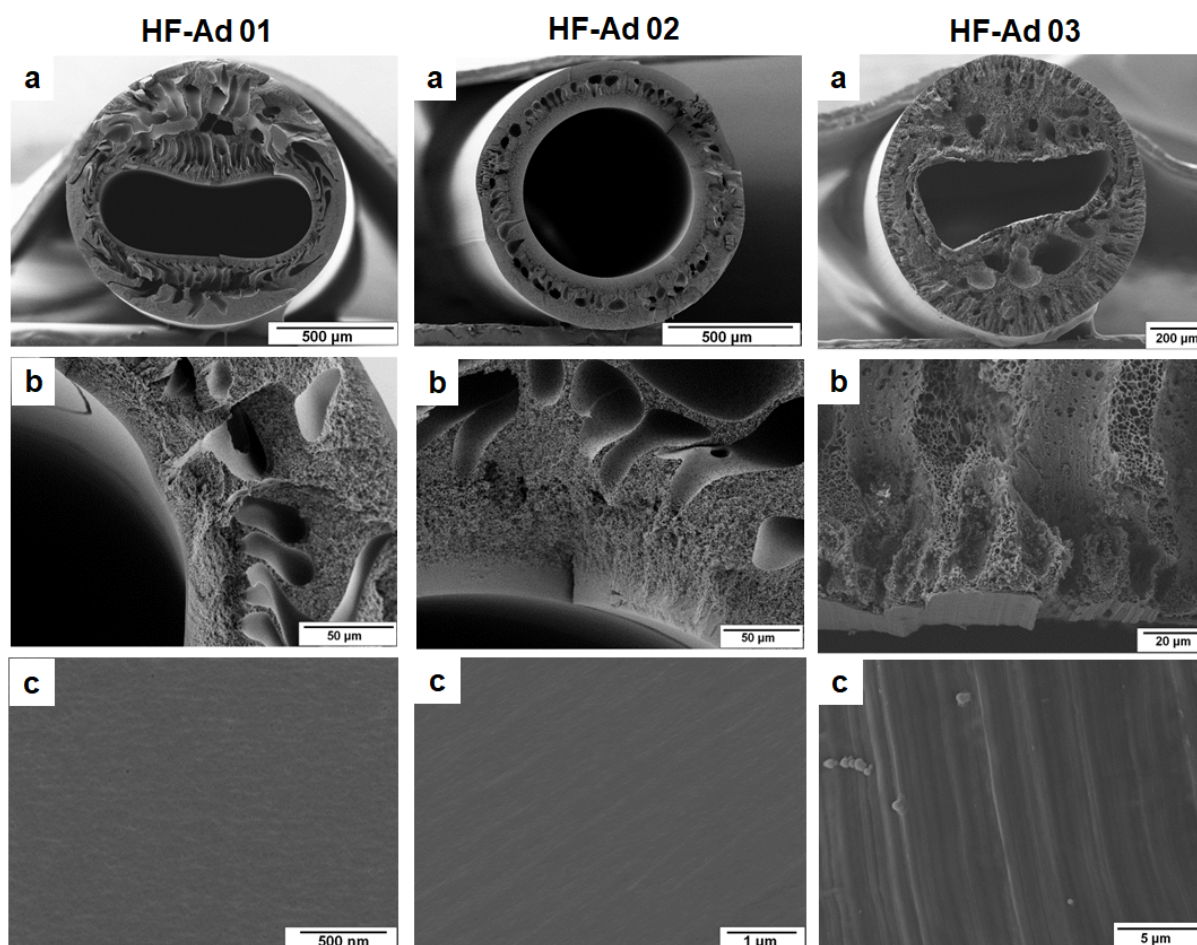
Figure 9.2 Hollow fibers HF-Ad 01, HF-Ad 02, and HF-Ad 03: **(a)** Cross-section of the hollow fiber; **(b)** Cross-sectional structure near the lumen side surface; **(c)** Inner surface or lumen side surface of the hollow fiber.[2]

The morphology of the hollow fiber membranes prepared by the NIPS process was dependent on the components and composition of the dope solution and bore fluid together with the spinning parameters.[102, 124, 125] The SEM images in **Figure 9.2** show that the different additives led to different morphological structures, while the concentration and composition of PESU and sPESU10 were kept constant in the solution (25% of PESU/sPESU10 (60/40) in the solution). The irregular lumen contour of the hollow fibers in the experiments resulted from the mass transfer and hydrodynamic instability as it was observed and explained in previous studies.[50] However, that discussion is out of the scope of this current study. Although the morphology of the hollow fibers HF-Ad 01, HF-Ad 02, HF-Ad 03 (fabricated from three different solution compositions) were different, the water permeance through all of them were too low to be measured. Only a few drops of water permeated through these hollow fibers after 24 h of measurement time at a transmembrane pressure of 1 bar. This circumstance may arise from the non-porous inner surface of the hollow fibers and/or the absence of pore interconnectivity.[2]

9.3 Spinning with Different Bore Fluids

Since the impermeability to water of the hollow fibers listed in **Table 9. 1** may arise from a higher degree of swelling of the sulfonated polymers,[126] the amount of sulfonated polymer in the dope solutions was decreased. The spinning dope solution was prepared by keeping a constant blend ratio for PESU and sPESU10 (90 wt.% PESU and 10 wt.% sPESU10), and the hollow fibers were spun by using different bore fluids. The compositions of the spinning dopes and bore fluids are listed in **Table 9.3**. The spinning parameters are listed in **Table 9.4**. The morphological features of these hollow fibers from SEM micrographs are shown in **Figure 9.3**.

Table 9.3 Compositions of the spinning solutions and
water flux of the hollow fibers[2]

Membrane code	Polymer concentration & composition[a]	Solvent and additive concentration	Bore fluid composition[b]	Water flux [L m^{-2} h^{-1} bar^{-1}]
HF-Bf 01	25% PESU/sPESU10 (90/10)	75% NMP	Water (100)	Too little to be measured
HF-Bf 02	25% PESU/sPESU10 (90/10)	75% NMP	Water/glycerol (50/50)	
HF-Bf 03	25% PESU/sPESU10 (90/10)	75% NMP	Water of pH 2 (100)	
HF-Bf 04	25% PESU/sPESU10 (90/10)	75% NMP	Water of pH 11 (100)	

[a]Polymer concentration and composition are expressed as x% A/B (y/z), where x is the total polymer concentration in weight% in the solution, and y and z are the weight percentage of polymer A and B, respectively, in the polymer blend; [b] bore fluid composition is expressed as C/D (v/w), where v and w are the concentration of C and D, respectively, in weight% in the total bore fluid content.

Table 9.4 Spinning parameters of the hollow fibers shown in **Figure 9.3**[2]

Membrane ID	Flow rate of bore fluid	Flow rate of polymer solution	Air gap, L_{Air}
HF-Bf 01	1 mL/min	0.5 mL/min	10 cm
HF-Bf 02	1 mL/min	0.5 mL/min	10 cm
HF-Bf 03	1 mL/min	1 mL/min	10 cm
HF-Bf 04	1 mL/min	1 mL/min	10 cm
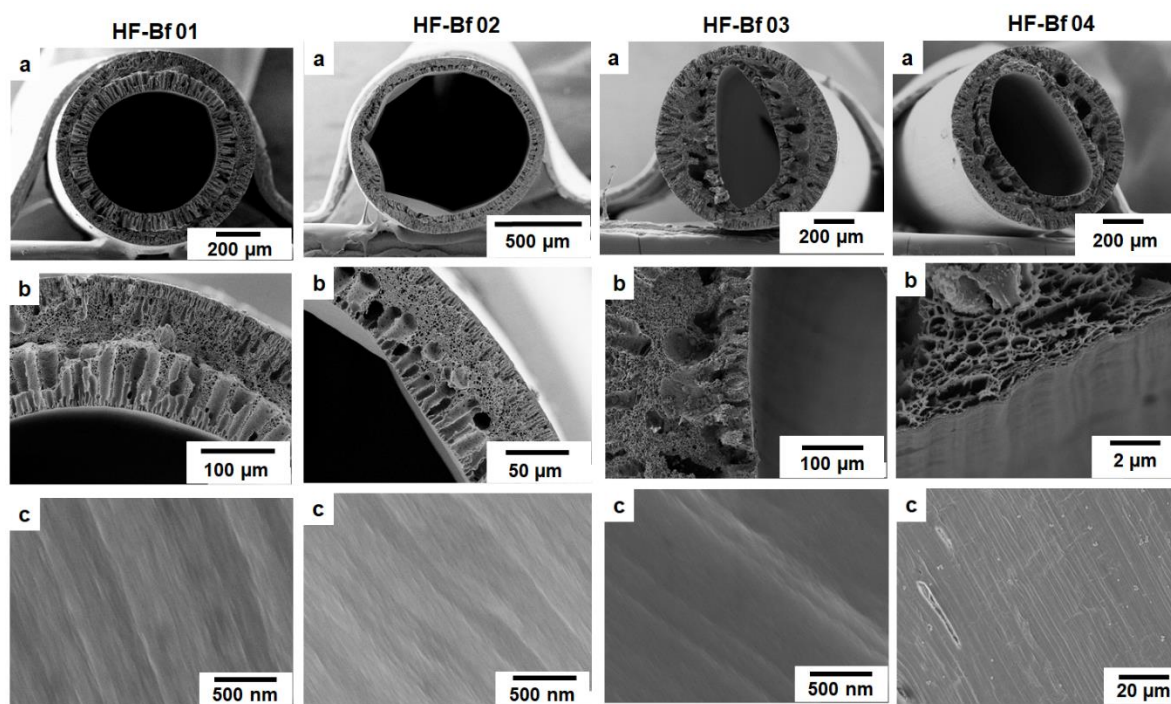
Figure 9.3 Hollow fibers HF-Bf 01, HF-Bf 02, HF-Bf 03, and HF-Bf 04: **(a)** Cross-section of the hollow fiber; **(b)** Cross-sectional structure near the lumen side surface; **(c)** Inner surface or lumen side surface of the hollow fiber.[2]

The experiments with the different bore fluids resulted in hollow fibers with a dense-looking inner surface with a thick skin layer on the lumen side (**Figure 9.3**). When water or water/glycerol mixture were used as a bore fluid, no open porous inner surface was created (HF-Bf 01 and HF-BF 02). Moreover, the skin layer at the lumen side turned out to be much thicker (shown in **Figure 9.4**) when the weak non-solvent glycerol was added to the bore fluid to spin the dope solution with an increased concentration of sPESU10 (compositions are listed in **Table 9.5**). This phenomenon is more likely to happen if the solvent outflow from the dope solution is faster than the inflow of non-solvent (water/glycerol) into the nascent fiber.[51, 127] A closed cell-like structure was dominating in the cross-sectional area of these hollow fibers. When the weak non-solvent glycerol was replaced and the hollow fibers were spun with the

bore fluids of acidic and basic water, the same scenario was reflected with a dense inner surface and a closed cell-like structure throughout the thickness of the hollow fibers (**Figure 9.3**). A sufficiently high polymer concentration of the spinning solution with a higher outflow of the solvent from the dope solution may follow the route to vitrify the polymers at the lumen side first, and may cause the formation of a thick layer near the inner surface. This thick inner side surface influences the solvent–non-solvent exchange during the spinning process, and the effect translates locally into a higher polymer content, which may bring the closed cell structure with a dense layer. So, the final membrane morphology is influenced by the degree of solvent outflow and non-solvent inflow during the coagulation process.[50, 97] This part led to the conclusion that the attempt of fabricating permeable hollow fibers was not successful, even with a lower concentration of sPESU10 in the dope solutions along with the use of different bore fluids in the spinning process.[2]
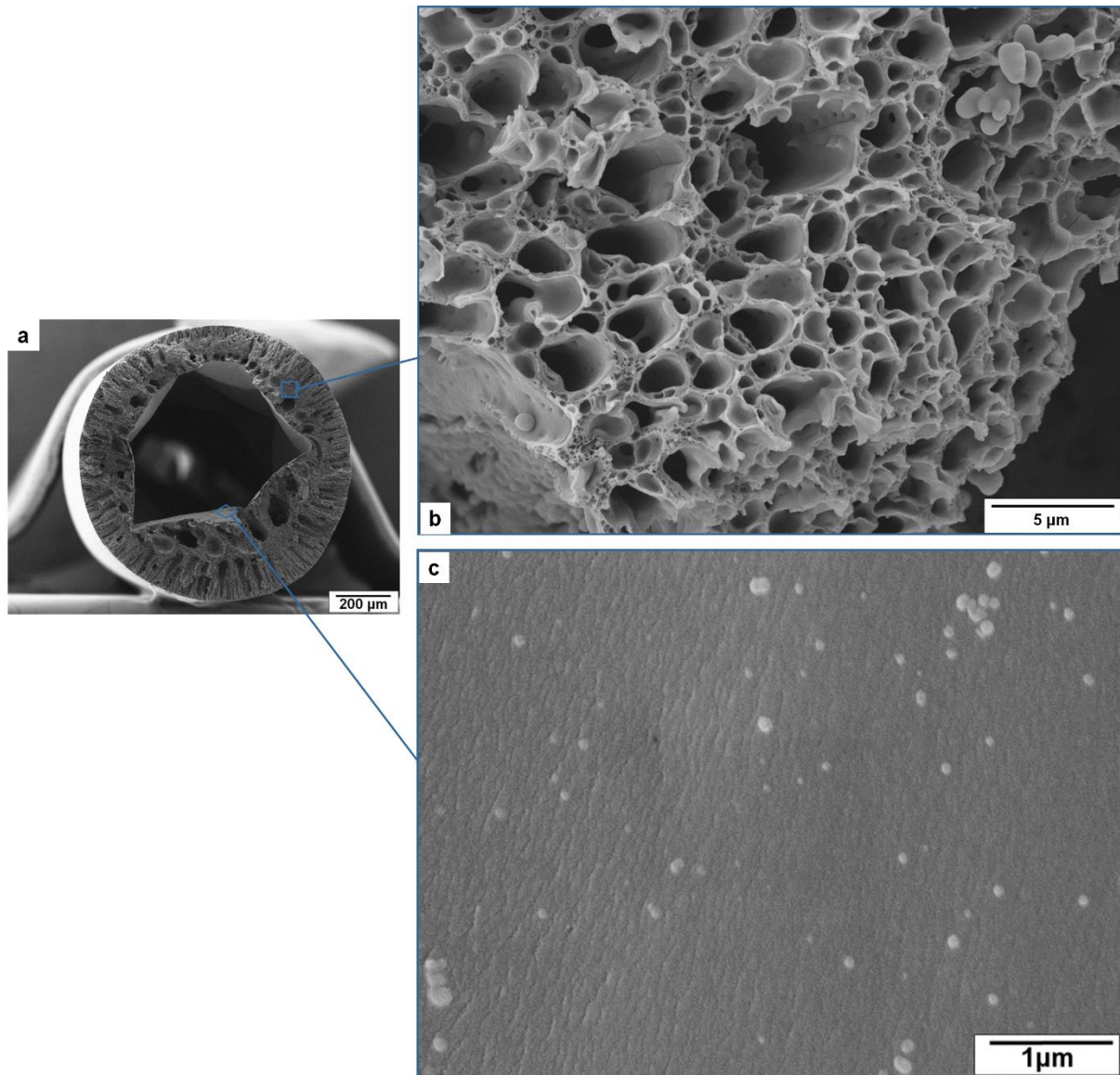
Figure 9.4 Hollow fiber membrane spun with the solution compositions and parameters referred in **Table 9.5** and **Table 9.6**, respectively: **(a)** Cross section of the hollow fiber; **(b)** Magnified image at the middle area of the cross section of the hollow fiber; **(c)** Inner surface of the hollow fiber.[2]

Table 9.5 Compositions of the spinning solutions
(hollow fiber is shown in **Figure 9.4**)[2]

Hollow fiber	Polymer concentration & composition[a]	Solvent concentration	Bore fluid composition[b]
Figure 9.4	25% PESU/sPESU10 (60/40)	75% NMP	Water/glycerol (50/50)

[a]Polymer concentration and composition are expressed as x% A/B (y/z), where x is the total polymer concentration in weight% in the solution, and y and z are the weight percentage of polymer A and B, respectively, in the polymer blend; [b] bore fluid composition is expressed as C/D (v/w), where v and w are the concentration of C and D, respectively, in weight% in the total bore fluid content.

Table 9.6 Spinning parameters of the hollow fibers shown in **Figure 9.4**[2]

Hollow fiber	Flow rate of bore fluid	Flow rate of polymer solution	Air gap, L_{Air}
Figure 9.4	1 mL/min	1.5 mL/min	10 cm

9.4 Analysis of the Inner Surface of the Hollow Fibers by XPS

In this section, the inner surface of the hollow fibers is analyzed by XPS. For this study, two different hollow fibers were chosen. In one case, the inner surface of HF-Bf 01 was analyzed where sPESU10 was used as a blend component in the dope solution. In the other case, the inner surface of HF-C 01 (solution composition and the spinning parameters are listed in **Table 9.7** and **Table 9.8**) was analyzed where a commercially available sulfonated polymer sPPSU5 was used as a blend component in the dope solution. Commercially available sPPSU polymers from BASF were synthesized from sulfonated monomers,[126] unlike sPESU10, which was prepared by the post-sulfonation of PESU.[2]

Table 9.7 Compositions of the spinning solutions and
water flux of the hollow fiber[2]

Membrane code	Polymer concentration & composition[a]	Solvent and additive concentration	Bore fluid composition[b]	Water flux [L m^{-2} h^{-1} bar^{-1}]
HF-C 01	20% PESU/sPPSU5 (90/10)	80% DMAc	Water (100)	22

[a]Polymer concentration and composition are expressed as x% A/B (y/z), where x is total polymer concentration in weight% in the solution, and y and z are the weight percentages of polymer A and B, respectively, in the polymer blend; [b]bore fluid composition is expressed as C (w), where w is the concentration of C in weight% in the total bore fluid content.

Table 9.8 Spinning parameters of the hollow fiber[2]

Membrane ID	Flow rate of bore fluid	Flow rate of polymer solution	Air gap, L_{Air}
HF-C 01	2 mL/min	1 mL/min	10 cm

Core level regions from the inner surfaces were recorded at different binding energies. In this study, the S2p region was validated very carefully to avoid the wrong interpretation of S2p$_{3/2}$ as S2p. For S2p, peak overlapping spin-orbit doublets were detected, and closely spaced spin-orbit components of S2p peak were detected at a 1.18 eV binding energy difference with an intensity ratio of around 0.5. The S2p region was deconvoluted, and the regions for two different sulfur species for sulfonyl groups (O=$\overset{|}{S}$=O) and sulfonic acid groups (-SO$_3$H) were identified. The spectra from XPS are shown in **Figure 9.5**, and the S2p regions are given in **Table 9.9** (peaks from the sulfur of sulfonic acid groups are termed with B). The near-surface coverage of sulfonated polymer was calculated by [S$_{(-SO3H)}$/S$_{(O=\overset{|}{S}=O)}$] × 100%.[2]

For example, $S_{(-SO3H)}$ is the peak area at $S2p_{1/2}$ B or at $S2p_{3/2}$ B, and $S_{(O=S=O)}$ is the peak area at $S2p_{1/2}$ or at $S2p_{3/2}$. The amount of S from (–SO$_3$H) groups to S from (O=S=O) groups is calculated to be around 34% ($16.89/49.78 \times 100\% = 33.9\%$, or $8.45/24.88 \times 100\% = 33.9\%$). This method is followed in every case to calculate the near-surface coverage of sulfonated polymer on the inner surface of the hollow fibers.[2]

Table 9.9 Sulfur regions from the inner surface of the hollow fibers HF-Bf 01 and HF-C 01[2]

Inner surface of HF-Bf 01						Inner surface of HF-C 01					
S 2p region from (O=S=O) groups			S 2p region from (-SO₃H) groups			S 2p region from (O=S=O) groups			S 2p region from (-SO₃H) groups		
Peak	Binding energy (eV)	Area %	Peak	Binding energy (eV)	Area %	Peak	Binding energy (eV)	Area %	Peak	Binding energy (eV)	Area %
S2p$_{3/2}$	167.38	49.78	S2p$_{3/2}$ B	167.78	16.89	S2p$_{3/2}$	167.37	59.93	S2p$_{3/2}$ B	167.77	6.74
S2p$_{1/2}$	168.56	24.88	S2p$_{1/2}$ B	168.96	8.45	S2p$_{1/2}$	168.55	29.96	S2p$_{1/2}$ B	168.95	3.37
Near-surface coverage of sPESU10 (% of Atoms)			**~34%**			Near-surface coverage of sPPSU5 (% of Atoms)			**~11%**		
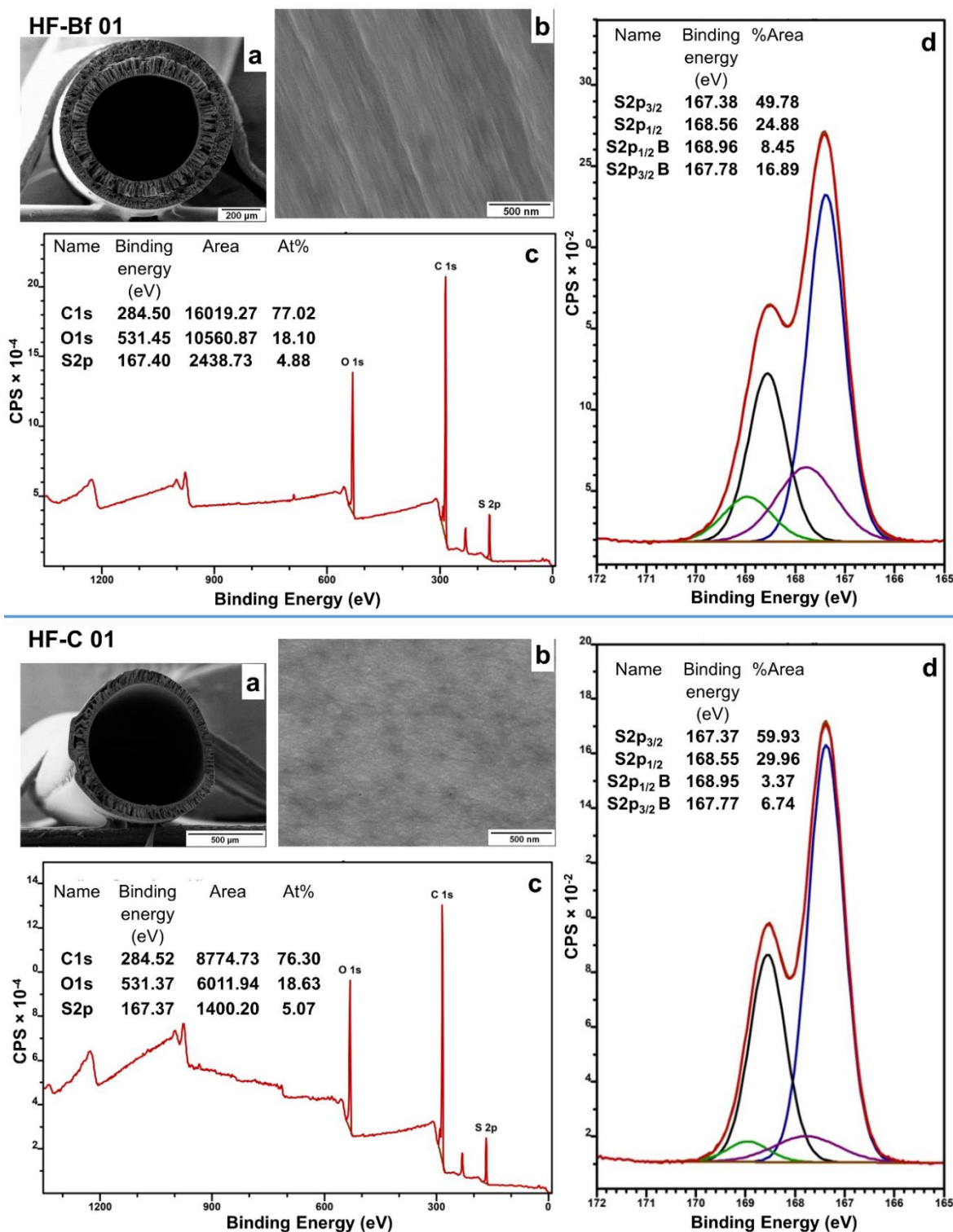
Figure 9.5 Elemental analysis of the inner surfaces of the hollow fibers HF-Bf 01 and HF-C 01. **(a)** Cross-section of the hollow fiber; **(b)** Inner surface of the hollow fiber; **(c)** X-ray photoelectron spectroscopy (XPS) survey spectrum of the components of the inner surface of the hollow fiber; **(d)** Deconvoluted S2p region from the XPS spectrum.[2]

The comparison between the inner surface analyses of the hollow fibers HF-Bf 01 and HF-C 01 led to the conclusion that the inner surface of the hollow fiber that contained sPESU10 (HF-Bf 01) was much enriched in sulfur from the sulfonic acid groups. Surface segregation was caused by the repulsive forces between the hydrophilic chains and the hydrophobic membrane matrix as soon as the bore fluid (coagulant) came into contact with the inner surface of the hollow fiber. When the spinning solution encountered the bore fluid, which was water, hydrophilic chains of sPESU10 tended to face toward the bore fluid side i.e., accumulated at the surface of the lumen side. This phenomenon of the preferential orientation of sulfonic acid groups toward water was explained in the previous works as well, where sulfonated polymers were used as a blend partner in membrane-casting solutions.[128, 129] From the analysis of HF-C 01, it was found that sulfonated chains were less abundant on the inner surface. The previous studies showed that the enrichment of sulfonic acid groups on the surface enhanced the permeation of water through the membrane, although the surface appeared non-porous. The enhanced permeance was often attributed to the increased bulk porosity and hydrophilicity.[11] Nevertheless, in this case, the hollow fiber that was spun with PESU/sPPSU5 (HF-C 01) showed some water permeance (22 L m^{-2} h^{-1} bar^{-1}) in spite of having less enrichment of sulfonic acid groups on the inner surface. However, the hollow fiber spun with PESU/sPESU10 (HF-Bf 01) was impermeable. The water permeance of hollow fibers depends on the overall pore structure (pore size, porosity) and pore interconnectivity.[7] In the case of HF-Bf 01, the missing interconnectivity of the pores throughout the cross-section might be a reason for impermeability.[2]

The permeability of HF-C 01 might be facilitated by other reasons as well. sPPSU5 is less hydrophilic compared to sPESU10 because of its lower degree of sulfonation. A higher degree

of swelling in the sPESU10 containing membranes could be a big contributor to the resistance to water flow. In the previous studies, it was shown that the membranes prepared with a polymer of higher degree of sulfonation led to a decrease in water flux values due to the increased swelling effect.[2, 126, 130]

9.5 Characterization and Performance of the Hollow Fiber Membranes Prepared with PSSNa/EG in the Dope Solution

The results from the previous sections had motivated the search of an additive system that can alter the morphology of the PESU/sPESU10 hollow fibers to a permeable one. In this study, PSSNa was dissolved in ethylene glycol (EG), and incorporated this into the spinning solution to examine the effect on the final hollow fiber membranes' performance.[2]

The solution compositions and the spinning parameters of the hollow fibers are listed in **Table 9.10** and **Table 9.11,** respectively. Morphological features from SEM are shown in **Figure 9.6**, and the results from the water flux measurements are shown in **Figure 9.7**.

Table 9.10 Compositions of the spinning solutions

(hollow fibers are shown in **Figure 9.6**)[2]

Membrane code[c]	Polymer concentration and composition[d]	Solvent and other additives concentration
HF-PESU-P/E0	18% PESU	82% NMP
HF-PESU-P/E1	18% PESU	67.9% NMP 13.4% EG 0.70% PSSNa
HF-sPESU10-P/E1	18% PESU/sPESU10 (60/40)	67.9% NMP 13.4% EG 0.70% PSSNa
HF-sPESU10-P/E2	15% PESU/sPESU10 (90/10)	59% NMP 24.7% EG 1.3% PSSNa
HF-sPPSU8.4-P/E0	25% PESU/sPPSU8.4 (60/40)	75% NMP
HF-sPPSU8.4-P/E1	18% PESU/sPPSU8.4 (60/40)	67.9% NMP 13.4% EG 0.70% PSSNa

[c]Membrane codes are indicated in a way where HF-PESU indicates that the dope solution contains PESU and HF-sPESU10 or HF-sPPSU8.4 indicate that the dope solution contains PESU and a sulfonated polymer; P/E0 refers to the absence of PSSNa/EG in the solution whereas P/E1 or P/E2 refer to the presence of PSSNa/EG in the solution. [d]Polymer concentration and compositions of the polymer blends are expressed as x% A/B (y/z), where x is the total polymer concentration in weight% in the solution, and y and z are the weight percentages of polymer A and B, respectively, in the polymer blend.

Table 9.11 Spinning parameters of the hollow fibers shown in **Figure 9.6**[2]

Membrane code	Flow rate of bore fluid [mL/min]	Flow rate of Polymer solution [mL/min]	Air-gap distance, L_{Air} [cm]	Bore fluid and coagulation bath solution
HF-PESU-P/E0				
HF-PESU-P/E1				
HF-sPESU10-P/E1				
HF-sPESU10-P/E2	2	1	10	Water
HF-sPPSU8.4-P/E0				
HF-sPPSU8.4-P/E1				

HF-PESU-P/E0

HF-PESU-P/E1

HF-sPESU10-P/E1

HF-sPESU10-P/E2

HF-sPPSU8.4-P/E0

HF-sPPSU8.4-P/E1
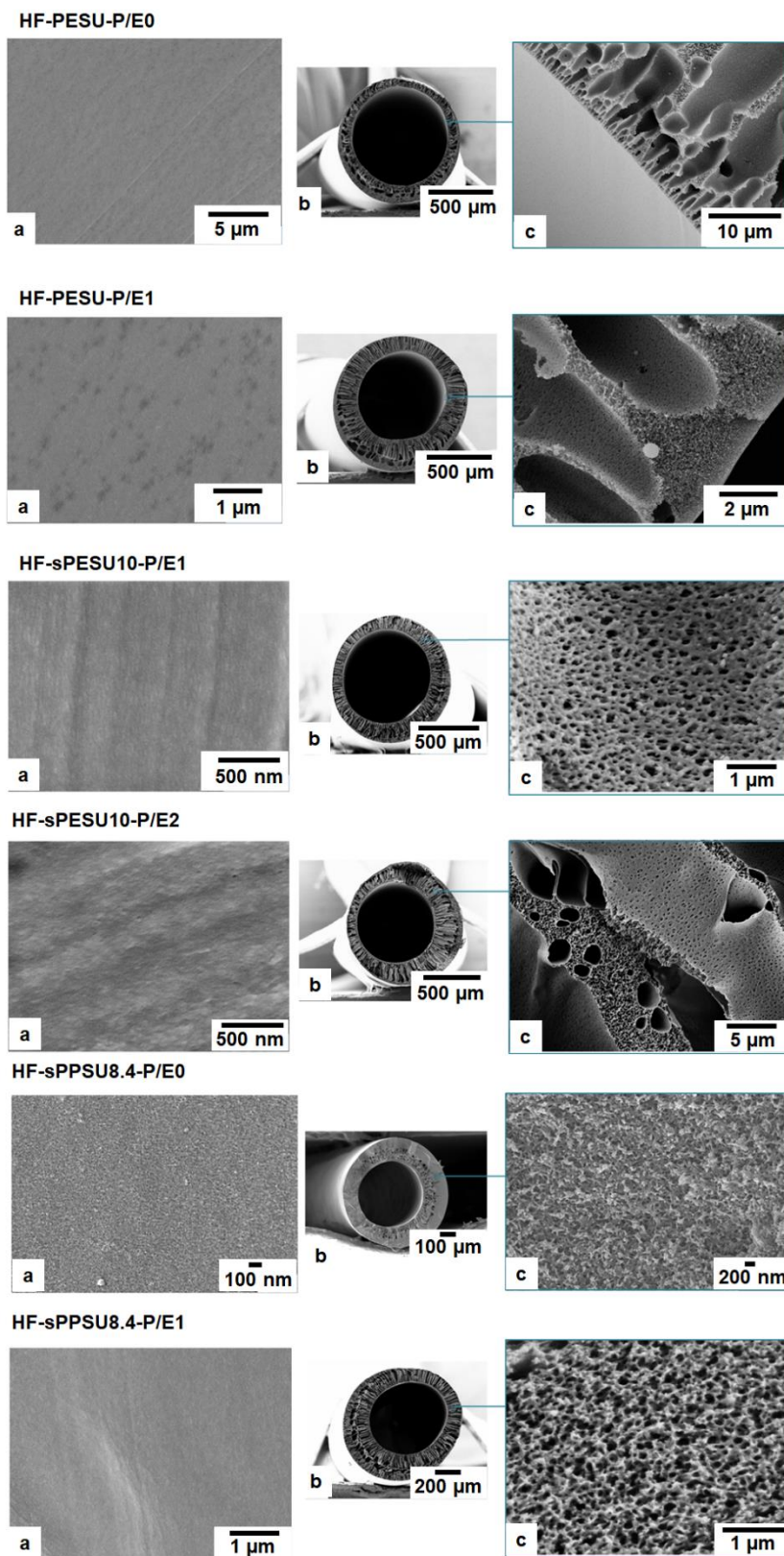
Figure 9.6 Hollow fibers spun with the dopes listed in **Table 9.10**: **(a)** Inner surface or lumen

side surface of the hollow fiber; **(b)** Cross-section of the hollow fiber; **(c)** Cross-sectional structure near the lumen side surface or in the middle section of the hollow fibers.[2]

In the previous sections, it is shown that the hollow fibers that were spun with PESU/sPESU10 containing dope solutions were impermeable to water. From **Figure 9.7**, it can be seen that the PESU/sPESU10 and PSSNa/EG containing dope solutions resulted in hollow fibers (HF-sPESU10-P/E1 and HF-sPESU10-P/E2) that showed high values of water flux. Moreover, from **Figure 9.7**, it is observed that the addition of PSSNa/EG in the PESU containing dope solution increased the water flux value of the hollow fiber membranes (comparison between HF-PESU-P/E0 and HF-PESU-P/E1) as well. However, in the case of PSSNa/EG addition to the PESU dope solution, the increase in water flux was not as much as in the case of PSSNa/EG addition to the PESU/sulfonated polymer blend dope solutions. In the case of PESU membranes (HF-PESU-P/E1 and HF-PESU-P/E0), the pure water flux increases to 340 L m^{-2} h^{-1} bar^{-1} from 125 L m^{-2} h^{-1} bar^{-1} upon the addition of PSSNa/EG to the PESU solution. The thickness and the morphological features of the hollow fibers play a vital role in determining the permeation or water flux of the membranes, which is also dependent on the solution system and the spinning parameters. The most notable part of the polyelectrolyte addition is that it led to the fabrication of permeable PESU/sPESU10 hollow fibers. PESU/sPESU10 (60/40) and PESU/sPESU10 (90/10) containing membranes (HF-sPESU10-P/E1 and HF-sPESU10-P/E2) showed water flux values of around 450 L m^{-2} h^{-1} bar^{-1} and 700 L m^{-2} h^{-1} bar^{-1}, respectively. The effect of PSSNa/EG was also examined for a dope solution where a commercially available sulfonated polymer sPPSU8.4 was used. From **Figure 9.7**, it is noticeable that the addition of PSSNa/EG in the dope solution of HF-sPPSU8.4-P/E1 showed about a fourfold increase in the value of water flux compared to its counterpart where this additive was not used, i.e., HF-sPPSU8.4-P/E0.[2]
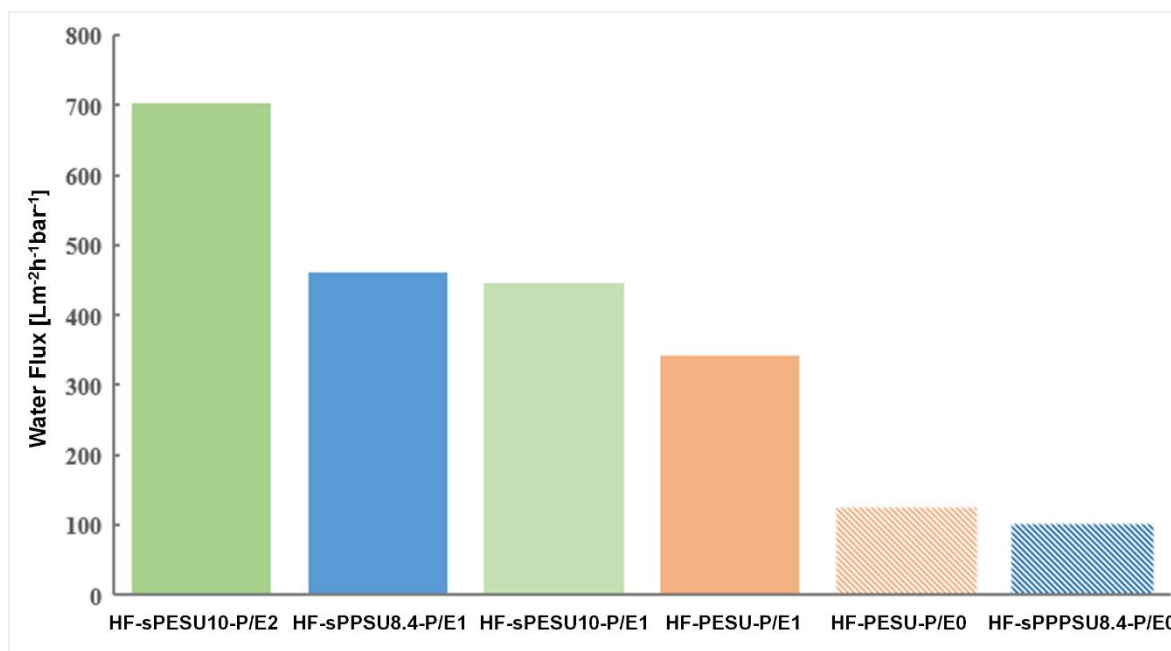
Figure 9.7 Water flux of the hollow fiber membranes spun from the dope solutions listed in **Table 9.10** after half an hour.[2]

It has to be noted that the total polymer concentrations were reduced in the case of PSSNa/EG additive incorporation, and this rendered into the decreased aggregation of polymer molecules through chain entanglement, which helped to increase the pore size and porosity as well[129, 131]. From **Figure 9.6**, it is observed that PSSNa/EG containing dope solutions resulted in hollow fibers (HF-PESU-P/E1, HF-sPESU10-P/E1, HF-sPESU10-P/E2, and HF-sPPSU8.4-P/E1) that showed finger-like structures extended from the lumen side to the outer edge, and an interconnectivity of the porous structure throughout the cross-section.[2]

The inner surfaces of the hollow fibers HF-sPESU10-P/E1 and HF-sPESU10-P/E2 were examined by X-ray photoelectron spectroscopy (XPS). **Figure 9.8** and **Table 9.12** show that the near-surface coverage by the sulfonic acid groups of the hollow fiber HF-sPESU10-P/E1

is about 25.6%, and that of the hollow fiber HF-sPESU10-P/E2 is about 16%. That means that the near-surface coverage by the sulfonic acid groups was less at the inner surface of the hollow fiber that showed a higher water flux (HF-sPESU10-P/E2). So, as seen before in section 9.4, the higher concentration of the more hydrophilic groups on the surface is less influential on water permeation in comparison to the overall pore structure and pore interconnectivity throughout the thickness of the hollow fiber. It has to be mentioned that the fluorine and nitrogen peaks from HF-sPESU10-P/E1 might have originated from the grease used in the piston to press the dope solution, and the sodium peak in HF-sPESU10-P/E2 might have come from any impurities or the additive system that was not properly washed off from the surface of this sample.[2]

Table 9.12 Sulfur regions from the inner surfaces of the hollow fibers
HF-sPESU10-P/E1 and HF-sPESU10-P/E2[2]

Inner surface of HF-sPESU10-P/E1						Inner surface of HF-sPESU10-P/E2					
S 2p region from (O=S=O) groups			S 2p region from (-SO$_3$H) groups			S 2p region from (O=S=O) groups			S 2p region from (-SO$_3$H) groups		
Peak	Binding energy (eV)	Area %	Peak	Binding energy (eV)	Area %	Peak	Binding energy (eV)	Area %	Peak	Binding energy (eV)	Area %
S2p$_{3/2}$	167.59	53.07	S2p$_{3/2}$ B	167.99	13.60	S2p$_{3/2}$	167.58	57.57	S2p$_{3/2}$ B	167.98	9.10
S2p$_{1/2}$	168.77	26.53	S2p$_{1/2}$ B	169.17	6.80	S2p$_{1/2}$	168.76	28.78	S2p$_{1/2}$ B	169.16	4.55
Near-surface coverage of sPESU10 (% of Atoms)			**~25.6%**			Near-surface coverage of sPESU10 (% of Atoms)			**~16%**		

HF-sPESU10-P/E1

Name	Binding energy (eV)	%Area
S2p$_{3/2}$	167.59	53.07
S2p$_{1/2}$	168.77	26.53
S2p$_{1/2}$ B	169.17	6.80
S2p$_{3/2}$ B	167.99	13.60

Name	Binding energy (eV)	Area	At%
C1s	284.71	19699.95	72.36
N1s	401.71	110.91	0.23
O1s	531.71	15135.90	18.98
S2p	167.71	3666.03	8.03
F1s	688.71	488.46	0.41

HF-sPESU10-P/E2

Name	Binding energy (eV)	%Area
S2p$_{3/2}$	167.58	57.57
S2p$_{1/2}$	168.76	28.78
S2p$_{1/2}$ B	169.16	4.55
S2p$_{3/2}$ B	167.98	9.10

Name	Binding energy (eV)	Area	At%
C1s	284.70	22506.53	74.99
O1s	531.70	15797.32	17.96
S2p	167.70	3487.98	6.93
Na1s	1071.20	295.30	0.12

Figure 9.8 Elemental analysis of the inner surfaces of the hollow fibers HF-sPESU10-P/E1 and HF-sPESU10-P/E2: **(a)** Cross-section of the hollow fiber; **(b)** Inner surface of the hollow fiber; **(c)** XPS spectrum from the inner surface of the hollow fiber; **(d)** Deconvoluted S2p region from the XPS spectrum.[2]

129

The phase inversion process of membrane formation is influenced by both thermodynamic and kinetic factors. The composition of the PSSNa/EG-associated solution was varied until the solution started to be opaque. The addition of PSSNa/EG altered the dope composition as well as the thermodynamic stability, and thus influenced the precipitation kinetics.[132, 133] Previous studies showed that if PSSNa is bound to the membrane surface, then it might increase the water permeance by inducing more hydrophilicity to the membrane surface.[134] However, from this study, it was assumed that the PSSNa/EG additive system helped in the reorganization of the matrix forming polymer chains during the phase inversion process. Moreover, since the polyelectrolyte PSSNa is water soluble, as is EG, due to the intrusion of water molecules from the lumen side of the hollow fiber during the spinning and from the shell side during the precipitation in the coagulation bath, PSSNa was washed away along with the low molecular weight component EG. This statement was verified by TGA and NMR measurements which is shown in the next section.[2]

9.6 TGA and NMR Analysis

From **Figure 9.9a**, for the samples PESU, sPESU10, HF-sPESU10-P/E1, and HF-sPESU10-P/E2 it is seen that the first step of the weight loss corresponds to the loss of water. Since the water molecules bound to the sulfonic acid groups leave at higher temperature this step extends beyond 100 $^{\circ}$C for the samples which carry sulfonated polymers. The weight loss step at around 300 $^{\circ}$C corresponds to the loss of sulfonic acid groups. This step is very pronounced and started at a lower temperature for sPESU10. The weight loss observed in this step does not account for a significant mass loss for the hollow fiber HF-sPESU10-P/E1 (PESU/sPESU10 (60/40) blend) and is not even noticeable for the hollow fiber HF-sPESU10-P/E2 ((PESU/sPESU10

(90/10) blend). The mass loss step at around 400 °C associates with the fragmentation of the polymer main chain. This step started at slightly lower temperature for sPESU10 and HF-sPESU10-P/E1 than that for pure PESU polymer. Samples with sulfonated polymers showed lower decomposition temperatures and this might be observed since the presence of sulfonic acid groups in the PESU structure induced enhanced asymmetry. Therefore, the less regularity in the structure brought out less stability. This phenomenon was showed in previous works as well.[2, 122, 135-137]

In case of PSSNa, after the exclusion of water from the sample two major weight loss steps were seen at around 330 °C and 470 °C. Comparison among the mass loss spectra shows that the hollow fibers HF-sPESU10-P/E1 and HF-sPESU10-P/E2 did not retain any noticeable amount of the additive (PSSNa/EG). The comparative study on the TGA measurements of HF-sPPSU8.4-P/E0 and HF-sPPSU8.4-P/E1 is shown in **Figure 9.9b**. Here it is seen that the hollow fiber spun with PSSNa/EG containing dope solution did not show any difference in degradation behavior compared to the hollow fiber spun with a dope solution without PSSNa/EG. These results indicate that the additive system (PSSNa/EG) acted as a porogen for this system. The NMR study of the hollow fibers further affirmed this observation (**Figure 9.10**). PSSNa shows three characteristic peaks at 1.7 ppm, 6.4 ppm, and 7.4 ppm. However, from **Figure 9.10a** and **b** it is seen that the hollow fibers spun with PSSNa/EG carrying dope solution did not show any characteristic peak of PSSNa.[2]
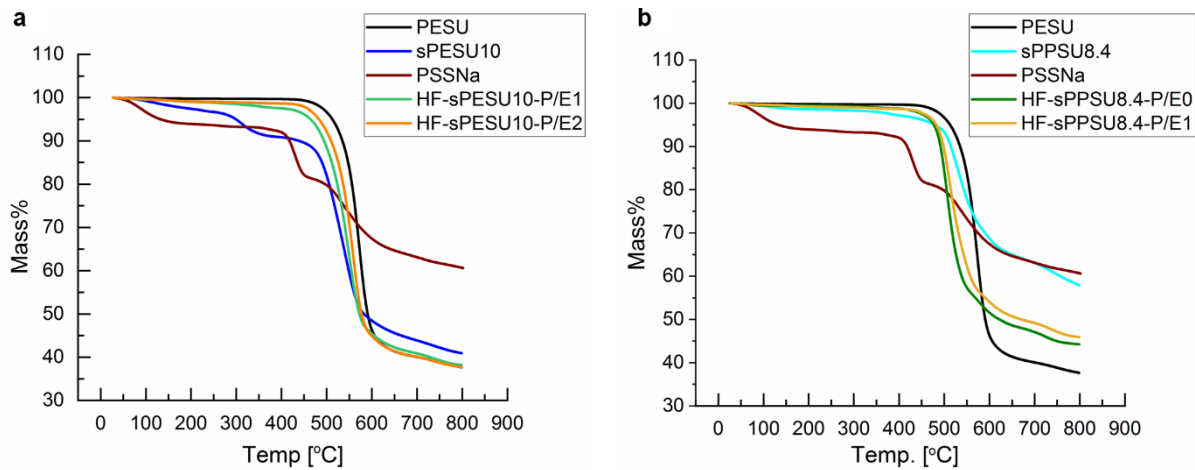
Figure 9.9 TGA of polymers, PSSNa and hollow fibers.[2]
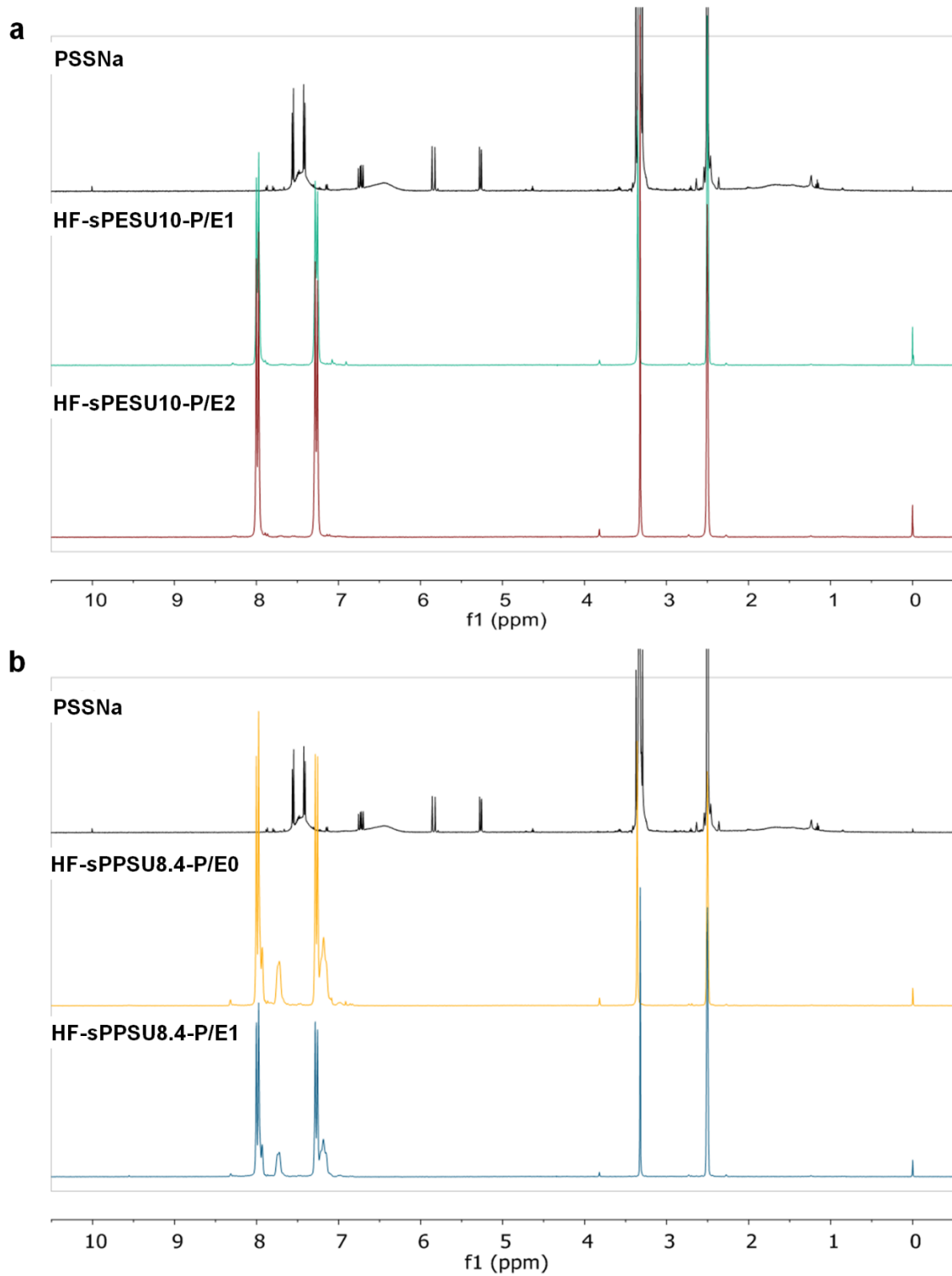
Figure 9.10 ^{1}H-NMR spectra of PSSNa and hollow fibers.[2]

Chapter 10

Results and Discussion

Continuous Production of Macroporous Films: an Alternative to Breath Figure Assembly

Despite the need for sophisticated instrumentation, breath figure assembly (BFA) methods are restricted to produce macroporous films on a tiny scale so far. The current chapter narrates the fabrication of macroporous films in hollow fiber and flat sheet geometries which extend to adopt the method for continuous production of isoporous surfaces from commercially available low-priced polymer materials.

10.1 Porous Films

Porous polymeric films have earned an enormous attention in research because of their significant potential in many fields. This type of films extends their adoption as supporting media in tissue engineering, inorganic growth templates, optical materials, antireflection coating, catalysis, bio or gas sensing, dielectric materials for electronic devices, stamps for soft lithography, etching masks, etc. Many techniques are available nowadays to create surfaces with ordered uniform pores of nanometer to micrometer sizes. Foremost conceivable techniques are lithography, electron beam sculpting, colloidal templates, emulsion, breath figure assembly (BFA), block copolymer self-assembly, track etching, non-solvent induced phase separation of self-assembled block copolymers, etc.[29, 138-144] Fabrication of many functional nanoporous materials are guided by nanoarchitectonics which spans its field from soft templating to hard templating. Monolayer or multilayer self-assembled lipid or the assembly of polymeric micelles to direct the porous inorganic structures, metal-organic frameworks (MOFs) have been of high research interest as well in recent years for the foreseeable utilization of the produced porous structures in fuel cells, separation technologies, catalysis, and many more in the near future.[3, 145-150]

Among all the methods for formulating ordered macroporous films, BFA is a captivating root because of its simplicity and cost effectiveness.[151-154] Research on isoporous structure

formation from both homopolymers and block copolymers had been clutched on this method for the last two and half decades after this nature inspired phenomenon first got recognized in the work of Widawski *et al.* in 1994.[155] By the BFA method regular arrangements of micrometer sized pores are created by templating the droplets of water formed on cold surfaces. Even though this method does not require any sophisticated equipment, it requires steady state humidity all over the film on which the macroporous structure of high regularity can be built up on. However, the mode of processing does not promise yet a large scale production of films with uniformity in the pore sizes. A continuous process of making honeycomb structures in flat sheet geometry from commercially available polymers was first disclosed by FUJIFILM Corporation which includes the requirement of control over humidity around the production line as well and the final film was obtained after going through several steps.[156] Moreover, the ordered hexagonal structure formation in a dry environment reported before involved the spin coating of the water containing solution. But the spin coating method is limited by the range of area of the porous film it can produce in a single shot.[3, 140]

Along with the flat sheet geometry porous films need to be framed on substrates with cylindrical, spherical, or concave surfaces for many applications, too. Contriving macroporous structure on a non-planar surface is still a challenge even in a small scale and the strategy of transferring porous film on curved surface requires sophisticated arrangement. Some attempts to fabricate porous structures on non-planar substrates by the BFA method involved macro-patterned thin films on a bas-relief pattern,[157] transfer of the colloidal monolayer on a curved surface,[158, 159] casting of a film forming solution on TEM grids, sugar crystal, or patterned silicon wafer,[160-162] combining the breath figure assembly with eletrospinning,[163] and etc. But all these approaches also face the challenge to produce isoporous structures on more than a square centimeter scale in one step.[3]

In 2016, Wang *et al.* introduced a method for creating an isoporous surface by spin coating of the pore forming material on a porous substrate filled with glycerol and the pores on a micrometer range formed by templating the droplets of glycerol.[164] However, large surfaces of isoporous films cannot be obtained by the spin coating. Widening this pore formation approach to processing methods different from spin coating would allow porous film formation in different geometries in a continuous manner beyond the BFA method.[3]

In this chapter, the formation of macroporous films in hollow fiber geometry from commercially available polymers in a continuous process is discussed. The potential for fabricating the macroporous film in a continuous manner is mentioned as well. In this work the knowledge of hollow fiber spinning (or, flat sheet casting) by non-solvent induced phase separation (NIPS) was combined with the pore formation mechanism by diffuse-in and condense-out behavior of glycerol.[3]

10.2 Fabrication of the Film in Hollow Fiber Geometry

The means applied to this work are comprised of some essential points- the spinning procedure requires a quadruple orifice spinneret where four different die gaps are designated to four different entities which are co-extruded by the dry-jet wet spinning method, the macroporous film in hollow fiber geometry is fabricated by the concept of diffuse-in condense-out behavior of glycerol, the macroporous film contains a support layer in the spinning stream to give mechanical integrity to the film for its handling afterwards.[3]

Polymer solutions and the bore fluids were prepared by stirring the respective components with the desired percentages (weight basis) in the sealed glass bottles for overnight. After complete

dissolution, solutions were kept in rest for some hours to remove the entrapped air bubbles. After that solutions and the bore fluid were filled in the different designated containers.[3]

For hollow fiber spinning, bore fluid and the solutions for support layer were extruded through the designated orifice of the spinneret by using gear pumps and the flow rates were determined in weight of the solution comes out of the pump in a minute i.e. g/min. Moreover, infusion pumps were used for purging glycerol and the macroporous film forming solutions through the designated gaps of the spinneret and flow rates were determined in volume of the solutions purged by the pumps in one minute that is mL/min.[3]

The main focus of this study was put on the dry-jet wet spinning method of hollow fiber production which is described in the earlier chapters. **Figure 10.1** depicts the spinning method schematically with a longitudinal and cross sectional view of the quadruple orifice spinneret (end of the spinneret) used in this study. This type of spinneret was employed for fabricating ceramic hollow fibers for solid oxide fuel cells and polymer hollow fibers for membranes.[165-167] Here the quadruple orifice spinneret served the purpose of co-extruding bore fluid, support layer forming solution, glycerol, and macroporous film forming layer solution (through the orifice 1, 2, 3, and 4, respectively in **Figure 10.1**). The dimensions of the die gaps at the spinneret end are listed in **Table 10.1**. Since the support layer solution is employed only as a guide in the spinning line for the macroporous film forming layer, there is a broad variety of the bore fluid and the support layer solution which can be chosen by considering the phase separation behavior of the support layer solution. Depending on the intended application of the macroporous film this layer can be removed later on. In principle ceramic materials can also be used as a support layer, but for the ease of extrusion with our existing spinning facilities only a polymer solution was applied for this purpose.[3]
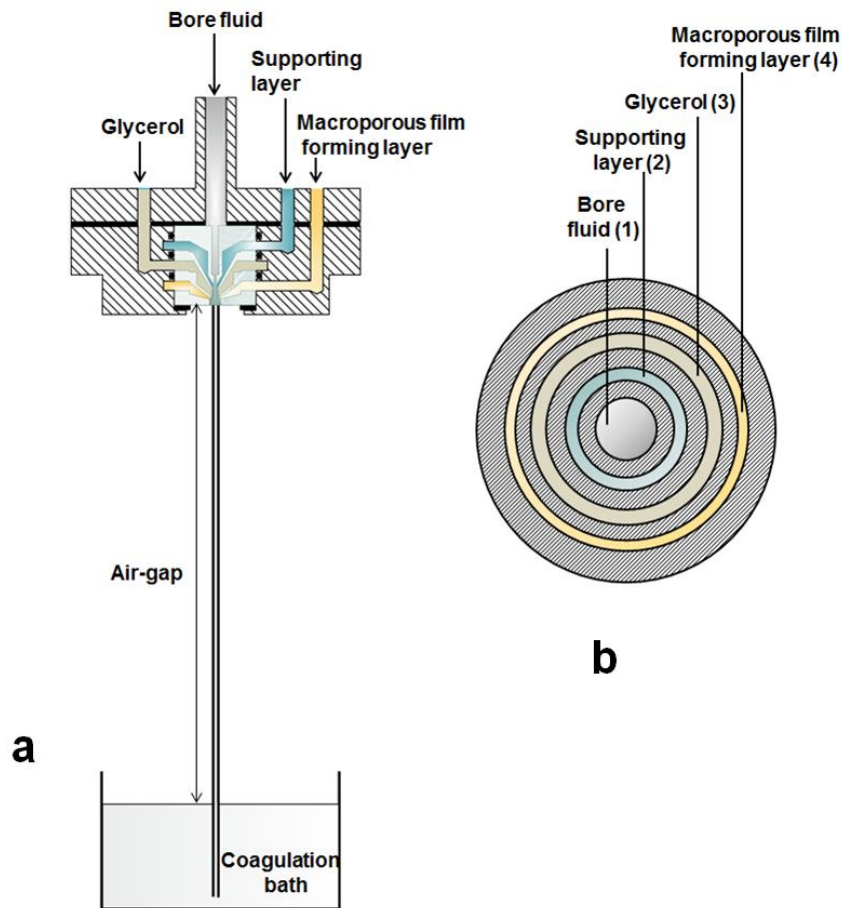
Figure 10.1 (a) Dry-jet wet spinning method of hollow fiber fabrication where a quadruple orifice spinneret is used for co-extruding four different entities through the spinneret; **(b)** Cross sectional view of the exit of the quadruple orifice spinneret; 1,2,3,4 are the four orifices of the spinneret which dimensions are listed in **Table 10.1**.[3]

Table 10.1 Dimension of the end of the quadruple orifice spinneret[3]

Orifice no.	Die gap (µm)
1	300
2	200
3	180
4	100

10.2.1 Macroporous Structure Formation

The macroporous structure formation in hollow fiber geometry by templating the glycerol droplets is illustrated in **Figure 10.2**. The porous film forming solution contained a homopolymer or a block copolymer in a highly volatile solvent. After exiting from the spinneret, the volatile solvent starts to evaporate from the surface of the film forming solution and brings down the temperature. Meanwhile glycerol starts to diffuse into the film forming solution. The solvent of the support layer solution exchanges with the non-solvent of the bore fluid in the meantime and the solidification of the support layer solution starts which gives rigidity to the hollow fiber along the spinning axis (**Figure 10.2i**). When glycerol reaches its saturation level in the solvent of the film forming solution, it forms droplets and condenses out of the film. These droplets act as template for the pore formation on the surface of the film and the film forming solution commences to solidify around the glycerol droplets (**Figure 10.2ii**). The hollow fiber immersed into the coagulation bath and gets precipitated after the exchange of solvents of the support layer solution, rest solvent in the film forming solution, and glycerol with water accomplishes (**Figure 10.2iii**). After drying this fiber, a thin polymeric film in hollow fiber geometry with macroporous structure on its surface is obtained and this layer encircles the support layer hollow fiber.[3]
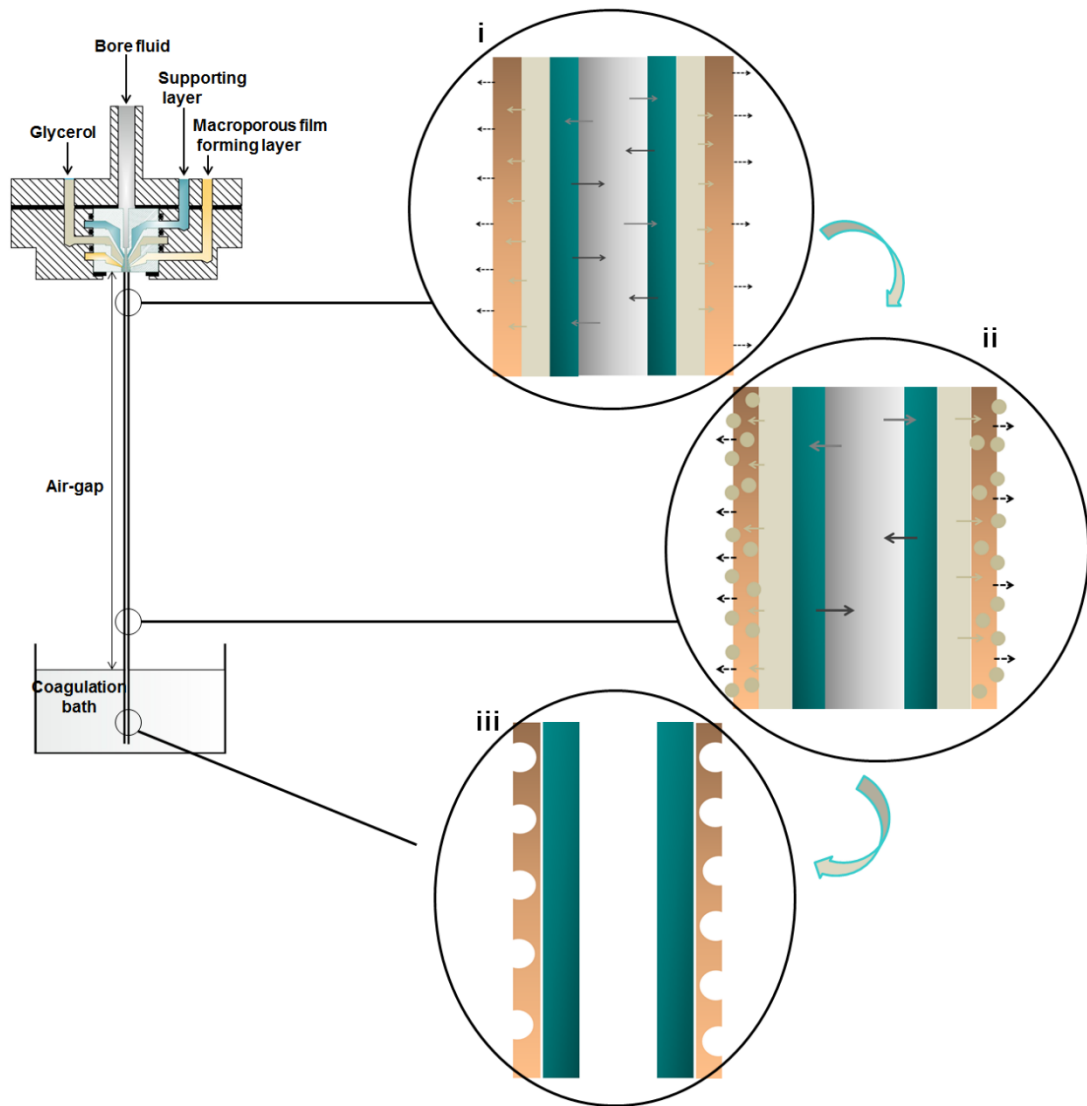
Figure 10.2 Mechanism of macroporous film formation in hollow fiber geometry. Left part of the picture shows the dry-jet wet spinning method for hollow fiber production. Right part of the picture depicts the mass transfer phenomena in the hollow fiber; **i.** Solvent and non-solvent exchange between bore fluid and the support layer solution, evaporation of the volatile solvent from the porous film forming layer and meanwhile glycerol diffusion into the porous film forming layer. **ii.** Solvent and non-solvent exchange between bore fluid and supporting layer solution continues, glycerol gets saturated in the solvent of the film forming solution and forms droplets which condense out afterwards. **iii.** Porous film formed in hollow fiber geometry with support layer underneath. Since different polymers are used for preparing supporting layer solution and the porous film forming layer solution, these two layers typically delaminate from each other.[3]

10.2.2 Macroporous Film Formation by Commercial Polymers

Two different commercial polymers are chosen to validate this process of macroporous film formation. One is cellulose acetate (CA 398-30 Eastman) and another one is a star block copolymer of polystyrene-*b*-polybutadiene-*b*-polystyrene (PS-*b*-PB-*b*-PS) (StyroClear® GH 62 from BASF).[3]

The experiments are divided into three groups according to the combination of solutions chosen for the spinning. They are listed in **Table 10.2** with the designated orifice of the quadruple orifice spinneret (shown in **Figure 10.1** and Table **10.1**) they are purged through and the spinning parameters are summarized in **Table 10.3.** All spinning experiments were done in an environment where temperature varied from 20-30 $^{\circ}$C and relative humidity was 21-33%. The scanning electron micrographs of the outer surface and the cross section of the films from the three different groups of experiments (Group 1, 2, 3 in **Table 10.2**) are presented in **Figures 10.3**, **10.4**, and **10.6**, respectively.**[3]**

Table 10.2 Solutions purged through the different orifices of the spinneret[3]

Group	1	2	3
Bore fluid (Orifice 1)	Water/NMP/PEG400 (40/30/30)**a)**	Water (100)**a)**	Water/NMP/PEG400 (40/30/30)**a)**
Support layer solution (Orifice 2)	PESU/NMP/PEG400/Water (16/40.5/40.5/3)**a)**	PESU/NMP/PEG400/Water (16/40.5/40.5/3)**a)**	PESU/NMP/PEG400/Water(16/40.5/40.5/3)**a)**
Pore former (Orifice 3)	Glycerol	Glycerol	Glycerol
Film forming solution (Orifice 4)	CA/1,4-dioxane (8/92)**a)**	CA/1,4-dioxane (12/88)**a)**	GH 62/THF (12/88)**a)**

a)The ratios of the components in the solutions are expressed in wt.%.

Table 10.3 Spinning parameters for the experiments of Group 1, 2, and 3 from **Table 10.2**[3]

	Flow rate of Bore fluid (in g min^{-1})	Flow rate of Support layer solution (in g min^{-1})	Flow rate of Glycerol (in mL min^{-1})	Flow rate of Film forming solution (in mL min^{-1})	Air gap (in cm)
Group 1	1	2	0.1	0.1	
Group 2	1	2	0.1	0.1	10
Group 3	1	2	0.05	0.05	

Figure 10.3 Film forming solution: 8% CA in 1,4-dioxane (Group 1 in **Table 10.2**); **(a)** A schematically drawn hollow fiber where the macroporous outer layer film encircles the support layer hollow fiber; **(b)** Cross sectional view of the porous film under scanning electron microscope (SEM); **(c)** Surface of the film under SEM; **(d)** Pore size distribution [2724 number of pores in 39.54 x 10^3 μm^2 of the measured area] of the surface of the film forming layer measured by IMS V15Q4 (Imagic Bildverarbeitung AG, Glattbrugg, Switzerland). [3]
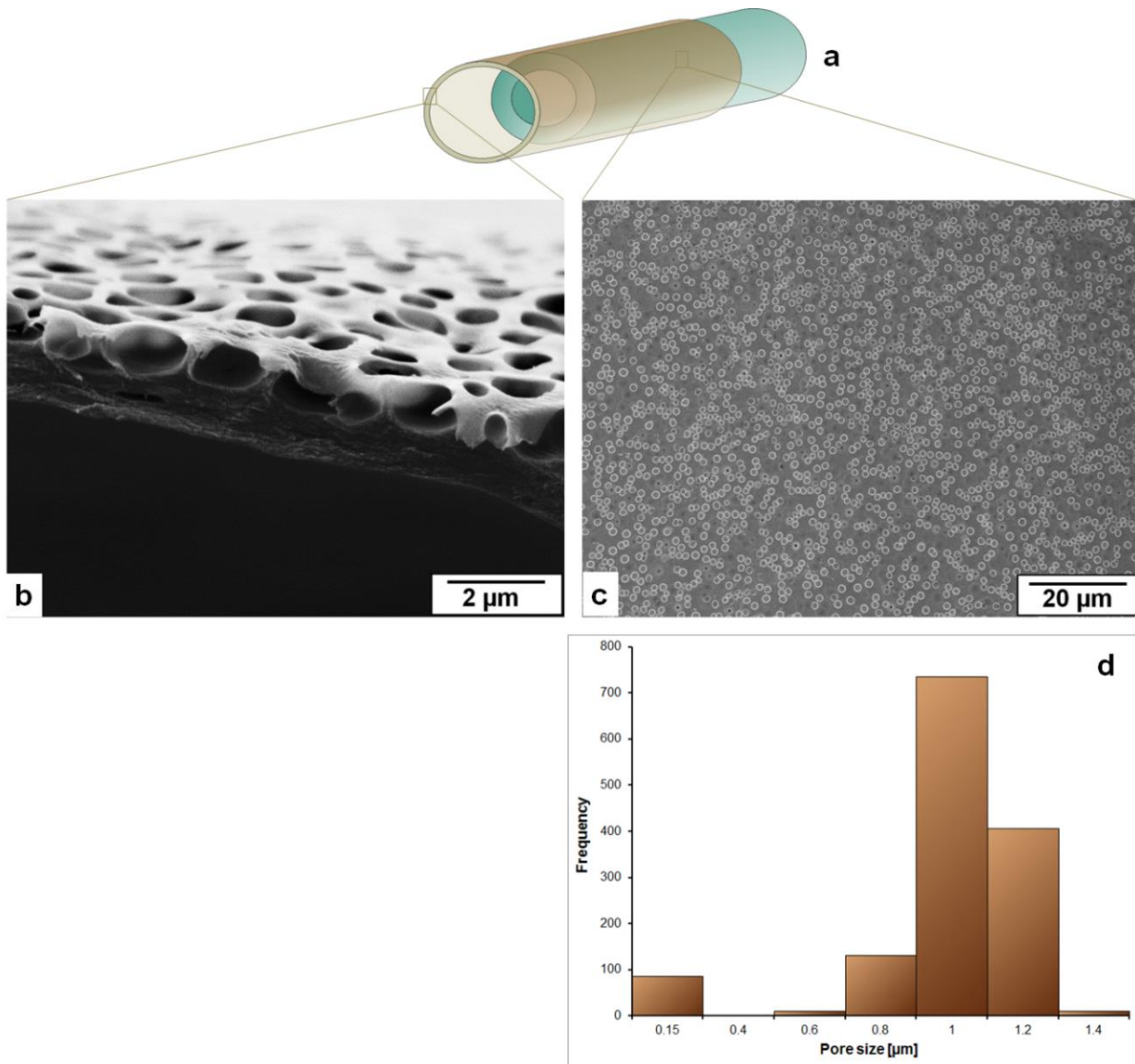
Figure 10.4 Film forming solution: 12% CA in 1,4-dioxane (Group 2 in **Table 10.2**); **(a)** A schematically drawn double layer hollow fiber where the macroporous outer layer encircles the support layer hollow fiber; **(b)** Cross sectional view of the porous film under scanning electron microscope (SEM); **(c)** Surface of the film under SEM; **(d)** Pore size distribution [1384 number of pores in 10.04 x 10^3 μm^2 of the measured area] of the surface of the film forming layer measured by IMS V15Q4 (Imagic Bildverarbeitung AG, Glattbrugg, Switzerland). [3]

Figure 10.3 shows that 8% solution of cellulose acetate (CA) in 1,4- dioxane as a film forming solution created pores on the surface with a broad distribution of pore diameters from less than

1 µm to more than 2.5 µm and the surface porosity from the analyzed section was found about

15%. The average film thickness was 2.3 µm. Moreover, the pore depth was almost equal to

the film thickness. As the concentration of cellulose acetate increases from 8% to 12% (**Figure**

10.4) the pore sizes accumulated in a narrower distribution mainly with diameters from 0.9 to

1.3 µm. The surface porosity measured in the analyzed section was about 10%. The average

film thickness got to 2 µm and the pore depth was about half of the film thickness. Although

the results shown in **Figures 10.3** and **10.4** are the outcome of same spinning parameters (listed

in **Table 10.3**), the reason for the different pore sizes and depths may lie in the solution

properties and that can be pointed as follows:[3]

i. In spite of using the same solvent higher concentration of polymer decreased the surface

tension of the solution which means that the difference in surface energy of glycerol and the

film forming solution was higher when 12% of CA solution was used compared to 8% CA

solution (surface tension of the solutions, solvents, and glycerol are listed in **Table 10.4**).[3]

ii. If the 8% concentration of CA was too low to stabilize the glycerol droplets then the

coalescence of droplets could have led to a broader distribution of pore size.[3]

iii. Glycerol dissolves in 1,4-dioxane but aggregates into droplets above a certain concentration

and the higher concentration of polymer in 1,4-dioxane might develop higher resistance for the

growth of the droplets to the surface.[3]

Table 10.4 Surface tension of the solutions, solvents, and glycerol[3]

	Glycerol	1,4-dioxane	THF	8% CA solution in 1,4-dioxane	12% CA solution in 1,4-dioxane	12% GH 62 solution in THF
Surface tension (in mN/m)	64.4	33.6	28.8	33.2	29.2	29.1

A decrease of pore size with increasing solution concentration was also observed in the previous work by Wang *et al.* where pores formed on the spin coated polymer solution templating the glycerol droplets.[164] But as reported in several works on pore formation by breath figure assembly,[151] the chances to have the reverse trend in pore size with increasing solution concentration can also not be nullified with this present mechanism. Different combinations of polymers and solvents, molecular weight of the polymer, structure of the polymer, solution concentration can be of further research interest for tuning the size and the order of the pores on the film surface.[3]

Glycerol has limited solubility in 1,4-dioxane[164] (used for CA solution) and in tetrahydrofuran (THF)[168] (used for Styro Clear® GH 62 solution). In this work, from the spinneret exit to the coagulation bath these highly volatile solvents evaporate from the film forming solution while diffused glycerol forms droplets in the film forming solution at lower concentrations of glycerol than in pure 1,4-dioxane or THF. Because of the continuous evaporation of the solvent from the macroporous film forming layer, the temperature drops down at the solution-air interface and the glycerol droplets condense out at the surface. If the glycerol droplets are stabilized at the surface then they act as template for the pore formation. The stabilization of glycerol

droplets in the surface is also governed by the spinning parameters and this supposition is
supported by comparing the surface structures obtained at different air-gaps.[3]

In **Figure 10.5** three images of the surfaces are shown which are spun in hollow fiber geometry
with different spinning parameters engaging the same solutions for bore fluid, support layer,
film, and glycerol. The solution compositions (as of Group 1 in **Table 10.2**) and the spinning
parameters are listed in **Table 10.5**.[3]

Table 10.5 Spinning parameters applied for the experiments of **Figure 10.5**[3]

| Figure no. | Flow rate | | | | Air gap |
	Bore fluid: (Water/NMP/PEG400 = 40/30/30) (in g/min)	Support layer solution (PESU/NMP/PEG400/water = 16/40.5/40.5/3) (in g/min)	Glycerol (in mL/min)	Film forming layer (CA/1,4-dioxane = 8/92) (in mL/min)	(in cm)
10.5a	2	2	0.1	0.2	10
10.5b	2	2	0.1	0.2	25
10.5c	2	3	0.2	0.2	25
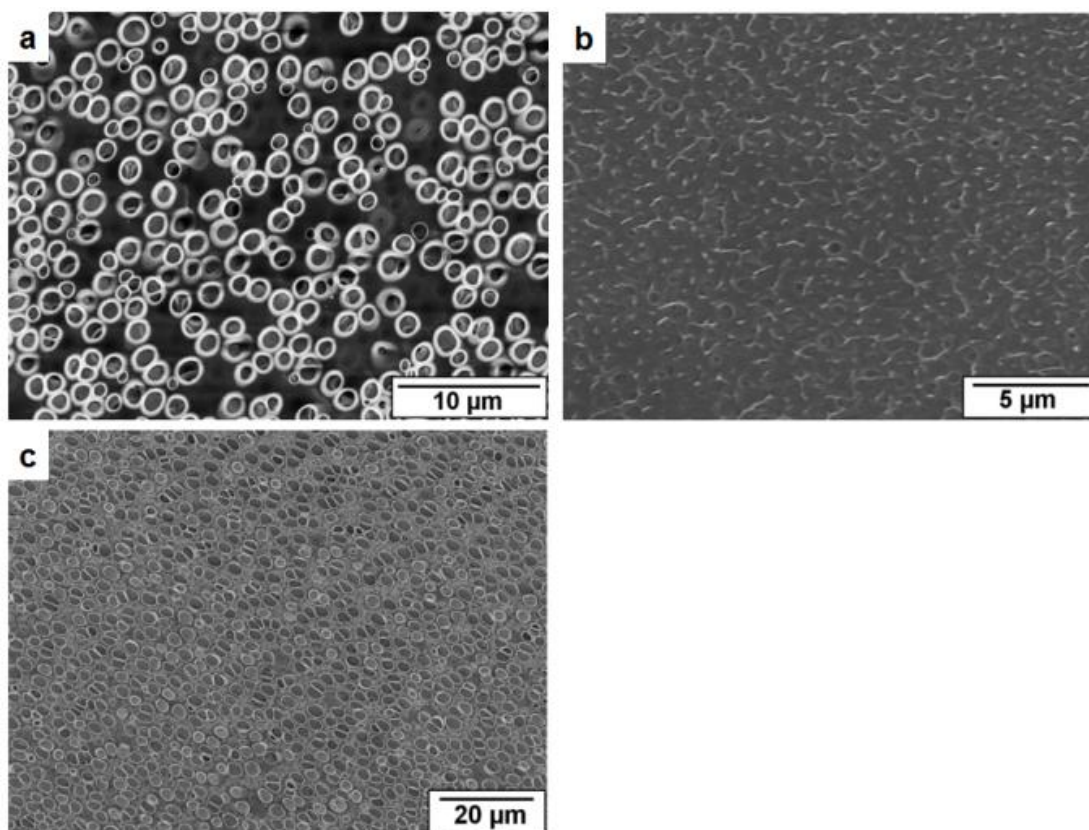
Figure 10.5 SEM images of the surfaces of the films spun with air gap of 10 cm **(a)**, 25 cm **(b)**, and 25 cm with higher flow rates **(c)**. Spinning parameters are listed in **Table 10.5**.[3]

As seen, the surface of the fiber spun with 10 cm air gap distance carries pores (**Figure 10.5a**). With the same flow rates of the bore fluid and dope solutions, increased air-gap (25 cm) i.e. longer time span in the air fades away the pores (**Figure 10.5b**). In contrast, pores are revived on the surface with air gap of 25 cm when the fiber strand plunges into the coagulation bath in a shorter time which is maintained by applying higher flow rate to the extruded solution/s (**Figure 10.5c**). From this observation it is of clear evidence that the pore formation not only is dependent on the solution properties but also on the spinning parameters which results in the optimum time for the pore formation on the surface of the film in hollow fiber geometry.[3]

The pore formation with the residing time of the fiber in the air might be explained as 1,4-dioxane of boiling point 101 ºC has slow rate of evaporation and evaporation of 1,4-dioxane promotes condensing out of the glycerol droplets at the cooled surface. But the polymer dissolved in 1,4-dioxane carries some residual solvent at the late stage of solvent evaporation. The residual solvent decreases the glass transition temperature of the solvated polymer film which promotes the relaxation of the chains at the surface. So at this stage if the solvated film stays for long enough time in the air then the glycerol droplets are not stabilized and cavities cannot be formed on the surface templating the droplets. The effect of residual solvent in the polymer film on the pore formation is also evidenced in the BFA mechanism when the evaporation rate of the solvent is slow.[169] Moreover, the effect of increased air gap distance for pore formation is expelled when it is coupled with higher flow rate of polymer solution/s, i.e. having shorter time span of the fiber strand in the air. Furthermore, the surface of the fiber which is spun with longer distance between spinneret and coagulation bath might come up against pore shape stability because of higher elongational stretching of the thin film originated by gravity. That might result in elongated pores (**Figure 10.5c**).[3]

The consequence of using polymers of different structures and behavior is substantiated by choosing a commercially available star block copolymer of polystyrene and polybutadiene (StyroClear® GH 62). Because of its inherent nano-scale heterogeneity this copolymer appears transparent. StyroClear® GH 62 (BASF) is an asymmetric star block copolymer with polybutadiene core and polystyrene external blocks.[170] Such star-shaped block copolymers self-assemble in a variety of ordered structure because of the intramolecular phase separation of the blocks.[3, 70, 171]

12% solution of GH 62 in THF by the applied pore forming mechanism coupled with dry-jet wet spinning creates the film with thickness of less than 1 µm and with the surface containing pores of narrower size distribution from 60 nm to 210 nm as majority (**Figure 10.6**). The sharp decrease in pore size using a GH 62 solution compared to a CA solution may be caused by the microphase separation of the block copolymer which favors creation of smaller pore sizes. The previous studies on this commercial star block copolymer showed that it can equilibrate in a lamellar morphology. Obviously the structure formed in this study (**Figure 10.6**) does not resemble the equilibrium morphology. The multilayered pores and the decreased size of pores could be the result of the following reasons: because of the higher segment density in star polymers they may form a solid polymer layer faster around the glycerol-solution interface. The star block copolymer is dissolved in THF which is a selective solvent for PS blocks and so if the star block copolymer forms quasi-spherical micelles in THF then aggregates of these micelles possess higher rigidity to conserve the glycerol droplets. The larger difference of surface tension between glycerol and THF compared to glycerol and 1,4-dioxane (**Table 10.4**) leads to a smaller size of the droplets. And if they do not coalesce, then they will form pores by stacking in multiple layers through the film thickness. Similar arguments were advocated also for the porous films which were devised by BFA using both star and nonamphiphilic block copolymers.[3, 151, 172, 173]
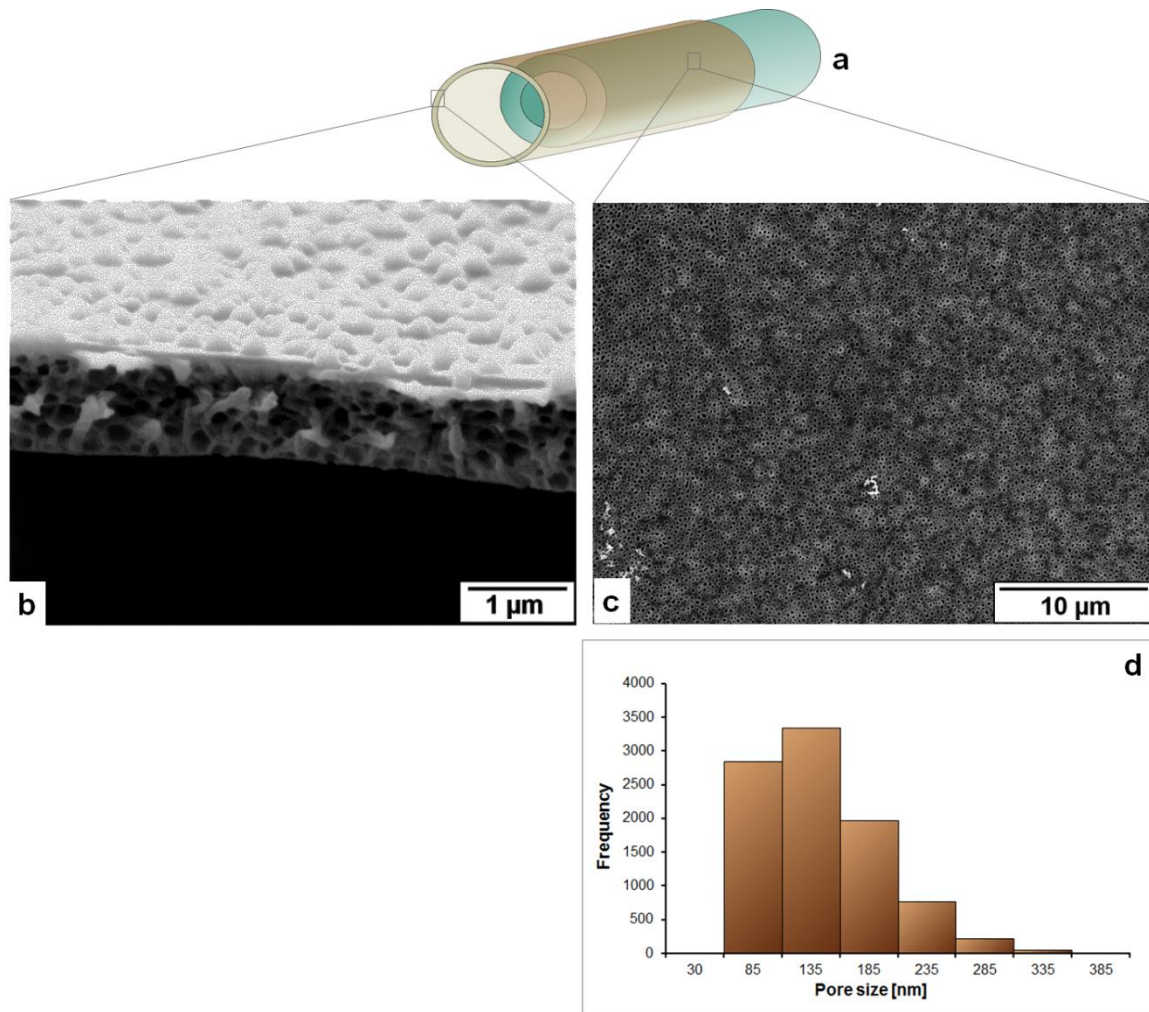
Figure 10.6 Film forming solution: 12% Styro Clear® GH 62 in THF (Group 3 in **Table 10.2**); **(a)** A schematically drawn double layer hollow fiber where the macroporous outer layer encircles the support layer hollow fiber; **(b)** Cross sectional view of the porous film under scanning electron microscope (SEM); **(c)** Surface picture of the porous layer taken by SEM; **(d)** Pore size distribution [9206 number of pores in 1.09 x 10^3 μm^2 of the measured area] of the surface of the film forming layer measured by IMS V15Q4 (Imagic Bildverarbeitung AG, Glattbrugg, Switzerland).[3]

10.3 Macroporous Structure Formation in Flat Sheet Geometry

Pore formation in a continuous manner by the mechanism of glycerol diffuse-in condense-out is also possible in flat sheet geometry. An in-house built casting machine (illustrated in **Figure 10.7a**) was used for this purpose. It was equipped with two doctor/casting blades. One casting

blade was already in-built in the machine and the other one was fixed a few cm ahead of it. The device was equipped with nonwoven support on which the casting was performed. Glycerol was casted on the nonwoven with the first casting blade following the macroporous film forming solution on top of the glycerol layer by the second casting blade. The film forming solution was purged from the container to the designated blade in the casting machine by using a gear pump. The nonwoven with glycerol and the film forming layer was dipped in the coagulation bath (water) after passing a distance in air and then was collected on a roll. The film forming solution consisted of 8% cellulose acetate (CA) in 1,4-dioxane and the casting was operated at around 20 $^{\circ}$C temperature and 28% relative humidity. Although the order in pore size and pore arrangement on the surface was missing, the pore formation by glycerol in a continuous manner is evident in flat sheet geometry, too, as can be seen in **Figure 10.7b**. The optimized combination of the speed of the nonwoven, the gaps between the blades' ends and the support layer, and solution composition may lead to a better control of the pore arrangement on the surface. Using nonwoven as a support layer causes infiltration of glycerol downward through this support. For avoiding this downward flow of the pore forming component other supports e.g. metallic or polymeric foils can be also used in the proposed instrumentation for porous film formation in flat sheet geometry.[3]
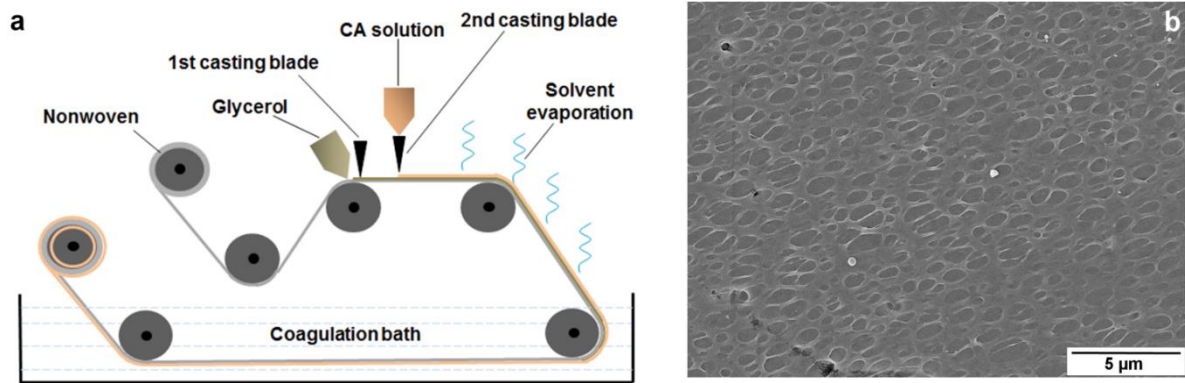
Figure 10.7 (a) Casting machine equipped with two casting blades; first one is for glycerol and the second one is for the film forming solution; **(b)** SEM image of the surface of the film casted with the machine depicted in **a** by using 8% CA solution in 1,4-dioxane.[3]

Chapter 11

Summary

11.1 Summary

The work aimed to fabricate double layer isoporous hollow fiber membranes by co-extrusion of the layers. The ease in fabrication and to minimize the usage of the tailor-made polymers for the selective layer were the line of reasoning to go for this method. To formulate the way from the idea to the aspired goal the hollow fiber membrane fabrication method was analyzed and optimized.

To fabricate the isoporous structure on the membrane surface by the SNIPS method, PS-*b*-P4VP was chosen as the outer layer forming material. The structure formation of PS-*b*-P4VP was studied and optimized in flat sheet geometry beforehand. Afterwards the PS-*b*-P4VP solution was employed in co-extrusion. The major problem appeared in co-extrusion was delamination between the support layer and the selective layer. To solve this problem different commercially available polymers were used as the support layer beneath the PS-*b*-P4VP layer and different spinning parameters and conditions were tested. Nevertheless, none of them ensured the fabrication of delamination free double layer hollow fibers.

The double layer hollow fiber with the seamless interface was fabricated by implementing the idea of interfacial bond formation between the layers. To do so, a commercial polymer, polyethersulfone (PESU) was functionalized to sulfonated polyethersulfone (sPESU) and the blend of PESU and sPESU was used as a supporting layer forming material. Interfacial hydrogen bond formation between the pyridine groups of PS-*b*-P4VP and the acid groups of sPESU favored in-process integration between the two layers in the spinning line. This method of *in-situ* hydrogen bond formation might be an attractive route for making isoporous composite membranes in other geometries as well and can also be applied for other processing methods.[1]

The double layer hollow fiber containing a PS-*b*-P4VP outer layer and a PESU/sPESU inner layer prepared in this study was impermeable to water due to the formation of a rather dense inner layer. Therefore, hollow fibers of PESU/sulfonated polymer blend solutions were fabricated and investigated to find out the dope compositions that would constitute a support layer with less resistance. PESU/sPESU blend solutions were spun with different additives and different bore fluids. Single layer hollow fibers containing a PESU/sPESU blend were also found to be impermeable to water, although from XPS it was seen that their surface was rich in sulfonic acid groups. The addition of ethylene glycol and poly(sodium 4-styrene sulfonate) to the spinning dopes of PESU/sPESU blends formed permeable hollow fiber membranes. Addition of this additive system increased the water permeation of PESU/sulfonated polyphenylenesulfone (sPPSU) blend hollow fibers as well. The result showed that the permeance of the hollow fibers containing a blend of PESU/sulfonated polymer was mainly dependent on the morphological features and pore interconnectivity, rather than on the presence of hydrophilic groups on the surface.[2]

Although the ethylene glycol and poly(sodium 4-styrene sulfonate) additive system improved the water flux of the single layer PESU/sulfonated polymer hollow fibers, this recipe may lead to a different morphological structure when it will be applied as a support layer material for a composite membrane by co-extrusion.[111] Moreover, to favor good interfacial integrity between the layers of a composite membrane, the compositions of the co-extruded solutions near the interfacial region have to be far-off from their phase separation region in the phase diagram for a longer time.[99] Therefore the solution compositions shown here to achieve permeable PESU/sulfonated polymer blend hollow fibers are subject to change while being employed as a support layer in co-extrusion. In spite of these difficulties, since the hollow fiber geometry promises higher productivity, the proposed method would be worth to be investigated

further for the formation of composite hollow fiber membranes with isoporous surface and this PhD work sets the stage for future research.

The work on co-extrusion led to an innovative approach for the fabrication of macroporous films which carries its potential for many applications. A design is introduced to explore an alternative way of macroporous film formation other than the conventional ones. The pore formation by glycerol droplets welded with the equipment of hollow fiber spinning or flat sheet casting enables macroporous film formation in a continuous manner.

The fabrication of the films in hollow fiber geometry was carried out by a concentric quadruple orifice spinneret through which four different liquids were co-extruded simultaneously. The utilization of "diffuse-in, droplet formation, and then condense-out" behavior of glycerol in a hollow fiber spinning method formulated macroporous films in a single step. Moreover, this method of film formation in a continuous manner was also verified to produce macroporous films in flat sheet geometry by using two casting blades in a casting machine.[3]

The presented method of pore formation can be applied to create ordered assemblies of inorganic nanoparticles in nonplanar and planar geometries by using nanoparticle precursors in the film forming solutions. Accordingly, the method is expected to offer a continuous process to create micropatterned surfaces which may find their way to applications in catalysis, sensing, templating, cell culture, or in microelectronics.[3]

Chapter 12

Reference

Reference

[1] N. Noor, J. Koll, M. Radjabian, C. Abetz, V. Abetz, *Macromolecular Rapid Communications* **2016**, *37*, 414.

[2] N. Noor, J. Koll, N. Scharnagl, C. Abetz, V. Abetz, *Membranes* **2018**, *8*, 54.

[3] N. Noor, J. Koll, C. Abetz, H. Notzke, V. Abetz, *Scientific Reports* **2017**, *7*, 8050.

[4] R. W. Baker, "Overview of Membrane Science and Technology", in *Membrane Technology and Applications*, 2nd edition, John Wiley & Sons, Ltd England, **2004**, p. 1.

[5] "https://www.mrwa.com/WaterWorksMnl/Chapter%2019%20Membrane%20Filtration.pdf".

[6] "https://en.wikipedia.org/wiki/Membrane_technology".

[7] Y. Li, T.-S. Chung, *Journal of Membrane Science* **2008**, *309*, 45.

[8] "Protein Purification & Isolation Market by Technology (Precipitation, Dialysis, Electrophoresis, Western Blotting, Ion Exchange & Affinity Chromatography) by Product (Instruments, Kits, Reagents, Resins) by Application & End User - Global Forecast to 2020", MarketsandMarkets Research Pvt. Ltd. **2015**.

[9] R. G. Harrison, "*Protein Purification process engineering"*, Marcel Dekker, New york, **1994**.

[10] S. Roe, "*Protein Purification techniques"*, 2nd edition, Oxford University Press, **2001**.

[11] L.-F. Fang, H.-Y. Yang, L. Cheng, N. Kato, S. Jeon, R. Takagi, H. Matsuyama, *Industrial & Engineering Chemistry Research* **2017**, *56*, 11302.

[12] C. Christy, S. Vermant, *Desalination* **2002**, *147*, 1.

[13] A. N. Cherkasov, A. E. Polotsky, *Journal of Membrane Science* **1996**, *110*, 79.

[14] M. E. Warkiani, A. A. S. Bhagat, B. L. Khoo, J. Han, C. T. Lim, H. Q. Gong, A. G. Fane, *ACS Nano* **2013**, *7*, 1882.

[15] S. Kuiper, C. J. M. van Rijn, W. Nijdam, M. C. Elwenspoek, *Journal of Membrane Science* **1998**, *150*, 1.

[16] T. Yanagishita, K. Nishio, H. Masuda, *Journal of Vacuum Science & Technology B: Microelectronics and Nanometer Structures Processing, Measurement, and Phenomena* **2007**, *25*, L35.

[17] M. Gironès, I. J. Akbarsyah, W. Nijdam, C. J. M. van Rijn, H. V. Jansen, R. G. H. Lammertink, M. Wessling, *Journal of Membrane Science* **2006**, *283*, 411.

[18] S. Ishan, A. Amit, S. J. Suhas, *Journal of Micromechanics and Microengineering* **2009**, *19*, 025025.

[19] K. Han, W. Xu, A. Ruiz, P. Ruchhoeft, S. Chellam, *Journal of Membrane Science* **2005**, *249*, 193.

[20] M. E. Warkiani, L. Chen, C.-P. Lou, H.-B. Liu, R. Zhang, H.-Q. Gong, *Journal of Membrane Science* **2011**, *369*, 560.

[21] C. Park, J. Yoon, E. L. Thomas, *Polymer* **2003**, *44*, 6725.

[22] M. A. Hillmyer, "Nanoporous Materials from Block Copolymer Precursors", in *Block Copolymers II*, V. Abetz, Ed., Springer Berlin Heidelberg, Berlin, Heidelberg, **2005**, p. 137.

[23] D. A. Olson, L. Chen, M. A. Hillmyer, *Chemistry of Materials* **2008**, *20*, 869.

[24] E. A. Jackson, M. A. Hillmyer, *ACS Nano* **2010**, *4*, 3548.

[25] X. Li, C.-A. Fustin, N. Lefevre, J.-F. Gohy, S. D. Feyter, J. D. Baerdemaeker, W. Egger, I. F. J. Vankelecom, *Journal of Materials Chemistry* **2010**, *20*, 4333.

[26] A.-V. Ruzette, L. Leibler, *Nature Materials* **2005**, *4*, 19.

[27] F. S. Bates, G. H. Fredrickson, *Physics Today* **1999**, *52*, 32.

[28] K.-V. Peinemann, V. Abetz, P. F. W. Simon, *Nature Materials* **2007**, *6*, 992.

[29] V. Abetz, *Macromolecular Rapid Communications* **2015**, *36*, 10.

[30] S. Rangou, K. Buhr, V. Filiz, J. I. Clodt, B. Lademann, J. Hahn, A. Jung, V. Abetz, *Journal of Membrane Science* **2014**, *451*, 266.

[31] J. I. Clodt, V. Filiz, S. Rangou, K. Buhr, C. Abetz, D. Höche, J. Hahn, A. Jung, V. Abetz, *Advanced Functional Materials* **2013**, *23*, 731.

[32] A. Jung, V. Filiz, S. Rangou, K. Buhr, P. Merten, J. Hahn, J. Clodt, C. Abetz, V. Abetz, *Macromolecular Rapid Communications* **2013**, *34*, 610.

[33] P. Madhavan, P.-Y. Hong, R. Sougrat, S. P. Nunes, *ACS Applied Materials & Interfaces* **2014**, *6*, 18497.

[34] M. Radjabian, J. Koll, K. Buhr, U. A. Handge, V. Abetz, *Polymer* **2013**, *54*, 1803.

[35] M. Radjabian, J. Koll, K. Buhr, U. Vainio, C. Abetz, U. A. Handge, V. Abetz, *Polymer* **2014**, *55*, 2986.

[36] J. Hahn, V. Filiz, S. Rangou, B. Lademann, K. Buhr, J. I. Clodt, A. Jung, C. Abetz, V. Abetz, *Macromolecular Materials and Engineering* **2013**, *298*, 1315.

[37] C. Höhme, J. Hahn, B. Lademann, A. Meyer, B. Bajer, C. Abetz, V. Filiz, V. Abetz, *European Polymer Journal* **2016**, *85*, 72.

[38] R. M. Dorin, W. A. Phillip, H. Sai, J. Werner, M. Elimelech, U. Wiesner, *Polymer* **2014**, *55*, 347.

[39] T. He, M. H. V. Mulder, H. Strathmann, M. Wessling, *Journal of Membrane Science* **2002**, *207*, 143.

[40] R. Hilke, N. Pradeep, A. R. Behzad, S. P. Nunes, K.-V. Peinemann, *Journal of Membrane Science* **2014**, *472*, 39.

[41] J. Hahn, J. I. Clodt, C. Abetz, V. Filiz, V. Abetz, *ACS Applied Materials & Interfaces* **2015**, *7*, 21130.

[42] D. S. Marques, U. Vainio, N. M. Chaparro, V. M. Calo, A. R. Bezahd, J. W. Pitera, K.-V. Peinemann, S. P. Nunes, *Soft Matter* **2013**, *9*, 5557.

[43] K.-V. P. Suzana Pereira Nunes, "Membrane Preparation", in *Membrane Technology in the Chemical Industry* 2nd edition, WILEY-VCH Verlag GmbH & Co. KGaA, Weinheim, Germany, **2006**, p. 9.

[44] M. Mulder, "Introduction", in *Basic Principles of Membrane Technology*, Springer Netherlands, Dordrecht, **1996**, p. 1.

[45] R. W. Baker, "Membrane Transport Theory", in *Membrane Technology and Applications*, 2nd edition, John Wiley & Sons Ltd England, **2004**, p 15.

[46] R. W. Baker, "Membranes and Modules", in *Membrane Technology and Applications*, 2 edition, John Wiley & Sons, Ltd England, **2004**, p. 89.

[47] R. Safi, M. Karimi, A. Madhi, *Polymer Bulletin* **2015**, *72*, 1763.

[48] H. Strathmann, P. Scheible, R. W. Baker, *Journal of Applied Polymer Science* **1971**, *15*, 811.

[49] J. G. Wijmans, C. A. Smolders, "Preparation of Asymmetric Membranes by the Phase Inversion Process", in *Synthetic Membranes: Science, Engineering and Applications*, P.M. Bungay, H.K. Lonsdale, and M.N. de Pinho, Eds., Springer Netherlands, Dordrecht, **1986**, p. 39.

[50] N. Peng, N. Widjojo, P. Sukitpaneenit, M. M. Teoh, G. G. Lipscomb, T.-S. Chung, J.-Y. Lai, *Progress in Polymer Science* **2012**, *37*, 1401.

[51] Y. Liu, G. H. Koops, H. Strathmann, *Journal of Membrane Science* **2003**, *223*, 187.

[52] J. G. Wijmans, J. P. B. Baaij, C. A. Smolders, *Journal of Membrane Science* **1983**, *14*, 263.

[53] S. A. McKelvey, W. J. Koros, *Journal of Membrane Science* **1996**, *112*, 29.

[54] C. Cohen, G. B. Tanny, S. Prager, *Journal of Polymer Science: Polymer Physics Edition* **1979**, *17*, 477.

[55] L. Broens, F. W. Altena, C. A. Smolders, D. M. Koenhen, *Desalination* **1980**, *32*, 33.

[56] A. J. McHugh, L. Yilmaz, *Journal of Polymer Science: Polymer Physics Edition* **1985**, *23*, 1271.

[57] A. J. Reuvers, J. W. A. van den Berg, C. A. Smolders, *Journal of Membrane Science* **1987**, *34*, 45.

[58] C. A. Smolders, A. J. Reuvers, R. M. Boom, I. M. Wienk, *Journal of Membrane Science* **1992**, *73*, 259.

[59] a. V G Levich, V. S. Krylov, *Annual Review of Fluid Mechanics* **1969**, *1*, 293.

[60] R. Matz, *Desalination* **1972**, *10*, 1.

[61] H. Strathmann, K. Kock, P. Amar, R. W. Baker, *Desalination* **1975**, *16*, 179.

[62] H. Strathmann, K. Kock, *Desalination* **1977**, *21*, 241.

[63] S. S. Shojaie, W. B. Krantz, A. R. Greenberg, *Journal of Membrane Science* **1994**, *94*, 281.

[64] T. s. Chung, E. R. Kafchinski, *Journal of Applied Polymer Science* **1997**, *65*, 1555.

[65] T. S. Chung, X. Hu, *Journal of Applied Polymer Science* **1997**, *66*, 1067.

[66] M. R. Pekny, J. Zartman, W. B. Krantz, A. R. Greenberg, P. Todd, *Journal of Membrane Science* **2003**, *211*, 71.

[67] K. Y. Wang, D. Fei Li, T.-S. Chung, S. Bor Chen, *Chemical Engineering Science* **2004**, *59*, 4657.

[68] V. B.-d.-F. Abetz, A. ; Gohy, Jean-François, "Morphologies in block copolymers", in *Controlled and living polymerizations*, K.M. A. H. E. Müller, Ed., Wiley-VCH, **2009**, p. 493.

[69] J.-F. Gohy, "Block Copolymer Micelles", in *Block Copolymers II*, V. Abetz, Ed., Springer Berlin Heidelberg, Berlin, Heidelberg, **2005**, p. 65.

[70] R. Adhikari, R. Godehardt, W. Lebek, S. Goerlitz, G. H. Michler, K. Knoll, *Macromolecular Symposia* **2004**, *214*, 173.

[71] L. Leibler, *Macromolecules* **1980**, *13*, 1602.

[72] F. S. Bates, G. H. Fredrickson, *Annual Review of Physical Chemistry* **1990**, *41*, 525.

[73] a. G H Fredrickson, F. S. Bates, *Annual Review of Materials Science* **1996**, *26*, 501.

[74] M. W. Matsen, F. S. Bates, *The Journal of Chemical Physics* **1997**, *106*, 2436.

[75] I. W. Hamley, V. Castelletto, *Progress in Polymer Science* **2004**, *29*, 909.

[76] M. W. Matsen, F. S. Bates, *Macromolecules* **1996**, *29*, 1091.

[77] W. A. Phillip, M. A. Hillmyer, E. L. Cussler, *Macromolecules* **2010**, *43*, 7763.

[78] C. Stegelmeier, V. Filiz, V. Abetz, J. Perlich, A. Fery, P. Ruckdeschel, S. Rosenfeldt, S. Förster, *Macromolecules* **2014**, *47*, 5566.

[79] L. Oss-Ronen, J. Schmidt, V. Abetz, A. Radulescu, Y. Cohen, Y. Talmon, *Macromolecules* **2012**, *45*, 9631.

[80] D. S. Marques, R. M. Dorin, U. Wiesner, D.-M. Smilgies, A. R. Behzad, U. Vainio, K.-V. Peinemann, S. P. Nunes, *Polymer* **2014**, *55*, 1327.

[81] S. Förster, M. Zisenis, E. Wenz, M. Antonietti, *The Journal of Chemical Physics* **1996**, *104*, 9956.

[82] M. Antonietti, S. Heinz, M. Schmidt, C. Rosenauer, *Macromolecules* **1994**, *27*, 3276.

[83] Y. Li, W. B. Krantz, T.-S. Chung, *AIChE Journal* **2007**, *53*, 2470.

[84] R. G. Larson, *Rheologica Acta* **1992**, *31*, 213.

[85] N. Widjojo, T.-S. Chung, D. Y. Arifin, M. Weber, V. Warzelhan, *Chemical Engineering Journal* **2010**, *163*, 143.

[86] O. M. Ekiner, G. Vassilatos, *Journal of Membrane Science* **2001**, *186*, 71.

[87] B. A. Wolf, *Macromolecules* **1984**, *17*, 615.

[88] R. Horst, B. A. Wolf, *Macromolecules* **1992**, *25*, 5291.

[89] T.-S. Chung, *Journal of Membrane Science* **1997**, *126*, 19.

[90] C. Cao, T.-S. Chung, S. B. Chen, Z. Dong, *Chemical Engineering Science* **2004**, *59*, 1053.

[91] J.-J. Qin, J. Gu, T.-S. Chung, *Journal of Membrane Science* **2001**, *182*, 57.

[92] S. S. J., *Journal of Applied Polymer Science* **1997**, *65*, 1359.

[93] X. Miao, S. Sourirajan, H. Zhang, W. W. Y. Lau, *Separation Science and Technology* **1996**, *31*, 141.

[94] T. Liu, D. Zhang, S. Xu, S. Sourirajan, *Separation Science and Technology* **1992**, *27*, 161.

[95] M.-C. Yang, M.-T. Chou, *Journal of Membrane Science* **1996**, *116*, 279.

[96] C. Y. Feng, K. C. Khulbe, T. Matsuura, A. F. Ismail, *Separation and Purification Technology* **2013**, *111*, 43.

[97] X.-M. Li, T. He, *Polymers for Advanced Technologies* **2008**, *19*, 801.

[98] M. Mulder, "*Basic Principles of Membrane Technology"*, Kluwer Academic Publishers, Dordrecht, The Netherlands, **1996**.

[99] C. C. Pereira, R. Nobrega, C. P. Borges, *Journal of Membrane Science* **2001**, *192*, 11.

[100] X.-M. Li, Y. Ji, Y. Yin, Y.-Y. Zhang, Y. Wang, T. He, *Journal of Membrane Science* **2010**, *352*, 173.

[101] C. C. Pereira, R. Nobrega, K. V. Peinemann, C. P. Borges, *Journal of Membrane Science* **2003**, *226*, 35.

[102] D. F. Li, T.-S. Chung, R. Wang, Y. Liu, *Journal of Membrane Science* **2002**, *198*, 211.

[103] S. P. Nunes, R. Sougrat, B. Hooghan, D. H. Anjum, A. R. Behzad, L. Zhao, N. Pradeep, I. Pinnau, U. Vainio, K.-V. Peinemann, *Macromolecules* **2010**, *43*, 8079.

[104] G. Markus, R. Sofia, F. Volkan, B. Kristian, B. Sabrina, A. Clarissa, A. Volker, *Macromolecular Chemistry and Physics* **2013**, *214*, 1037.

[105] C. J. Isabel, R. Sofia, S. Anne, B. Kristian, H. Janina, J. Adina, F. Volkan, A. Volker, *Macromolecular Rapid Communications* **2013**, *34*, 190.

[106] D. Li, T.-S. Chung, R. Wang, *Journal of Membrane Science* **2004**, *243*, 155.

[107] Y. Zhang, R. A. Mulvenna, B. W. Boudouris, W. A. Phillip, *Journal of Materials Chemistry A* **2017**, *5*, 3358.

[108] Y. Liu, T. Liu, Y. Su, H. Yuan, T. Hayakawa, X. Wang, *Journal of Membrane Science* **2016**, *506*, 1.

[109] D. Li, T.-S. Chung, R. Wang, *Journal of Membrane Science* **2004**, *243*, 155.

[110] W. Albrecht, K. Kneifel, T. Weigel, R. Hilke, R. Just, M. Schossig, K. Ebert, A. Lendlein, *Journal of Membrane Science* **2005**, *262*, 69.

[111] Q.-C. Xia, J. Wang, X. Wang, B.-Z. Chen, J.-L. Guo, T.-Z. Jia, S.-P. Sun, *Journal of Membrane Science* **2017**, *539*, 392.

[112] S. A. Hashemifard, A. F. Ismail, T. Matsuura, *Journal of Membrane Science* **2011**, *375*, 258.

[113] S. P. Sun, K. Y. Wang, N. Peng, T. A. Hatton, T.-S. Chung, *Journal of Membrane Science* **2010**, *363*, 232.

[114] L. Setiawan, L. Shi, W. B. Krantz, R. Wang, *Journal of Membrane Science* **2012**, *423-424*, 73.

[115] T.-S. Chung, L. Y. Jiang, Y. Li, S. Kulprathipanja, *Progress in Polymer Science* **2007**, *32*, 483.

[116] N. Widjojo, T. S. Chung, W. B. Krantz, *Journal of Membrane Science* **2007**, *294*, 132.

[117] N. Widjojo, T.-S. Chung, S. Kulprathipanja, *Journal of Membrane Science* **2008**, *325*, 326.

[118] S. Bondzic, J. de Wit, E. Polushkin, A. J. Schouten, G. ten Brinke, J. Ruokolainen, O. Ikkala, I. Dolbnya, W. Bras, *Macromolecules* **2004**, *37*, 9517.

[119] M. R. Hammond, R. Mezzenga, *Soft Matter* **2008**, *4*, 952.

[120] P. Madhavan, K.-V. Peinemann, S. P. Nunes, *ACS Applied Materials & Interfaces* **2013**, *5*, 7152.

[121] Y. Li, W. B. Krantz, T. S. Chung, *AIChE Journal* **2007**, *53*, 2470.

[122] R. Guan, H. Zou, D. Lu, C. Gong, Y. Liu, *European Polymer Journal* **2005**, *41*, 1554.

[123] F.-J. Fu, S. Zhang, S.-P. Sun, K.-Y. Wang, T.-S. Chung, *Journal of Membrane Science* **2013**, *443*, 144.

[124] D. Wang, K. Li, W. K. Teo, *Journal of Membrane Science* **1999**, *163*, 211.

[125] K. Y. Wang, T. Matsuura, T.-S. Chung, W. F. Guo, *Journal of Membrane Science* **2004**, *240*, 67.

[126] N. Widjojo, T.-S. Chung, M. Weber, C. Maletzko, V. Warzelhan, *Chemical Engineering Journal* **2013**, *220*, 15.

[127] J. A. van't Hof, A. J. Reuvers, R. M. Boom, H. H. M. Rolevink, C. A. Smolders, *Journal of Membrane Science* **1992**, *70*, 17.

[128] H. Wu, X. Li, C. Zhao, X. Shen, Z. Jiang, X. Wang, *Industrial & Engineering Chemistry Research* **2013**, *52*, 5772.

[129] F. Ma, H. Ye, Y.-Z. Zhang, X.-L. Ding, L.-G. Lin, L. Zhao, H. Li, *Desalination and Water Treatment* **2014**, *52*, 618.

[130] Y. Feng, G. Han, L. Zhang, S.-B. Chen, T.-S. Chung, M. Weber, C. Staudt, C. Maletzko, *Polymer* **2016**, *99*, 72.

[131] K. Kimmerle, H. Strathmann, *Desalination* **1990**, *79*, 283.

[132] Y. Feng, G. Han, T.-S. Chung, M. Weber, N. Widjojo, C. Maletzko, *Journal of Membrane Science* **2017**, *531*, 27.

[133] I. M. Wienk, R. M. Boom, M. A. M. Beerlage, A. M. W. Bulte, C. A. Smolders, H. Strathmann, *Journal of Membrane Science* **1996**, *113*, 361.

[134] M. Liu, C. Zhou, B. Dong, Z. Wu, L. Wang, S. Yu, C. Gao, *Journal of Membrane Science* **2014**, *463*, 173.

[135] R. Guan, H. Dai, C. Li, J. Liu, J. Xu, *Journal of Membrane Science* **2006**, *277*, 148.

[136] Y. Li, T. S. Chung, *Journal of Membrane Science* **2008**, *308*, 128.

[137] F. Lufrano, I. Gatto, P. Staiti, V. Antonucci, E. Passalacqua, *Solid State Ionics* **2001**, *145*, 47.

[138] M. S. Park, J. K. Kim, *Langmuir* **2005**, *21*, 11404.

[139] M. S. Park, W. Joo, J. K. Kim, *Langmuir* **2006**, *22*, 4594.

[140] M. S. Park, J. K. Kim, *Langmuir* **2004**, *20*, 5347.

[141] L.-S. Wan, J.-W. Li, B.-B. Ke, Z.-K. Xu, *Journal of the American Chemical Society* **2012**, *134*, 95.

[142] S. Walheim, E. Schäffer, J. Mlynek, U. Steiner, *Science* **1999**, *283*, 520.

[143] K.-V. Peinemann, V. Abetz, P. F. W. Simon, *Nat Mater* **2007**, *6*, 992.

[144] K. Sakakibara, J. P. Hill, K. Ariga, *Small* **2011**, *7*, 1288.

[145] M. Victor, J. Qingmin, K. Yuichiro, M. Taizo, S. Fa-Kuen, W. K. C.-W., A. Katsuhiko, Y. Yusuke, *Bulletin of the Chemical Society of Japan* **2015**, *88*, 1171.

[146] B. Jiang, C. Li, J. Tang, T. Takei, J. H. Kim, Y. Ide, J. Henzie, S. Tominaka, Y. Yamauchi, *Angewandte Chemie International Edition* **2016**, *55*, 10037.

[147] Y. Li, C. Li, B. P. Bastakoti, J. Tang, B. Jiang, J. Kim, M. Shahabuddin, Y. Bando, J. H. Kim, Y. Yamauchi, *Journal of Materials Chemistry A* **2016**, *4*, 9169.

[148] L. Sun, M. G. Campbell, M. Dincă, *Angewandte Chemie International Edition* **2016**, *55*, 3566.

[149] Y. Li, B. P. Bastakoti, Y. Yamauchi, *APL Materials* **2016**, *4*, 040703.

[150] T. Yamada, M. Sadakiyo, A. Shigematsu, H. Kitagawa, *Bulletin of the Chemical Society of Japan* **2015**, *89*, 1.

[151] A. Zhang, H. Bai, L. Li, *Chemical Reviews* **2015**, *115*, 9801.

[152] M. Hernandez-Guerrero, M. H. Stenzel, *Polymer Chemistry* **2012**, *3*, 563.

[153] H. Bai, C. Du, A. Zhang, L. Li, *Angewandte Chemie International Edition* **2013**, *52*, 12240.

[154] U. H. F. Bunz, *Advanced Materials* **2006**, *18*, 973.

[155] G. Widawski, M. Rawiso, B. Francois, *Nature* **1994**, *369*, 387.

[156] S. Washizu, H. Yamazaki, J. Yamanouchi, H. Naruse, "Honeycomb composite film, and method for producing the same", Fuji Photo Co., Ltd. **2006**, US 2006/0266463 A1.

[157] T. Ohzono, T. Nishikawa, M. Shimomura, *Journal of Materials Science* **2004**, *39*, 2243.

[158] F. Sun, W. Cai, Y. Li, L. Jia, F. Lu, *Advanced Materials* **2005**, *17*, 2872.

[159] F. Sun, J. C. Yu, *Angewandte Chemie International Edition* **2007**, *46*, 773.

[160] L. A. Connal, G. G. Qiao, *Advanced Materials* **2006**, *18*, 3024.

[161] J. Ding, J. Gong, H. Bai, L. Li, Y. Zhong, Z. Ma, V. Svrcek, *Journal of Colloid and Interface Science* **2012**, *380*, 99.

[162] L. Li, Y. Zhong, J. Gong, J. Li, C. Chen, B. Zeng, Z. Ma, *Soft Matter* **2011**, *7*, 546.

[163] H. Fashandi, M. Karimi, *Polymer* **2012**, *53*, 5832.

[164] Z.-H. Wang, W. Cheng, C.-H. Liu, J. Ma, W.-J. Zhang, J. Li, *Macromolecular Materials and Engineering* **2016**, *301*, 36.

[165] T. Li, Z. Wu, K. Li, *Journal of Membrane Science* **2014**, *449*, 1.

[166] T. Li, Z. Wu, K. Li, *Journal of Power Sources* **2015**, *273*, 999.

[167] R. A. Amaral, C. P. Borges, A. C. Habert, N. R. J. D. Mermier, *Chemical Engineering & Technology* **2016**, *39*, 1171.

[168] A. Glycerine Producers, "*Physical properties of glycerine and its solutions*", Glycerine Producers' Association, New York, **1963**.

[169] R. Takekoh, T. P. Russell, *Advanced Functional Materials* **2014**, *24*, 1483.

[170] J. Albuerne, A. B.-d. Fierro, C. Abetz, D. Fierro, V. Abetz, *Advanced Engineering Materials* **2011**, *13*, 803.

[171] N. Nestle, W. Heckmann, H. Steininger, K. Knoll, *Analytica Chimica Acta* **2007**, *604*, 54.

[172] L. Li, J. Li, Y. Zhong, C. Chen, Y. Ben, J. Gong, Z. Ma, *Journal of Materials Chemistry* **2010**, *20*, 5446.

[173] M. H. Stenzel, C. Barner-Kowollik, T. P. Davis, *Journal of Polymer Science Part A: Polymer Chemistry* **2006**, *44*, 2363.

Chapter 13

Appendix

13.1 T_g of the Polymers
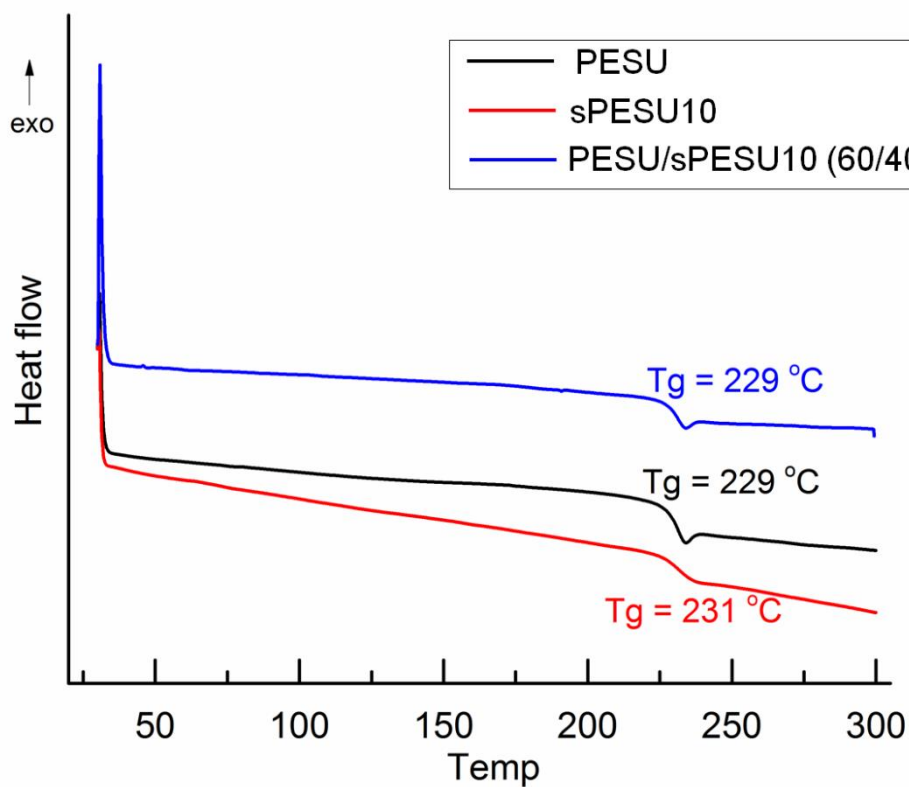
Figure 13.1 DSC thermograms of pure PESU, sPESU10, and the blend of PESU and sPESU10 (60 wt.% PESU and 40 wt.% sPESU10).

The glass transition temperature, T_g of pure PESU appeared at 229 °C. Sulfonation of PESU to 10% DS increased the T_g and it was found at 231 °C. The blend of PESU and sPESU10 where the majority part consisted of PESU did not show any difference in T_g.

13.2 Rheological Properties of the Solutions
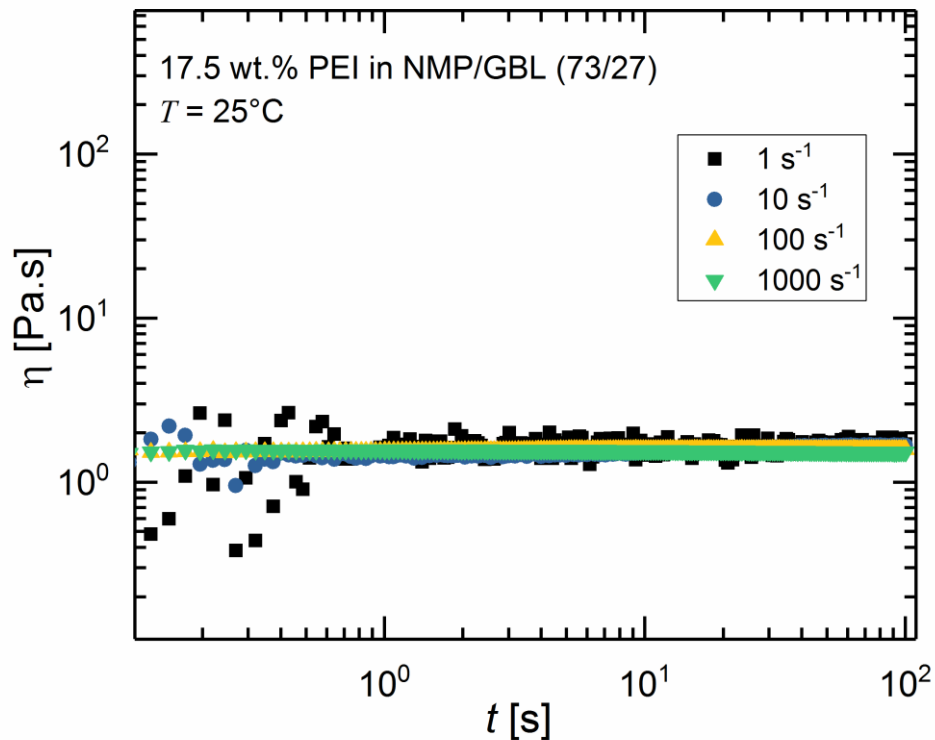
Figure 13.2 Transient viscosity (η) as a function of time (t) of 17.5 wt.% PEI in NMP and GBL (NMP/GBL: 73/27 (wt./wt.)) for different shear rates at 25 ºC. This solution showed slightly shear thinning behavior at higher shear rate. The transient viscosity showed a constant value with time for the same shear rate. Moreover, The effect of increase in shear rate is not much evident from this solution.
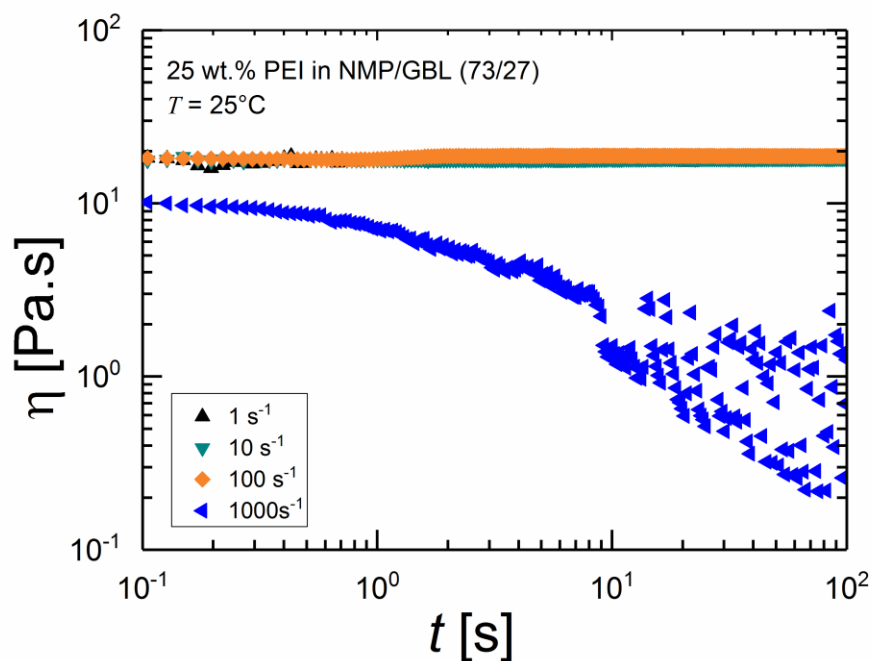
Figure 13.3 Transient viscosity (η) as a function of time (*t*) of 25 wt.% PEI in NMP and GBL (NMP/GBL: 73/27 (wt./wt.)) for different shear rates at 25 °C. This solution showed shear thinning behavior at higher shear rate.
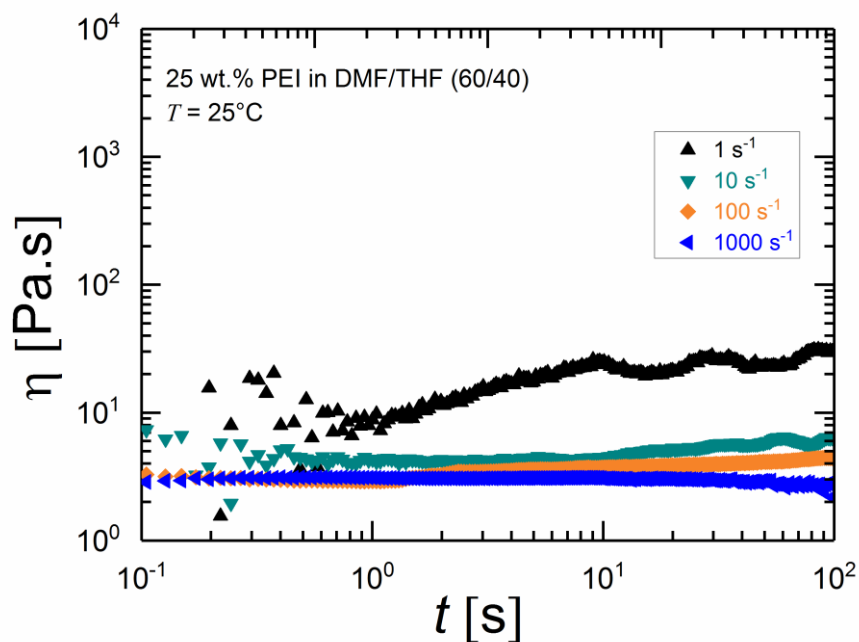
Figure 13.4 Transient viscosity (η) as a function of time (*t*) of 25 wt.% PEI in DMF and THF (DMF/THF: 60/40 (wt./wt.)) for different shear rates at 25 °C. This solution showed slightly shear thinning behavior at higher shear rate.
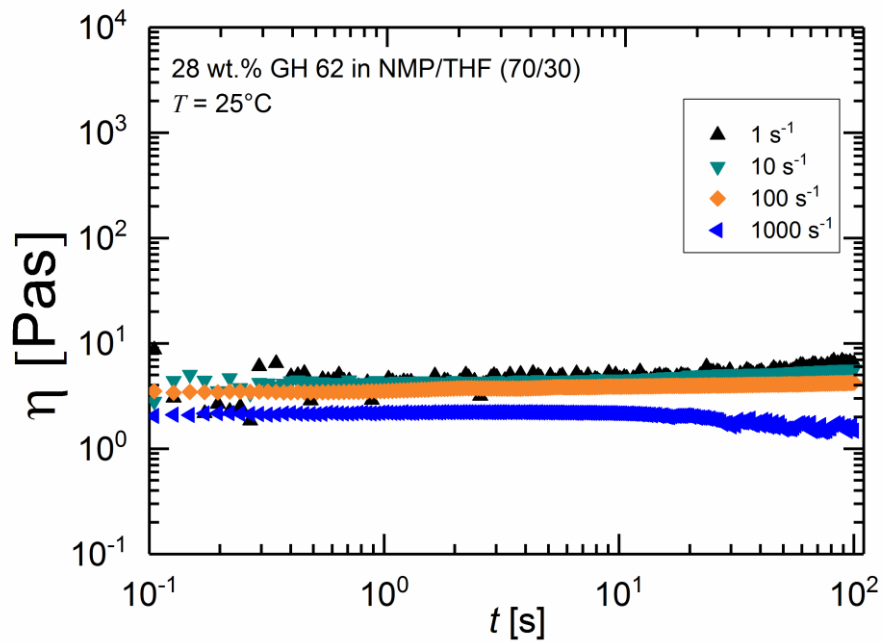
Figure 13.5 Transient viscosity (η) as a function of time (*t*) of 28 wt.% GH 62 in NMP and THF (NMP/THF: 70/30 (wt./wt.)) for different shear rates at 25 °C. This solution showed shear thinning behavior at higher shear rate.
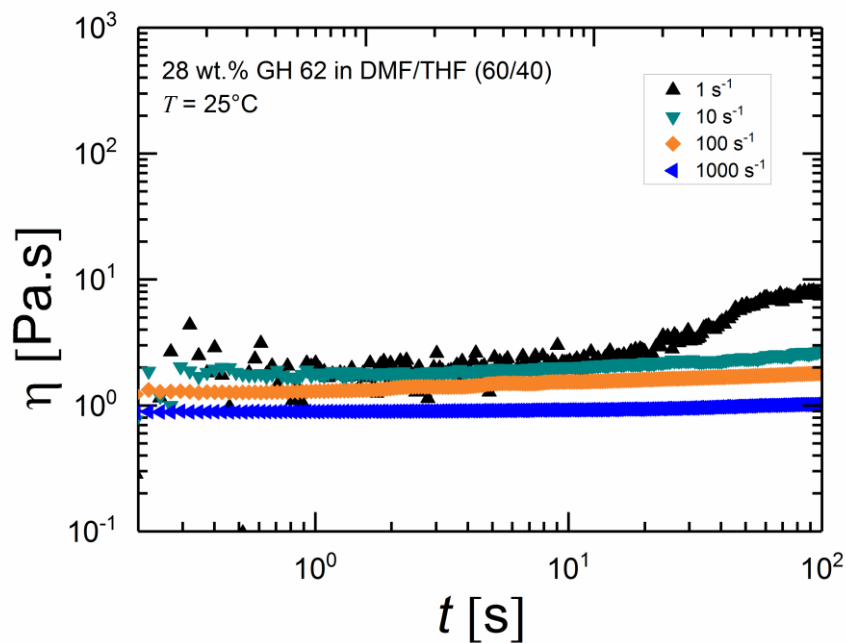
Figure 13.6 Transient viscosity (η) as a function of time (*t*) of 28 wt.% GH 62 in DMF and THF (DMF/THF: 60/40 (wt./wt.)) for different shear rates at 25 °C. This solution showed shear thinning behavior at higher shear rate.
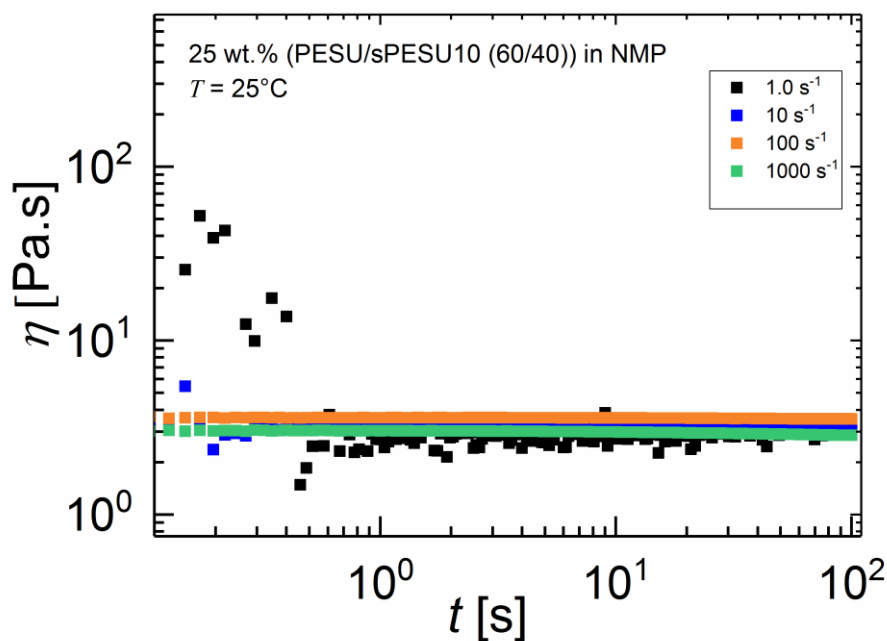
Figure 13.7 Transient viscosity (η) as a function of time (t) of 25 wt.% (PESU/sPESU10: 60/40 (wt./wt.) in NMP for different shear rates at 25 °C. The solution showed slightly shear thinning behavior at higher shear rate.
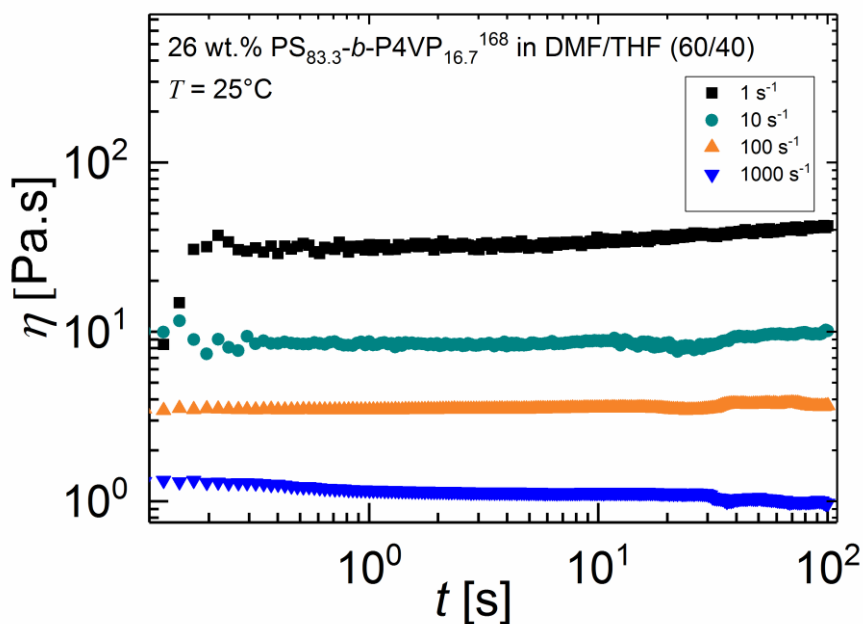
Figure 13.8 Transient viscosity (η) as a function of time (t) of 26 wt.% $PS_{83.3}$-b-$P4VP_{16.7}$[168] in DMF and THF (DMF/THF: 60/40 (wt./wt.) for different shear rates at 25 °C. The decrease in transient viscosity with increased shear rate is clearly detectable.

13.3 Toxicity of the Chemicals

Table 13.1 List of chemicals with GHS symbol and H- and P- phrases

Substance	GHS symbol	Hazard statement	Precautionary statement
1,4-dioxane	GHS02, GHS07, GHS08	H225, H319, H335, H351, EUH019, EUH066	P210, P233, P240, P281, P304 + P340, P308 + P313,P403 + P235
CaH₂	GHS02	H260	P223-P231 + P232 P370 + P378-P422
CHCl₃	GHS02, GHS07, GHS09	H302, H315, H319, H331, H336, H351, H361d, H372	P201, P261, P304 + P340 + P311, P305 + P351 + P338, P308 + P313, P403 + P233
ClSO₃H	-	H314, H335, EUH014	P260, P280, P303 + P361 + P353, P304 + P340 + P310, P305 + P351 + P338
DCM	GHS07, GHS08	H315, H319, H335, H336, H351, H373, H373	P260, P280, P305 + P351 + P338
DMAc	GHS07, GHS08	H312+ H332-H319 H360D	P201-P280 P305 + P351 + P338 P308 + P313
DMF	GHS 02, GHS07, GHS08	H360D, H226, H312+ H332, H319	P201, P210, P302+ P352, P305 + P351 + P338, P308 + P313
Ethylaluminium dichloride	GHS02, GHS05, GHS07, GHS08, GHS09	H225, H250, H261, H304, H314, H336, H361f, H373, H411, EUH014	P210, P231 + P232, P280, P301 + P310, P302 + P334, P303 + P361 + P353, P304 + P340 + P310, P305 + P351 + P338, P331, P422
GBL	-	H302, H318, H336	P261, P280, P305 + P351 + P338
NMP	GHS04, GHS02, GHS2A	H315,H319, H335, H360D,	P201, P302 + P352, P305 + P351 + P338, P308 + P313

Substance	GHS symbol	Hazard statement	Precautionary statement
SDS	-	H228, H302 + H332, H315, H318, H335, H412	P210, P261, P280, P302+P352, P305+P351+P338, P312
Sec-BuLi	GHS02, GHS05, GHS07, GHS08, GHS09	H225, H250, H260, H304, H314, H336, H410	P210, P222, P223, P231 + P232, P370 + P378, P422
Styrene	GHS02, GHS07	H226-H315-H319 H332	P305 + P351 + P338
THF	GHS02, GHS07, GHS12	H225,H319,H335,H351,EUH019	P210, P240, P305 + P351 + P338, P308 + P313, P403 + 233
4VP	GHS02, GHS05, GHS06	H226-H301-H314 H317	P280-P301 + P310 P305 + P351 + P338 P310

Acknowledgement

I dedicate this thesis to all the wonderful members of my family for being supportive to my every quest in life.

At the end, I want to remind you about all those vulnerable war affected people in today's world. We human beings have yet to walk a long way to secure safe drinking water, food, medical treatment, shelter, and education for every human being on this planet. Let's work on it. Let's STOP WAR wherever it is happening now. Let's live peacefully and let others live peacefully.

Curriculum Vitae

Lebenslauf entfällt aus datenschutzrechtlichen Gründen

Declaration of Oath

I hereby declare that this thesis on "Isoporous double layer hollow fiber by co-extrusion for membrane and other applications" accommodates the original work of my PhD. Several parts of this dissertation had been published in different peer-reviewed international journals and therefore, the similarities with those published works exist. All the sources used in this thesis are acknowledged. This dissertation is written by me and has not ever been submitted to any other university or institution to pursue a degree.

Nazia Noor